Assessment of the behaviour factor for structural wall buildings when incorporating soil-structure interaction.

by
Pieter Willem Wessels Visagie

Thesis presented in fulfilment of the requirements for the degree of Master of Engineering in Civil Engineering in the Faculty of Engineering at Stellenbosch University

Supervisor: Professor T.N. Haas
Co-supervisor: Professor G.P.A.G. van Zijl

March 2021

Declaration:

By submitting this thesis electronically, I declare that the entirety of the work contained therein is my own, original work, that I am the sole author thereof (save to the extent explicitly otherwise stated), that reproduction and publication thereof by Stellenbosch University will not infringe any third party rights and that I have not previously in its entirety or in part submitted it for obtaining any qualification.

March 2021

Abstract:

Structural walls in low- to medium-rise buildings are relatively stiff and have short fundamental periods of vibration. The short periods produce large equivalent lateral forces and overturning moments, which result in large foundations.

The principle of capacity design requires the use of an overstrength foundation in order to ensure that the hinge mechanism forms in the predicted region of the structural wall. The hinge region is then suitably detailed to resist the seismic action in a ductile manner and therefore dissipate energy. This overstrength foundation requirement can result in excessive foundation sizes for structural walls with shallow foundations.

Soil-structure interaction has beneficial effects for most building structures under seismic action. However, incorporating soil-structure interaction in the analysis influences the fundamental period, damping and ductility and will therefore influence the behaviour factor. The behaviour factor is necessary for linear methods (force-based methods) to predict the nonlinear behaviour of the structure.

This study assesses the current behaviour factor for reinforced concrete walls, as prescribed by SANS 10160-4 (2017), when soil-structure interaction is incorporated in the analysis. The buildings are initially designed and detailed using linear methods, with the prescribed behaviour factor, and then tested using nonlinear methods that do not require the use of a behaviour factor.

The results of this study show that the behaviour factor prescribed by SANS 10160-4 (2017) is adequate (and possibly conservative) when soil-structure interaction is incorporated in the analysis, provided that the frame is designed to resist the additional loading caused by the rotation of the wall foundation.

Uittreksel:

Gewapende betonmure in lae- tot medium-verdieping geboue is relatief styf en het gevolglik kort fundamentele periodes. Die kort periodes lewer groot ekwivalente laterale kragte en omkeermomente, wat groot fondamente tot gevolg het.

Kapasiteitsontwerp beginsels vereis dat hiedie mure vir ‘n hoër omkeermoment ontwerp moet word sodat die skarniermaganisme in die voorspelde gebied van die muur vorm. Die skarnierstreek word dan toepaslik gedetailleer om seismiese werking op ‘n duktiele manier te weerstaan en sodoende energie te versprei. Hierdie vereiste kan lei tot oormatige fondamentgroottes vir mure met vlak fondamente.

Interaksie tussen die grond en die struktuur het voordelige effekte vir meeste geboue onder seismiese werking. Die insluiting van hierdie interaksie in die analise beïnvloed egter die fundamentele periode, demping en duktiliteit, dus beïnvloed dit dan ook die gedragsfaktor. Die gedragsfakor word gebruik in lineêre metodes (kraggebaseerde metodes) om die nie-lineêre gedrag van die struktuur voor te stel.

Hierdie studie evalueer die huidige gedragsfaktor vir gewapende betonmure, soos voorgeskryf deur SANS 10160-4 (2017), wanneer die interaksie tussen die grond en struktuur in die analise ingesluit word. Die geboue word aanvanklik ontwerp en gedetailleer met lineêre metodes, met die voorgeskrewe gedragsfaktor, en dan getoets met nie-lineêre metodes wat nie gebruik maak van ‘n gedragsfaktor nie.

Die resultate van hiedie studie toon dat die voorgeskrewe gedragsfaktor voldoende (en moontlik konserwatief) is wanneer die interaksie tussen die grond en struktuur in die analise ingesluit word, mits die raamwerk ontwerp is om die addisionele belasting, wat veroorsaak word deur die rotasie van die fundament, te weerstaan.

Acknowledgment:

I would like to express my gratitude to:

- Professors Trevor Haas and Gideon van Zijl for their feedback and sharing their insight.
- The Civil Engineering department at Stellenbosch University for allowing me to perform this study on a part time basis.
- Family and friends.

Table of Content:

Table of Figures:

List of Tables:

Abbreviations:

ADRS	Acceleration-displacement response spectrum
ASCE	American Society of Civil Engineers
BNWF	Beam-on-nonlinear Winkler foundation
CQC	Complete quadratic combination
CSM	Capacity spectrum method
DL	Dead load
FEMA	Federal Emergency Management Agency
LL	Live load
MDOF	Multi degree of freedom
NEHRP	National Earthquake Hazards Reduction Program
PEER	Pacific Earthquake Engineering Research centre
PGA	Peak ground acceleration
SDOF	Single degree of freedom
SEI	Structural Engineering Institute
SRSS	Square root sum of squares
SSI	Soil-structure interaction
THA	Time-history analysis

Nomenclature:

$\left(\frac{\tilde{T}}{T}\right)_{eff}$	Effective period lengthening ratio
H^*, h^*	Effective structural height
h_c	Dimension of the boundary element in the direction under consideration
h_{pl}, h_{cr}	Vertical extent of plastic/critical region
h_s	Storey height
h_w	Height of walls
h_x	Maximum horizontal spacing of legs of confinement reinforcement
$[\mathrm{K}]$	Stiffness matrix
$[\mathrm{M}]$	Mass matrix
Δ_u, d_u	Ultimate displacement
Δ_y, d_y	Yield displacement
$\{\Phi\}$	Displacement shape vector
Φ_i	Normalised drift pattern for floor i
A_B	Ground floor area of the structure or average floor area where setbacks occur at higher levels
A_c	Area of core of section enclosed by the centre lines of links
A_e	Area of effective concrete core midway between two links
A_{sb}	The area of confinement reinforcement in the boundary zone
$A_{sx}; A_{sy}$	Total area of transverse reinforcement running in the x and y direction
C_0	Modification factor for the transformation of a SDOF system to MDOF
C_1	Modification factor for to relate expected maximum inelastic displacement to displacement calculated for linear elastic response

C_2	Modification factor to represent the effect of pinched hysteresis shape, cyclic stiffness degradation, and strength deterioration on maximum displacement response
C_m	Effective mass factor
D_c	Concrete compression force
D_{se}	Steel compression force in boundary element
E_c	Modulus of elasticity of concrete
E_m	Area under the capacity curve
E_s'	Plane strain modulus
E_{sec}	Tangent modulus of elasticity of the concrete
E_{stl}	Modulus of elasticity for steel reinforcement
F^*	Force of an equivalent SDOF system
F_i	Equivalent lateral force for floor i
F_y	Yield force
G_0	Shear strain modulus adjusted to account for nonlinearity associated with ground shaking
G_n	Permanent load
H_s	Depth of soil stratum
I_1, I_2, I_s, I_F	Influence factors related to modulus of subgrade reaction
M_{qL}	Normalised moment resistance of the foundation
M_{ub}	Ultimate moment capacity of the foundation
M_w	Moment magnitude
Q_{ni}	Imposed loads
S_{Ad}	Design acceleration spectrum
T^*, T_e	Effective period of vibration
T_{eff}	Adapted effective period prescribed by FEMA 440
T_{xx}, T_{yy}	Rotational period about the x-axis and y-axis respectively

T_y, T_x	Translational period in the y-direction and x-direction respectively
V_{el}	Force of an equivalent elastic system
V_n	Design base shear
V_y	Yield force
W_n	Nominal sustained vertical load
Z_{se}	Steel tensile force in boundary element
Z_{sw}	Steel tensile force in wall web
a_0	Dynamic stiffness modifier
b_w	Wall width
d^*	Displacement of an equivalent SDOF system
d_e	Elastic displacement
d_m	Displacement at the formation of the first plastic mechanism
$d_{r\ i-j}$	Relative drift between storeys
d_s	Inelastic displacement
d_t	Target displacement
d_t^*	Target displacement for an equivalent SDOF system
d_y^*	Yield displacement of an equivalent SDOF system
f_c	Concrete compressive stress
f_c'	Unconfined concrete compressive strength
f_{cc}'	Confined concrete compressive strength
f_{cd}	Design compressive cube strength
$f_{ck,cyl}$	Characteristic concrete cylinder strength
f_{cu}	Characteristic concrete cube strength
f_l	Lateral pressure from transverse reinforcement
f_l'	Effective lateral confining pressure

$f'_{lx}; f'_{ly}$	Effective lateral confinement pressure in the x and y direction
f_n	Natural frequency
f_{sy}	Characteristic steel yield strength
f_y	Design steel yield strength
f_{yh}	Specified yield strength of the confining reinforcement
k_e	Confinement effectiveness ratio
k_{sh}	Horizontal stiffness of the base
k_{sr}	Rotational stiffness of the base
k_{sv}	Vertical stiffness of the base
k_v	Modulus of subgrade reaction
k_x, k_y	Translational stiffness in the x-direction and y-direction respectively
k_{yy}, k_{xx}	Rotational stiffness about the y-axis and x-axis respectively
l_c	Length of boundary element
l_w	Length of wall
m^*	Effective modal mass of an equivalent SDOF system
m_i	Mass of floor i
q_u	Soil bearing capacity
r_{max}	Maximum storey shear ratio
s_x	The vertical spacing of confinement reinforcement in the boundary element
u_f	Horizontal displacement of the foundation
$v_{s,30}$	Average value of propagation of S-waves in the upper 30m of the soil profile at shear strains of 10^{-5}, or less
v_{s0}	Shear wave velocity
x_n	Distance from the extreme compressive fibres to the neutral axis.
Δ_D	Design displacement
Δ_F	Displacement at the effective height of the wall due to a flexible foundation

α_{xx}	Surface stiffness modifier
β_{eff}	Adapted effective damping prescribed by FEMA 440
β_f	Foundation damping
β_{rd}	Radiation damping
β_s	Soil hysteretic damping
β_{xx}, β_{yy}	Radiation damping relating to rotation about the x-axis and y-axis respectively
β_y, β_x	Radiation damping relating to translation in the y-direction and x-direction respectively
γ_{conc}	Concrete density
γ_{soil}	Soil density
ε_c	Concrete compressive strain
ε_{cc}	Strain at peak stress for confined concrete
ε_{co}	Strain at peak stress for unconfined concrete
ε_{cu}	Concrete ultimate strain
ε_{sm}	Transverse reinforcement steel strain at maximum stress
ε_{su}	Steel ultimate strain
ε_{sy}	Steel yield strain
μ_Φ	Curvature ductility
μ_Δ	Displacement ductility
ξ_{hyst}	Hysteretic damping
ξ_{el}	Elastic damping
ξ_{eq}	Equivalent viscous damping
ρ_{cc}	Ratio of area of longitudinal reinforcement to area of core of section
ρ_e	Reinforcing content in the boundary element
ρ_t	Total reinforcing content
ρ_w	Reinforcing content in the web
φ_i	Load combination factor

ω_n	Angular frequency
a_1	Tension shift length
E_E	Total response due to seismic action
k_w	EN 1998-1 adjustment factor to the behaviour factor for walls of aspect ratios lower than 2
RRS_{bsa}	Response reduction factor for base slab averaging
RRS_e	Response reduction factor for embedment
S	Soil spectral factor
$S_{Ae}(T)$	Elastic acceleration spectrum
$S_{De}(T)$	Displacement spectrum
S_{DS}	Peak spectral design response
T_B, T_C, T_D, T_E	Corner periods to define response spectra
B	Foundation width
C	Damping coefficient dependent on the hysteretic rule
F	Lateral force
G	Effective shear strain modulus
H, h	Total height
L	Foundation length
M	Internal bending moment about the strong axis of the wall
N	Axial load applied to the wall
P	Axial load on foundation
R	Force reduction factor
T	Vibration period
c	Viscous constant of damping
g	Gravity acceleration, $9.81\ m/s^2$
k	Stiffness of the structure
m	Oscillator mass

q	Behaviour factor
t	Thickness
ti	Time
u	Ground absolute displacement
x	Mass absolute displacement
y	Relative displacement
Γ	Modal participation factor
Δ, d	Displacement
Ω	Overstrength factor
αV	Limit to the percentage reduction of the equivalent design base shear in ASCE/SEI 7-16
η	Spectral correction factor for damping
θ	Rotation angle
μ	Ductility
ξ, β	Damping coefficient
ρ	Redundancy factor
υ	Poisson's ration
χ	Inverse of the foundation bearing capacity
ψ	Soil stiffness to strength ratio

1 Introduction

Traditional force-based seismic design approaches require the use of a period dependent acceleration response spectrum to determine the equivalent base shear. The fundamental period of vibration is determined from empirical equations set out in codes of practice, or by more detailed methods using moment-curvature relationships and eigenvalue analyses. The fundamental period of vibration is a function of the mass of the structure and the horizontal stiffness of the lateral supporting elements.

Reinforced concrete shear wall buildings, known as "*building frame systems*" in SANS 10160-4 (2017), rely on the reinforced concrete shear walls to resist the lateral movement induced by a seismic event. The aspect ratio (ratio of wall height to wall length) of these walls should be prescribed in a way to ensure more ductile flexural behaviour rather than brittle shear behaviour under seismic excitation. The term *structural wall* rather than *shear wall* will be used in this investigation.

Structural walls in medium- to low-rise buildings are comparatively stiff and therefore have short fundamental periods. The short period produces large equivalent base shear forces and overturning moments. The axial forces due to gravity loads are small in medium- to low-rise buildings compared to high-rise buildings. This relatively low ratio of axial force to equivalent horizontal force results in large foundations.

In the principles of capacity design, specific lateral resistant elements referred to as the *critical region* are identified and suitably detailed to resist the seismic displacement demand through ductile behaviour. This can be seen as an element with enough local ductility to form a plastic hinge in order to dissipate energy, thereby protecting the rest of the structure (Pauley & Priestley, 1992, pp. 37-38). Design codes widely adopt the capacity design principles. Engineers follow this approach to identify hinge mechanisms, which improves the prediction of nonlinear structural behaviour. In the case of structural wall systems, without basements, this critical region is in the lower part of the wall, between the foundation and, generally, the first storey. To ensure that the hinge mechanism forms in the critical region before excessive foundation rotation, the foundation is designed to resist a moment larger than the moment resulting from a static analysis. This is termed the *overstrength moment*. The overstrength moment requirements will result in even larger foundations.

Soil-structure interaction (SSI) analysis is the evaluation of the combined response of the structure, foundation and soil under the foundation (NIST GCR 12-917-21, 2012, p. iii). Including this interaction in the analysis can improve the seismic response of a structure by period lengthening, kinematic effects, additional damping caused by soil hysteric damping and radiation damping. These effects generally reduce the seismic response and therefore produce smaller foundations.

Linear methods of analysis are force-based and require the use of a behaviour factor (or force-reduction factor) to simulate the nonlinear behaviour of a structure under seismic action. This behaviour factor is related to the ductility capacity and the fundamental period of vibration. SSI influences both the ductility and the fundamental period. Furthermore, due to the variation in assessing ductility and ductility capacity, there is no real uniformity in codified behaviour factors (Priestley, et al., 2007, pp. 13-14).

The purpose of this study is to assess the behaviour factor prescribed by the SANS 10160-4 (2017) for structural wall systems in low- to medium-rise building when SSI is incorporated in the analysis.

This study investigates a series of reinforced concrete wall building-frame systems. The investigation commences by assuming fixed foundations before incrementally reducing the foundation size to determine its effects. Reducing the foundation size increases the contribution of the structural frame in resisting seismic action. These structural systems are initially designed using linear methods with the prescribed behaviour factor and then assessed using nonlinear methods that are independent of a behaviour factor.

The outline of the document is as follows:

The literature review in Chapter 2 deals with traditional design methods, conventional calculations of the fundamental period, the behaviour factor and its relationship with ductility and period, soil-structure interaction, and current South African design requirements.

The development of the foundation moment-rotation relationships is set out in Chapter 3.

Chapter 4 discusses the factors that influence the investigation and defines the scope of the study. The chapter also addresses the methodology of the investigation.

The basis of the structural design for the linear static analyses using South African standards is explained in Chapter 5. The chapter also deals with the design characteristic strength of the material used.

Chapter 6 presents the numerical modelling method adopted. The chapter also deals with the mean material strengths assumed in the nonlinear models and the corresponding performance criteria. The difference between confined and unconfined concrete is discussed.

In Chapter 7, various procedures available to calculate the target displacement (displacement demand) from the output of the pushover analyses (or nonlinear static analyses) are presented and compared. The inclusion of SSI in the procedure is defined with reference to the results from the fixed base models.

Chapter 8 defines the approach used for nonlinear time-history analyses (THA). Ground motion records are chosen and matched to the appropriate design spectrum. The appropriate damping factors and soil stiffnesses are discussed.

The results of the nonlinear methods are presented and discussed in Chapter 9.

Chapter 10 concludes the outcome and explores further possible investigations.

2 Literature review

2.1 Dynamic response of buildings

The simplest form of a single degree of freedom (SDOF) oscillator subjected to ground motion is presented in Figure 2-1.

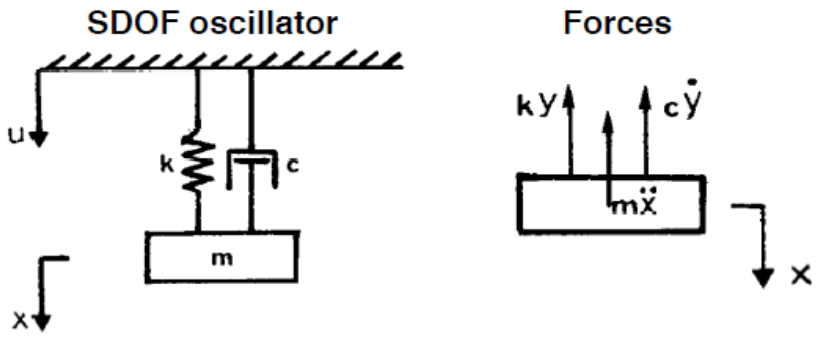

Figure 2-1: Single degree of freedom oscillator (Monteiro, 2019, L4 S. 11)

The equation of motion of a SDOF system subjected to an external force is expressed through Equation (2.1).

$$m\ddot{x} + c\dot{y} + ky = m\ddot{u} \qquad (2.1)$$

Where;

m	Oscillator mass
x	Mass absolute displacement
u	Ground absolute displacement
$y = x - u$	Relative displacement
k	Stiffness of the spring
c	Viscous constant of damping

Natural, angular frequency can be extracted as a characteristic of Equation (2.1):

$$\text{Angular frequency:} \quad \omega_n = \sqrt{\frac{k}{m}} \qquad (2.2)$$

It is useful to express damping relative to the frequency as:

$$\text{Damping coefficient:} \quad \xi = \frac{c}{2m\omega_n} \tag{2.3}$$

Substituting Equation (2.2) and (2.3) into Equation (2.1) and rearranging Equation (2.1) yield Equation (2.4).

$$\ddot{x} + 2\xi\omega_n\dot{y} + {\omega_n}^2 y = -\ddot{u} \tag{2.4}$$

The same approach can be followed for a SDOF oscillator under seismic action as in shown in Figure 2-2.

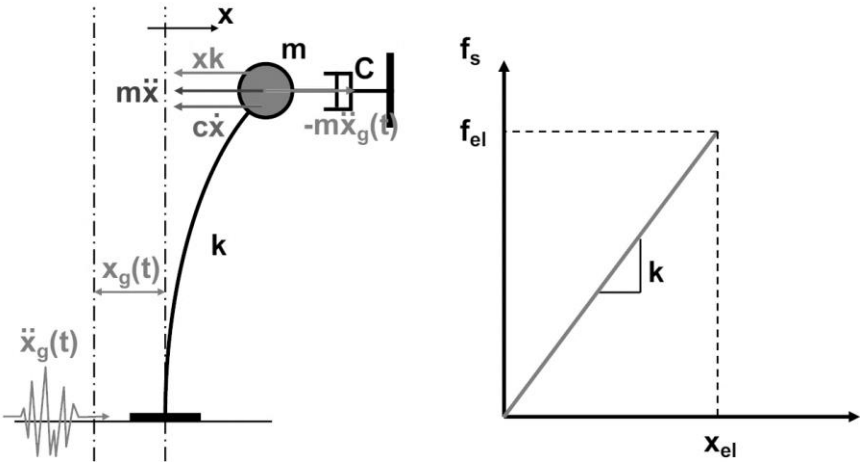

Figure 2-2: SDOF inverted pendulum under seismic action (Monteiro, 2019, p. 4-1)

The motion of a linear SDOF system subjected to seismic action is typically expressed as:

$$\ddot{x} + 2\xi\omega_n\dot{x} + \omega^2 x = -\ddot{x}_g \tag{2.5}$$

A parameter frequently used in seismic engineering is the natural period of vibration. This can be related to the angular frequency as defined in Equations (2.6) and (2.7).

$$\text{Natural frequency:} \quad f_n = \frac{\omega_n}{2\pi} \tag{2.6}$$

$$\text{Period:} \quad T = \frac{1}{f_n} = \frac{2\pi}{\omega_n} = 2\pi\sqrt{\frac{m}{k}} \tag{2.7}$$

2.2 Response spectra

Response spectra represent information regarding the peak response of a series of SDOF oscillators with different periods of vibration to a specific ground motion. The absolute acceleration and relative displacement are the quantities most useful for design purposes. Of the responses, the most commonly used by engineers is the elastic response with a specific elastic damping ratio plotted against the elastic period (Priestley, et al., 2007, p. 43).

Consider the 5 oscillators shown in Figure 2-3, each with a specific period of vibration and the same damping ratio. If these oscillators were to be subjected to a specific seismic action, it would be possible to plot the peak response of each oscillator, therefore creating a response spectrum.

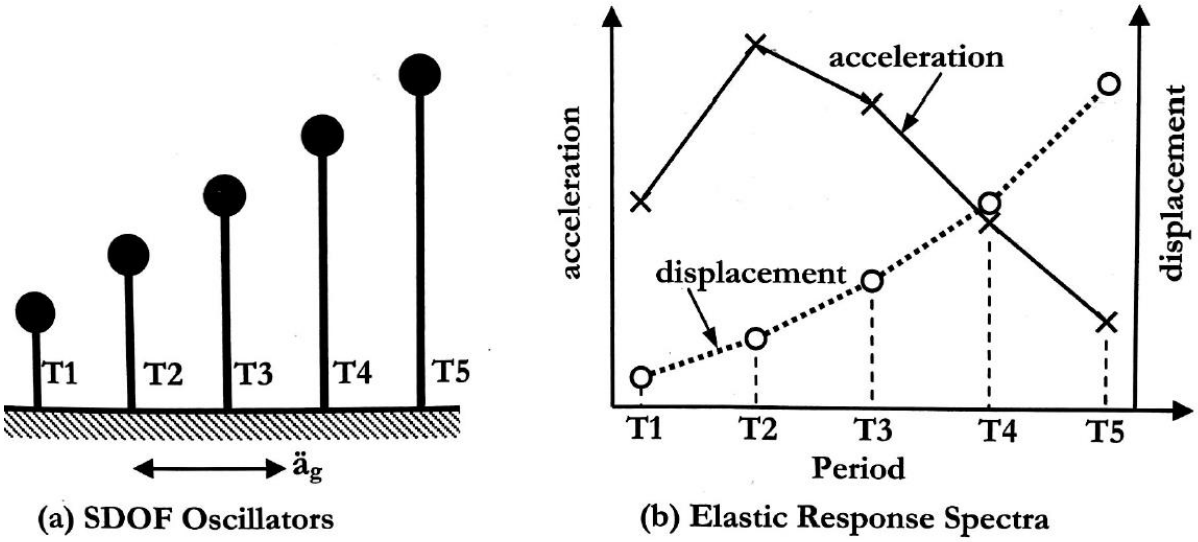

Figure 2-3: Formation of a response spectrum (Pauley & Priestley, 1992, p. 43)

Figure 2-4 illustrates the differences in spectra of varying damping ratios for a single seismic event. However, the response of a structure under seismic action is normally expected to be nonlinear. Procedures have been developed to determine the design spectrum for an inelastic system from the elastic spectrum (Chopra, 2012, pp. 257-305). The effects of inelastic behaviour on the response of a structure are considered in more detail in Section 2.5.

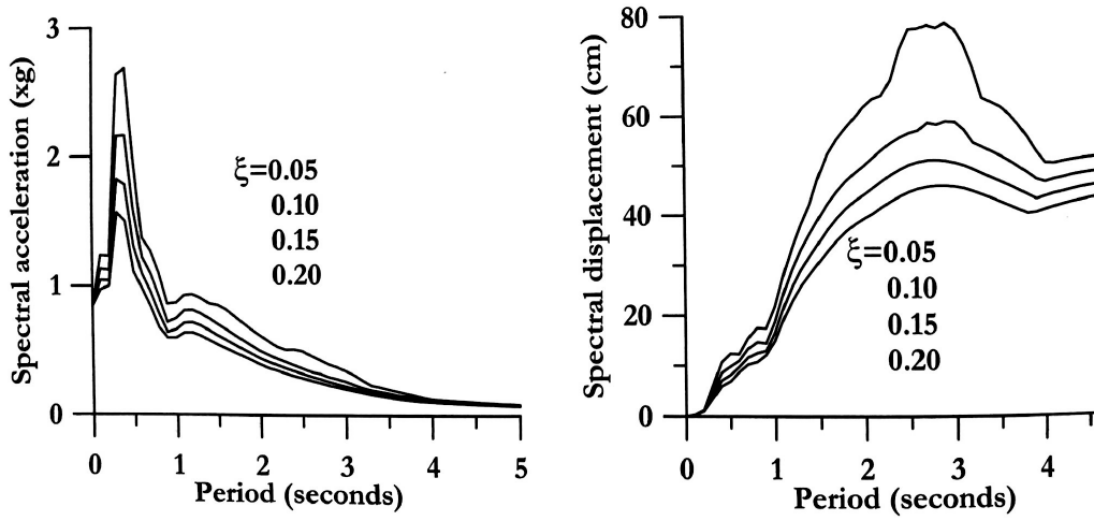

Figure 2-4: Normalised pseudo-acceleration and pseudo-displacement response spectrum for Northridge ground motion: ξ = 0,2,5,10, and 20% (Priestley, et al., 2007, p. 44)

2.3 Design spectra

Although response spectra provide engineers with valuable information regarding the behaviour of a structure, the practical application for design becomes more complex. A response spectrum provides specific information of all SDOF systems under a particular ground motion. Even if the ground motion were the same for every seismic event, predicting the response would still be difficult given the jagged shape and complexities in determining the modal shape and exact period when the response is likely to be nonlinear. A design spectrum, however, is derived from statistical analyses of several chosen ground motion records (Fardis, et al., 2005, p. 20). An envelope of the expected maximum of these responses can be represented as a smooth design spectrum.

As a practical example Chopra, (2012, p. 241) considers the scenario of a site in California that could be affected by ground motions from two different faults and therefore two different types of earthquakes. The characteristics of the two types will be different, as well as the effect on the specific site. The two design spectra would differ, as shown in Figure 2-5. The design spectra should be defined as the envelope of the two types of design spectra.

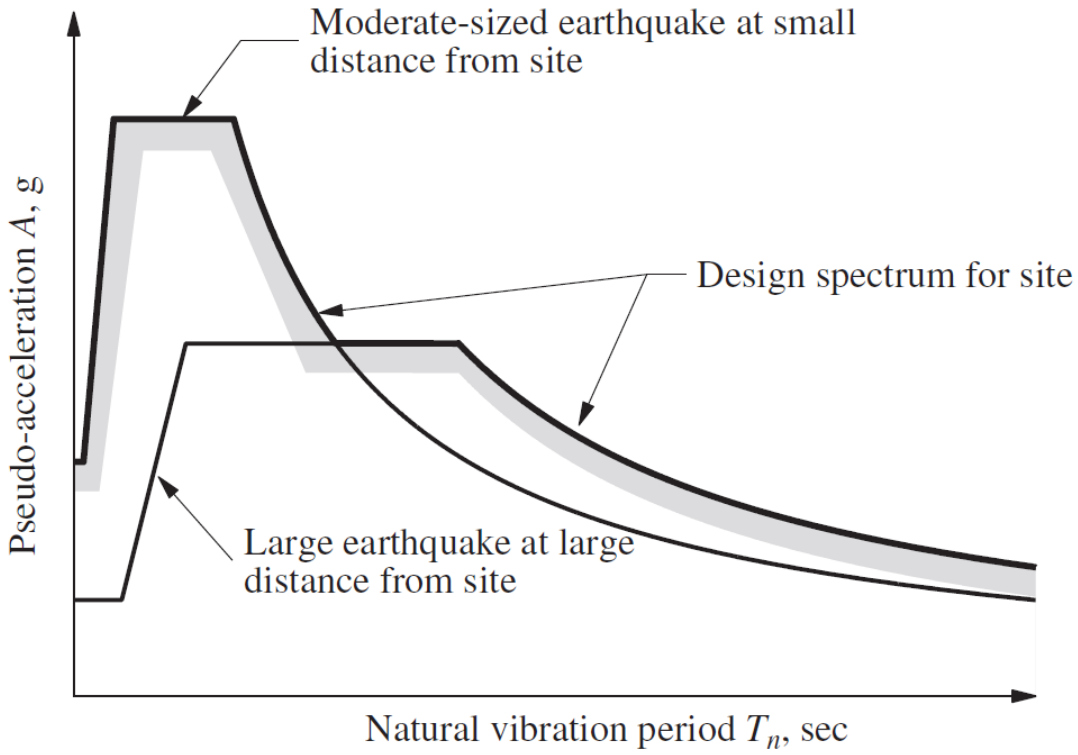

Figure 2-5: Two types of design spectra for a specific site (Chopra, 2012, p. 241).

The horizontal components of the ground motions are mainly caused by shear S-waves. Different types of soil will affect the propagation of these S-waves through the ground.

Design codes have developed design spectra for several types of soil, with the ground type classification mainly being related to the average value of propagation of S-waves in the upper 30m of the soil profile at shear strains of 10^{-5}, or less, $v_{s,30}$ (typically called the shear wave velocity).

South African National Standards (SANS 10160-4, 2017) specify the same spectra as Eurocode 8 (EN 1998-1, 2004). Figure 2-6 shows the typical horizontal elastic design response spectra for 5% damping, normalised by ground acceleration, a_g.

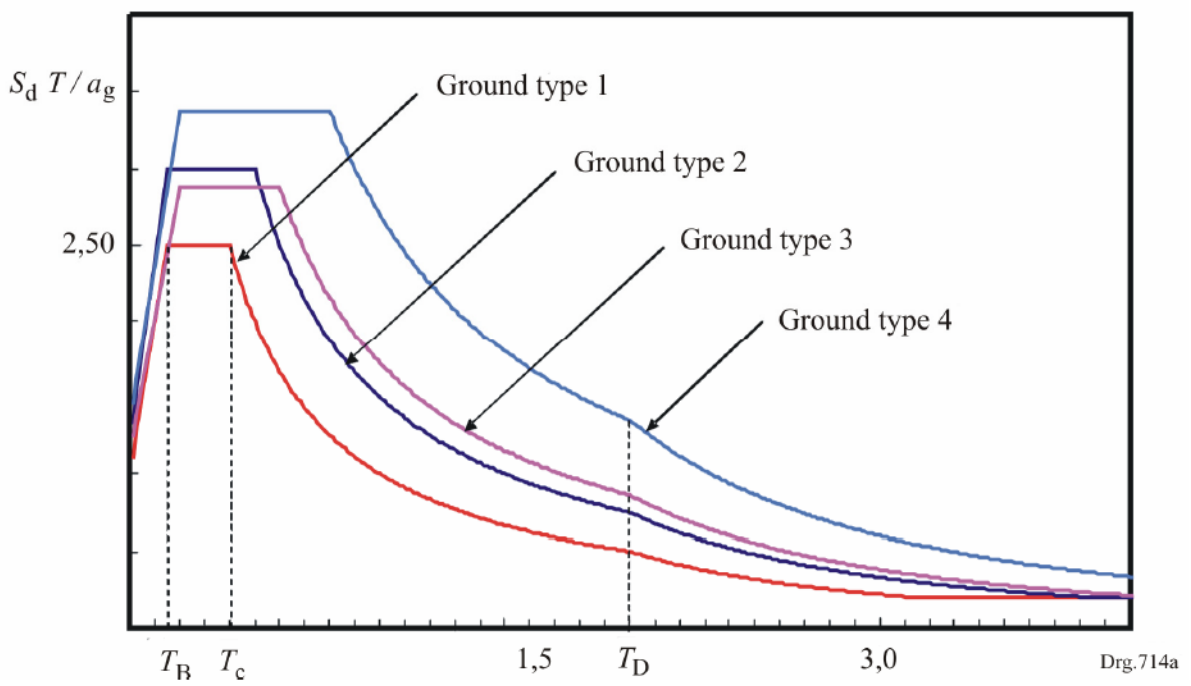

Figure 2-6: Elastic response spectra for different soil conditions. (SANS 10160-4, 2017),Type 1 (EN 1998-1, 2004)

With the three corner periods T_B, T_C and T_D representing changes in the shape of the idealised spectra:

Constant acceleration:	$T_B < T < T_C$
Constant velocity:	$T_C < T < T_D$
Constant displacement:	$T_D < T$

Considering Figure 2-6, an infinitely stiff structure, with a period of vibration T = 0 seconds, will experience the same acceleration as the peak ground acceleration (PGA), while a very slender structure, with a period of vibration approaching T = 4 seconds, will experience only mild absolute accelerations due to the ground motion. Figure 2-7 illustrates this principle.

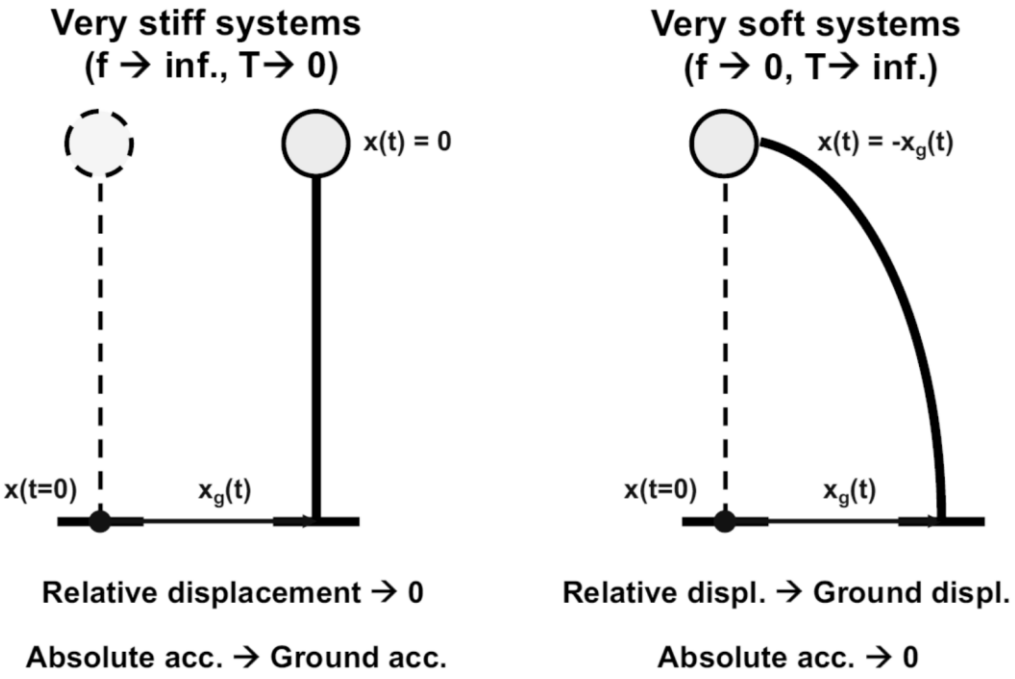

Figure 2-7: Structural responses with extreme period ranges (Monteiro, 2019, L4 S25).

Along with acceleration spectra, displacement spectra are a useful tool for engineers to predict the expected displacement of a structural system under seismic action (displacement demand), and therefore predicting the expected damage.

Codes typically derive displacement spectra in a simplified manner using Equation (2.8).

$$S_{De}(T) = g \times S_{Ae}(T)\left(\frac{T}{2\pi}\right)^2 \qquad (2.8)$$

Where $S_{De}(T)$ is the displacement spectrum, g is gravity acceleration and $S_{Ae}(T)$ is the elastic acceleration spectrum. Although the displacement spectra should ideally be developed separately, this relationship generally holds for periods less than 4 seconds. SANS 10160-4 (2017) does not explicitly provide information about displacement spectra, while Eurocode 8 provides such a definition in EN 1998-1 (2004), *Annex A*. The typical displacement response spectrum shape of Eurocode 8 is shown in Figure 2-8.

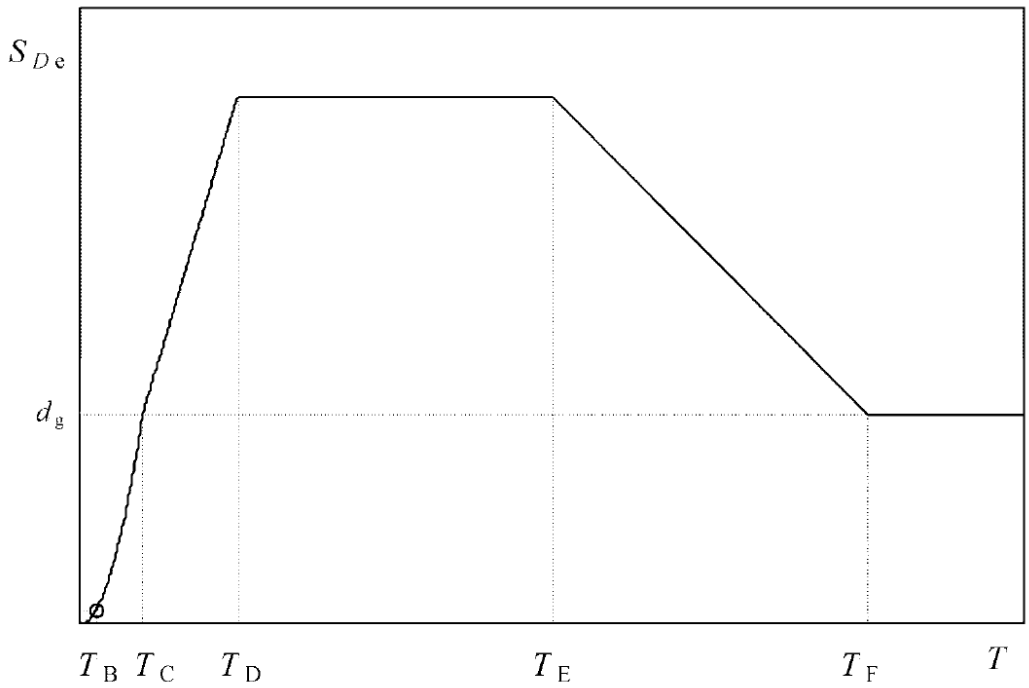

Figure 2-8: Eurocode 8, general form of displacement response spectrum

This shape agrees reasonably well with displacement spectra generated independently from accelerograms. The nonlinear shape between T_B and T_C will only be relevant for short elastic periods. The shape is essentially linear from T_C to T_D and then plateaus till T_E. From T_E the displacement decreases linearly to the peak-ground displacement. Table 2-1 indicates period ranges prescribed by EN 1998-1. This study will focus on periods ranges between T_C and T_E, which is typical for periods of low- to medium-rise structural wall buildings considering cracked sections.

Elastic design spectra are defined for a certain value of damping. Design codes typically specify 5% damping for building structures. In fact, structural systems will have unique damping values. Eurocode 8 utilizes a correction factor, η to allow engineers to adjust the elastic design spectra for values of damping other than 5%. EN 1998-1 (2004) equation 3.6 is presented in Equation (2.9).

$$\eta = \sqrt{\frac{10}{(5+\xi)}} \geq 0.55 \qquad (2.9)$$

The correction factor, η is used in EC 1998-1 (2004) to adjust the elastic response spectra through Equations (2.10) to (2.13).

$$0 \leq T \leq T_B \quad S_{Ae} = a_g \times S \left[1 + \frac{T}{T_B}(\eta \times 2.5 - 1)\right] \qquad (2.10)$$

$$T_B \leq T \leq T_C \quad S_{Ae} = a_g \times S \times \eta \times 2.5 \qquad (2.11)$$

$$T_C \leq T \leq T_D \quad S_{Ae} = a_g \times S \times \eta \times 2.5 \left[\frac{T_C}{T}\right] \qquad (2.12)$$

$$T_D \leq T \quad S_{Ae} = a_g \times S \times \eta \times 2.5 \left[\frac{T_C \times T_D}{T^2}\right] \qquad (2.13)$$

Where a_g is the ground acceleration normalised to gravity acceleration (*g*). The various period ranges and soil factors, S are defined in Table 2-1.

Table 2-1: Period range and soil factors for Type 1 earthquakes, adapted from EC 1998-1 (2004)

Ground Type	S	T_B	T_C	T_D	T_E	T_F
A	1	0.15	0.4	2	4.5	10.0
B	1.2	0.15	0.5	2	5.0	10.0
C	1.15	0.2	0.6	2	6.0	10.0
D	1.35	0.2	0.8	2	6.0	10.0
E	1.4	0.15	0.5	2	6.0	10.0

The minimum value of the damping correction factor, η = 0.55, corresponds to a maximum value of equivalent viscous damping of approximately 28%.

The effects of damping on acceleration and displacement response spectra is graphically illustrated in Figure 2-9.

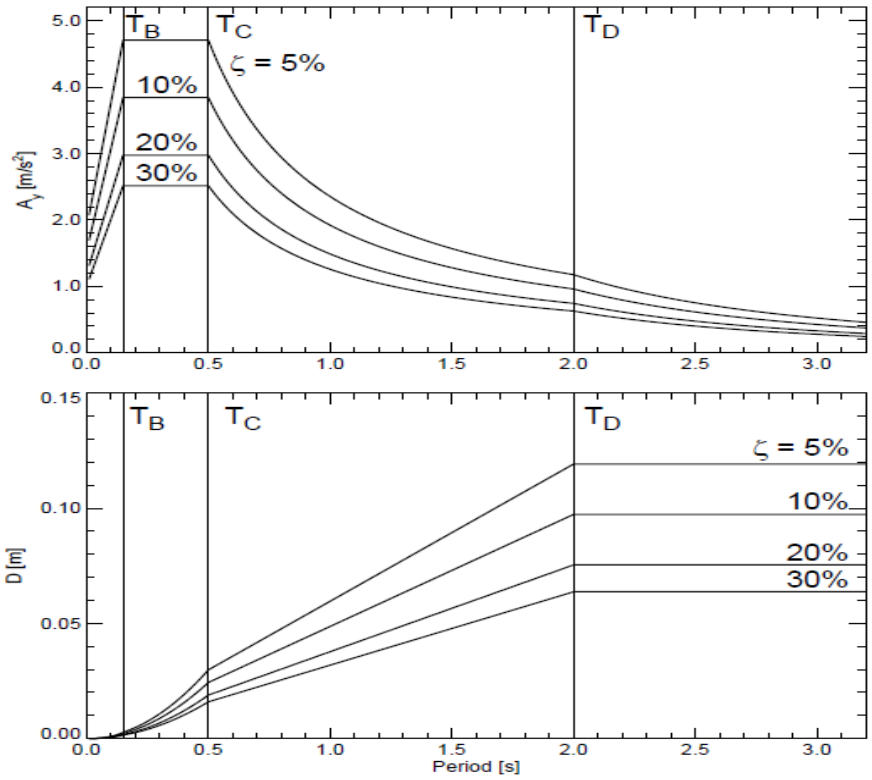

Figure 2-9: Damping effects on elastic response spectra (Bommer & Elnashai, 1999)

2.4 Period determination

Consider the basic equation to determine the period of vibration, presented in Equation (2.7), where the period (T) is a function of mass (m) and stiffness (k), repeated again for easy of reference.

$$T = 2\pi\sqrt{\frac{m}{k}}$$

For a reinforced concrete structure that is expected to behave nonlinearly, the stiffness (k) will change throughout the duration of the seismic event, as the concrete cracks and spalls and as the reinforcement yields. Determining the correct period for a reinforced concrete building under such conditions becomes complex.

Design codes typically provide height dependent empirical expressions that are considered conservative, as calculating equivalent base shear from a response acceleration spectrum with an underestimated period length will produce a larger value (not considering the period range between 0 and T_B). Calculating the displacement response using underestimated periods, however, will be unconservative.

SANS 10160-4 (2017) provides the same empirical formulae as Eurocode 8 (EN 1998-1, 2004) to calculate the fundamental period of vibration for the equivalent static lateral force method. SANS 10160-4 (2017) allows for alternative methods to be used "*in a properly substantiated analysis*", but limits the fundamental period to 1.4 times the period calculated using the empirical formulae.

Eurocode 8 encourages the use of the fundamental period based on mechanics, regardless of how its value compares with values calculated by prescribed empirical formulae (Fardis, et al., 2005).

As the structural wall cracks and deforms nonlinearly, it softens, which will then affect the fundamental period. Design codes typically account for this by allowing the use of an effective stiffness as a percentage of the elastic gross cross section stiffness, when calculating the fundamental period. More refined estimates will include a ratio of axial load to cross sectional property (Monteiro, 2019, p. 3-22).

Ideally, the stiffness of a reinforced concrete wall should be determined using moment-curvature analysis. The fundamental period can subsequently be calculated accurately using modal analysis (eigenvalue analysis). For force-based design, this should be an iterative procedure, as strength is related to the stiffness. A brief summary of the iteration is provided here:

1. Estimate the member stiffness using empirical formulae.
2. Calculate the fundamental period using eigenvalue analysis.
3. Calculate the equivalent base shear and moment using design spectra.
4. Design members and determine reinforcement required using characteristic material strength.
5. Perform a moment-curvature analysis to determine the stiffness of the members, as the reinforcement will affect the stiffness.
6. Calculate the fundamental period using new stiffness.
7. Repeat step 2 to 6 until the initial period and end period converges.

Considering SSI in the design will lengthen the fundamental period, but initial estimation of the effective stiffness becomes more complicated. As the foundation size decreases the *hinge mechanism* moves from the shear wall to the foundation-soil interface. The nonlinear behaviour of the wall element will then be affected by the

foundation, making the initial estimation for stiffness and period more difficult, than say, assuming a cracked stiffness as a percentage of the uncracked stiffness.

2.5 Ductility and force reduction

With an increase in the understanding of seismic response came the awareness that structures can resist seismic action at much higher levels than predicted using elastic inertial forces. This led to the development of the concept of ductility and force-reduction. (Priestley, et al., 2007, p. 4).

With this concept, certain structural elements with sufficient ductility can behave inelastically to protect the rest of the structure. Consider the simplified elastic and elastoplastic force-displacement relationship, as presented in Figure 2-10.

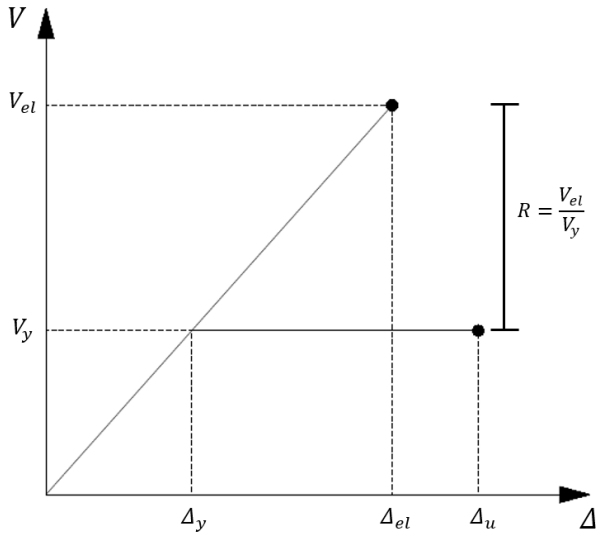

Figure 2-10: Force-displacement of an idealised inelastic system and an equivalent elastic system

From Figure 2-10 the displacement ductility is defined in Equation (2.14) as:

$$\mu_\Delta = \frac{\Delta_u}{\Delta_y} \qquad (2.14)$$

Where Δ_u and Δ_y is the ultimate displacement and yield displacement, respectively.

The force-reduction factor is presented in Equation (2.15) as:

$$R = \frac{V_{el}}{V_y} \qquad (2.15)$$

Where V_{el} is the force of an equivalent elastic system while V_y is the force for the elastoplastic system.

Several researchers have proposed a relationship between the force-reduction factor (*R*), ductility (μ) and period (*T*), called the "*R-μ-T relationship*". Commonly used approximations are *equal energy* and *equal displacement* principles. Figure 2-11 illustrates these approximations with a simplified elastoplastic system.

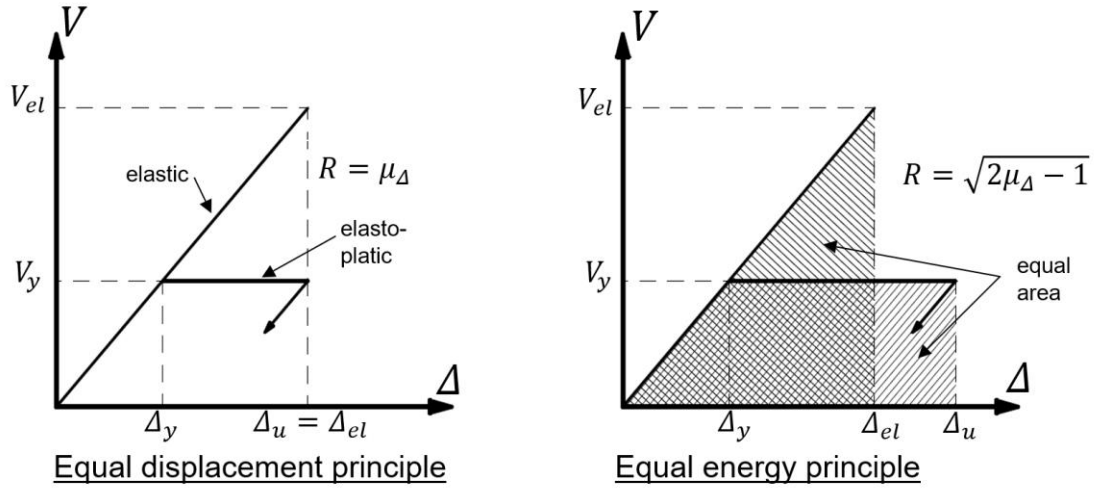

Figure 2-11: Equal displacement and equal energy principle (adapted from Monteiro (2019, p. 4-65))

The equal energy and equal displacement approximations can be expressed mathematically as presented in Equation (2.16).

$$R = \begin{cases} 1 & T < T_B \\ \sqrt{2\mu - 1} & T_B < T < T_C, \\ \mu & T_C, < T \end{cases} \qquad (2.16)$$

The corner period $T_{C'}$ is typically taken as T_C, as prescribed in design codes.

An illustration of the comparison between the force-reduction factor of a selected value of ductility and ductility from the medium of 20 ground motion records from the El Centro earthquake is shown in Figure 2-12 (Chopra, 2012, p. 289).

Chopra (2012, pp. 289-290) observes that for short period range the reduction factor tends to 1, for the long period range the reduction factor tends to the displacement ductility (μ), while for medium period range the relationship is rather irregular. Furthermore, these relationships are also dependent on the hysteretic characteristics of the structural system.

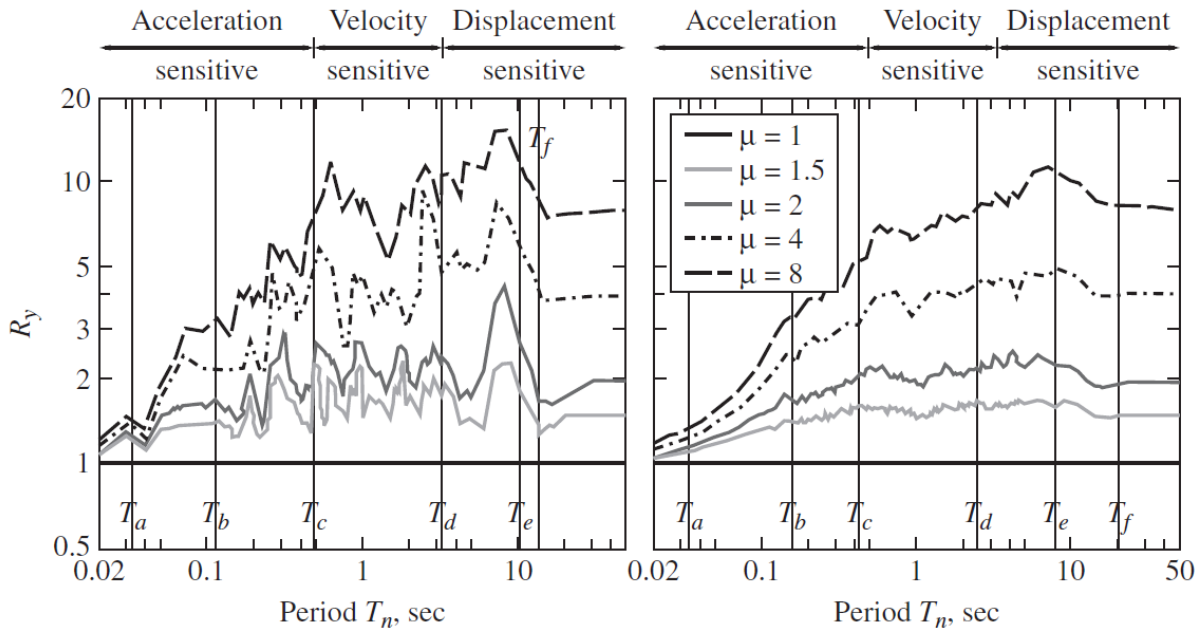

Figure 2-12: Comparison between force-reduction factor and ductility using 20 ground motions from the El Centro earthquake (Chopra, 2012, p. 289).

Research to define these relationships more accurately is ongoing. Design codes generally still adopt equal displacement and equal energy approximations as a basis for force reduction.

Eurocode 8 and SANS 10160-4 (2017) include this force reduction by means of a behaviour factor, q and is a combined effect of the force-reduction factor and an overstrength factor, Ω as presented in Equation (2.17).

$$q = R \times \Omega \qquad (2.17)$$

The overstrength can be seen as the structural strength redundancy inherent in code based structural design. The structural overstrength result from a number of factors, of which the main factors for the purposes of this investigation are:

- Material factors used in the design.
- Confinement effect of reinforced concrete members.
- Minimum reinforcement requirements.
- Elements that can add to resistance not considered in the design.

EN 1998-1 (2004), 3.2.2.5; describes the behaviour factor as "*an approximation of the ratio of the seismic forces that the structure would experience if its response was completely elastic with 5% viscous damping, to the seismic forces that may be used in the design, with a conventional elastic analysis model, still ensuring a satisfactory response of the structure*".

SANS 10160-4 (2017) prescribes a behaviour factor (q) for structural wall systems as 5, when strict rules for confinement reinforcement of the critical regions are adhered to. The detailing rules are taken from the ACI code, and the definition of the height of the plastic region is taken from the Swiss Code: SIA 262:2003 (Retief & Dunaiski, 2009, p. 181). Table 2-2 is an extract from the behaviour factors prescribed by SANS 10160 (2017).

Table 2-2: SANS 10160-4 (2017) prescribed behaviour factor for reinforced concrete walls (adapted from SANS 10160-4 Table 4)

Building Frame System	With reinforced concrete shear walls (detailed in accordance with SANS 10100-1 and Annex C)	**5**
	With reinforced concrete shear walls not detailed in accordance with and Annex A	2
	Ordinary braced steel frames	3

EN 1998-1 (2004) is more cautious but allows for explicit calculations to determine the ratio, α_u/α_1, where α_1 is the displacement at first yield and α_u is the displacement at which the global plastic mechanism is formed. This is typically determined using a nonlinear static (pushover) analysis. Table 2-3 presents the values prescribed by EN 1998 (2004) Table 5.1 for structural walls of ductility classes DCM and DCH.

Table 2-3: EN 1998-1 prescribed behaviour factor for reinforced concrete walls.

Structural Type	DCM	DCH
Frame system, dual system, coupled wall system	$3\ \alpha_u/\alpha_1$	$4.5\ \alpha_u/\alpha_1$
Uncoupled wall system	3	$4\ \alpha_u/\alpha_1$
Torsionally flexible system	2	3
Inverted pendulum system	1.5	2

The behaviour factor used by SANS 10160-4 and EN 1998-1 in the design acceleration spectrum expressions to reduce the elastic acceleration spectrum is presented in the Equations (2.18) to (2.21).

$$0 \leq T \leq T_B \quad S_{Ad} = a_g \times S\left[\frac{2}{3} + \frac{T}{T_B}\left(\frac{2.5}{q} - \frac{2}{3}\right)\right] \qquad (2.18)$$

$$T_B \leq T \leq T_C \quad S_{Ad} = a_g \times S\frac{2.5}{q} \qquad (2.19)$$

$$T_C \leq T \leq T_D \quad S_{Ad} = a_g \times S\frac{2.5}{q}\left[\frac{T_C}{T}\right] \; but \; \geq \beta \times a_g \qquad (2.20)$$

$$T_D \leq T \quad S_{Ad} = a_g \times S\frac{2.5}{q}\left[\frac{T_C \times T_D}{T^2}\right] \; but \geq \beta \times a_g \qquad (2.21)$$

The elastic spectrum (q = 1), with 5% damping and ground acceleration (a_g) of 0.1g, is compared to the design spectrum of q = 5 for ground type 3 as prescribed by SANS 10160-4 (2017) in Figure 2-13.

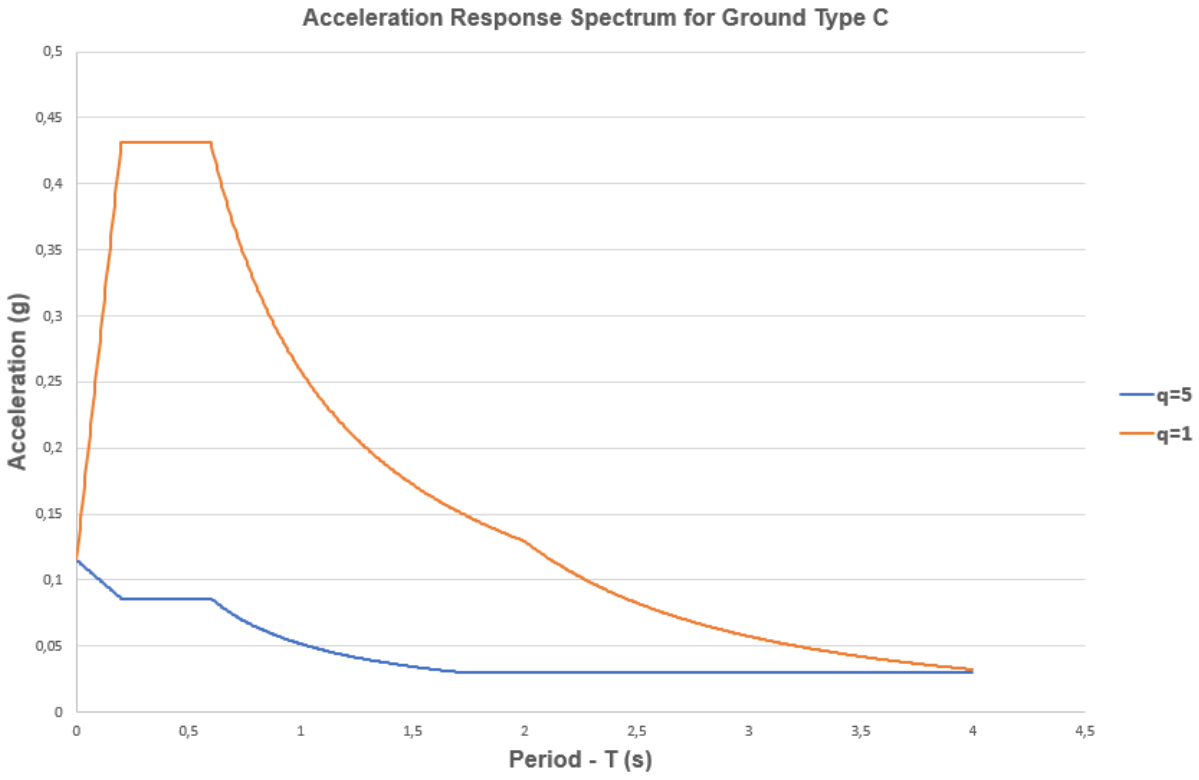

Figure 2-13: Comparison of design spectrum with q=1 and q=5 (ξ = 5%)

There is a significant reduction in equivalent forces when the behaviour factor of q = 5 is used.

Generally, when codes assume the equal displacement approximation, the behaviour factor does not affect the 5% damped displacement design spectra. Ductility does, however, influence damping. A design displacement spectrum can therefore be adjusted to accommodate an overdamped system similar to the adjustments used for an overdamped acceleration spectrum. This will be discussed in Chapter 7.

Le Roux (2010) assessed the behaviour factor for reinforced structural walls as prescribed by SANS 10160-4 using both the empirical formulae and moment-curvature analyses to determine the fundamental period. Le Roux tested several walls of different aspect ratios using direct displacement-based methods to determine their ductility capacity. The displacement capacity was limited to the drift limits. Ductility demand was tested using THA, with the conclusion that the behaviour factor was adequate for periods calculated from empirical formulae and periods obtained from moment-curvature analyses.

Le Roux (2010) considered fixed base structural walls where SSI is not considered. This study will focus on the effects of SSI on the behaviour factor for reinforced structural walls.

2.6 Damping

Damping is the measure of the rate at which free vibration decays over time. Figure 2-14 shows the differences between an undamped and a damped free vibration of a SDOF system. The damping also slightly influences the natural period. The period lengthening effects are typically negligible for the damping range applicable for most civil engineering structures.

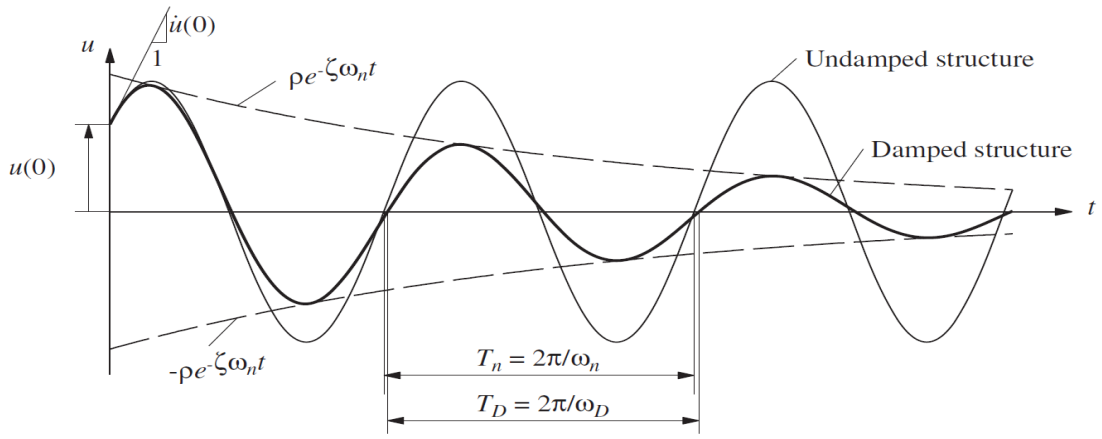

Figure 2-14: Effects of damping on free vibration (Chopra, 2012, p. 50)

If a system is *critically damped*, the damping ratio, ξ is equal to 1. This means that the damping ratio is 100% of a critically damped system and that the SDOF system will return to its original equilibrium position without oscillating. *Overdamped* systems have damping ratios larger than the critical damping ratios ($\xi > 1$), resulting in the SDOF system not oscillating, but returning to its original position at a slower rate than the critically damped system. Structural systems of interest have damping ratios much smaller than 1 and are termed *underdamped* systems. In underdamped systems the amplitude decreases with each cycle until the oscillator return to its original position, with the number of oscillations dependent on the damping ratio. (Chopra, 2012, pp. 49-50).

Figure 2-15 illustrates this principle.

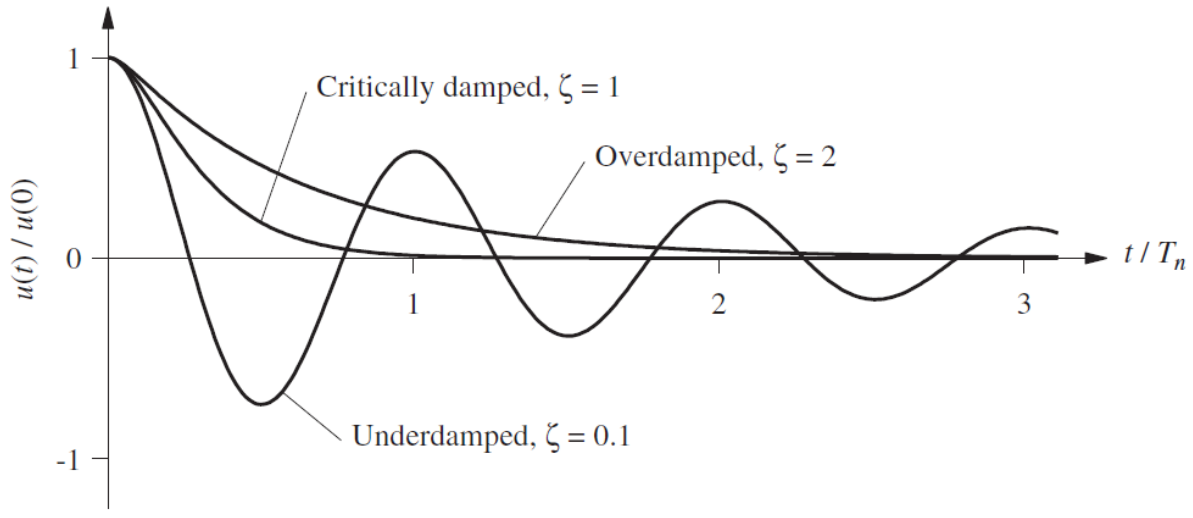

Figure 2-15: Free vibration of underdamped, overdamped and critically damped systems (Chopra, 2012, p. 59)

In structural engineering the term *equivalent viscous damping*, ξ_{eq} is typically used to represent damping. Equivalent viscous damping is the sum of the *hysteretic damping,* ξ_{hyst} and *elastic damping,* ξ_{el}:

$$\xi_{eq} = \xi_{el} + \xi_{hyst} \qquad (2.22)$$

Hysteretic damping is based on the energy absorbed by the hysteretic cyclic response of a nonlinear inelastic system. The energy absorbed is determined by integrating the force-displacement curve as shown in Figure 2-16.

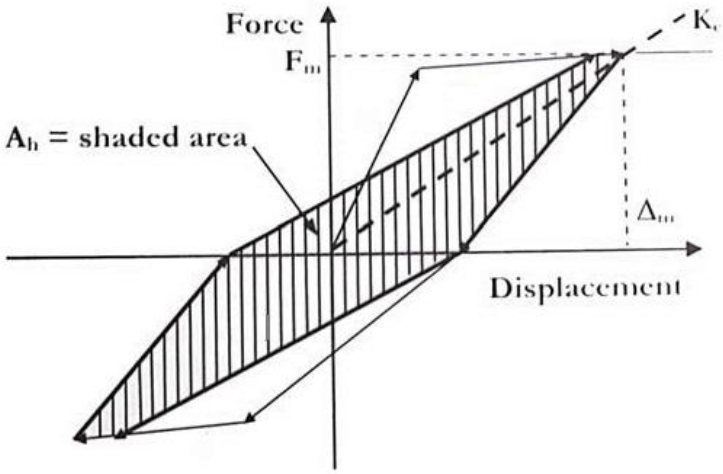

Figure 2-16: Hysteretic area for damping calculations (Priestley, et al., 2007, p. 77)

Elastic damping represents the damping not captured by the hysteretic model. Simplified hysteretic rules of a linear response in the elastic range will not model the absorption of energy correctly. Elastic damping is then calibrated to represent the hysteretic damping due to the nonlinearity in the elastic range.

Other typical factors that will contribute to elastic damping are:

- Structural damping due to foundation damping (see Chapter 2.7).
- Non-structural damping due to the hysteretic response of non-structural elements.
- Friction/sliding between structural and/or infill elements.

Various empirical expressions have been developed from parametric studies on various hysteretic rules (Monteiro, 2019, L4 S. 112). Priestley, et al. (2007, pp. 78-87) observe that the period dependent expressions proposed by Grant, et al., (2005) are

insignificant for periods longer than 1second. This simplification together with the expression from Dwairi & Kowalsky (2007) (presented in Equation (2.23)), are then used by Priestley, et al. (2007) to calibrate values for different structural systems of tangent stiffness proportionate damping and 5% elastic damping.

$$\xi_{hyst} = C \cdot \left(\frac{\mu - 1}{\mu\pi}\right) \qquad (2.23)$$

Where the coefficient C is depended on the hysteretic rule.

The expression for concrete wall buildings, typically represented by the Takeda Thin hysteretic rule, can be used to determine the displacement demand for the fixed base system and is expressed in Equation (2.24).

$$\xi_{hyst} = 0.05 + 0.444\left(\frac{\mu - 1}{\mu\pi}\right) \qquad (2.24)$$

As these are calibrated expressions, the values cannot be used for ranges of elastic damping other than 5%. As foundation damping will influence the elastic damping, the more detailed equations from Grant, et al., (2005) are applied when SSI is considered. The approach is discussed in Chapter 7.

2.7 Soil-structure interaction

2.7.1 Introduction

Soil-structure interaction (SSI) analysis is the evaluation of the combined response of the structure, the foundation and the soil under the foundation (NIST GCR 12-917-21, 2012, p. iii).

It has been recognised that soil-structure is an acceptable form of energy dissipation. The satisfactory performance of some structures subjected to seismic action could only be attributed to the soil-structure interaction. (Pauley & Priestley, 1992, p. 671).

Van der Merwe (2009) assessed the seismic response of a building by reducing the size of wall foundations and found that allowing the wall foundation to rock, could result in smaller foundations. The study was performed for regions experiencing moderate seismicity.

The South African standards do not explicitly set out specifications for soil-structure interaction. Eurocode 8 part 5 (EN 1998-5, 2004) lists the types of structures that require SSI analysis. These are structures where the interaction between the soil and the foundation could have a negative effect on the seismic response, therefore a “fixed base” analysis is likely to be unconservative.

These are unique structural systems, described by EN 1998-5: 6 as:

- Structures where the P-delta (second order) effects play a significant role.
- Structures with massive or deep-seated foundations, such as bridge piers and silos.
- Slender tall structures, such as towers and chimneys.
- Structures supported on very soft soil, with average shear wave velocity less than 100m/s.

Annex D of part 5 states: “*For the majority of common building structures, the effects of SSI tend to be beneficial, since they reduce the bending moment and shear forces in the various members of the superstructure*”. Eurocode 8 does not, however, provide more specific guidelines on the design and modelling aspects.

The Designers’ guide to Eurocode 8 (Fardis, et al., 2005, p. 250) states that a structure with a surface foundation can be sufficiently represented by an equivalent SDOF oscillator with adjusted period and damping, but does not provide specifics on methods to use. The Designers’ guide then refers to reports from Stewart, et al., (1999) as entries into to *Journal of the Geotechnical and Geo-environmental Engineering Division of the ASCE* for application of SSI.

ASCE reports, together with other US codes and technical guidelines, provide a more detailed procedure for evaluating and assessing structural systems with SSI. In this study, these guidelines are followed in a rational manner, while keeping within the framework of the South African national design codes and Eurocode 8.

Considering this interaction in the analysis can improve the seismic response of a structure by period lengthening, kinematic effects, as well as foundation damping effects caused by soil hysteric damping and radiation damping. These effects are discussed in the following subsections.

2.7.2 Period lengthening

Consider the SDOF oscillator shown in Figure 2-17.

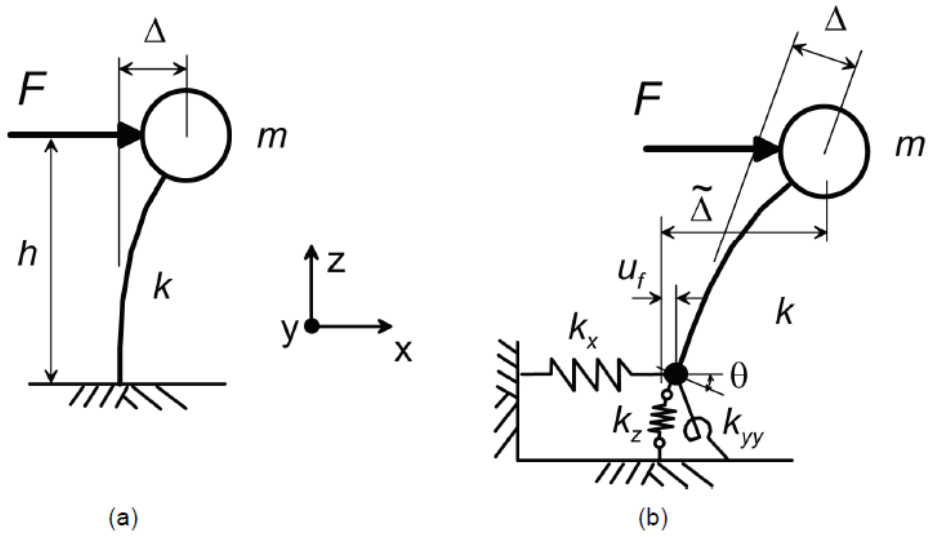

Figure 2-17:Schematic illustration of deflection caused by force applied to: (a) fixed-base structure; and (b) structure with vertical, horizontal, and rotational flexibility at its base (NIST GCR 12-917-21, 2012, p. 2-2).

A *fixed base* oscillator refers to the standard SDOF oscillator fully restrained to a base with infinite stiffness (no springs) while a *flexible base* oscillator refers to a SDOF oscillator connected to a flexible base (with springs).

The deflection, Δ under static force, F of the fixed base is presented in Equation (2.25).

$$\Delta = \frac{F}{k} \qquad (2.25)$$

Substituting Equation (2.25) with the period of vibration from Equation (2.7) the square of the period is expressed as in Equation (2.26).

$$T^2 = (2\pi)^2 \frac{m}{(F/\Delta)} = (2\pi)^2 \frac{m\Delta}{F} \qquad (2.26)$$

With reference to Figure 2-17, the deflection of the flexible base oscillator can be expressed by Equation (2.27).

$$\tilde{\Delta} = \frac{F}{k} + u_f + \theta \cdot h = \frac{F}{k} + \frac{F}{k_x} + \left(\frac{F \cdot h}{k_{yy}}\right) h \qquad (2.27)$$

Where u_f is the horizontal translation of the oscillator at its base and θ is the base rotation. The translational stiffness is defined as k_x, while the rotational stiffness is k_{yy}. The expression for the square of the period for the flexible base can then be expressed in Equation (2.28).

$$\tilde{T}^2 = (2\pi)^2 \frac{m\tilde{\Delta}}{F} = (2\pi)^2 m \left(\frac{1}{k} + \frac{1}{k_x} + \frac{h^2}{k_{yy}}\right) \qquad (2.28)$$

With Equations (2.26) and (2.28), the period ratio can be expressed through Equation (2.28).

$$\left(\frac{\tilde{T}}{T}\right)^2 = \frac{k}{m} \times m \times \left(\frac{1}{k} + \frac{1}{k_x} + \frac{h^2}{k_{yy}}\right) \qquad (2.29)$$

From Equation (2.29), the simplified classical period lengthening expression of Veletsos & Meek, (1974) is presented in Equation (2.30):

$$\frac{\tilde{T}}{T} = \sqrt{1 + \frac{k}{k_x} + \frac{kh^2}{k_{yy}}} \qquad (2.30)$$

Although earlier versions of ASCE 7 present the equation for period lengthening in a similar form, the latest ASCE/SEI 7-16 refers to the ratio, $\frac{\tilde{T}}{T}$, but does not provide an expression for this ratio. ASCE/SEI 41-17 specifies that the period extension should be determined using a mathematical model and stipulates that approximate periods shall not be used.

As mentioned in Section 2.4, the empirical formulae in design codes typically underestimate the period length to intentionally produce conservative values of design base shear. US codes also limit the period lengthening ratio to remain conservative with regard to equivalent base shear forces. NIST GCR 12-917-21 (2012), however, recommends that the lengthened period should be taken as the best estimate of the actual value. In this study the period extension is determined using eigenvalue

analysis of the structural models which is explicitly modelled with SSI elements. The modelling of the SSI elements is addressed in Chapters 3 and 6.

For design spectra, as presented in Figure 2-13, it can be observed that, apart from periods shorter than 0.6 seconds (not relevant to multi-storey buildings), lengthening the period should produce a smaller peak-ground acceleration and therefore smaller equivalent base shear forces.

2.7.3 Kinematic effects

Large stiff foundations can cause the foundation motion to deviate from the free-field motions due to *base slab averaging* and *embedment effect*. Simplistically, *base slab averaging* is caused by incoherence in the response of different parts of a single foundation, this results in an averaging effect over the foundation. Typically, ground motion reduces with depth, which is referred to as the *embedment effect.* The reader is referred to NIST GCR 12-917-21 (2012, Chapter 3) for a more detailed description.

Kinematic interaction will cause a decrease in the response of the building under seismic action. These effects are usually accounted for in the design by response spectrum modification factors called RRS_{bsa} and RRS_{e}. Where RRS_{bsa} is the response reduction factor for base slab averaging and RRS_{e} is the response reduction factor for foundation embedment. ASCE/SEI 41-17 and ASCE/SEI 7-16 propose empirical formulae to account for these effects. The product of RRS_{e} and RRS_{bse} is used to reduce the response spectrum. These factors are unrelated to the force-reduction factor (or behaviour factor).

This study is more concerned with the effects that would influence the behaviour factor, such as ductility and damping. The *RRS* was therefore, conservatively, not taken into consideration in the calculation of structural responses, therefore *RRS* is taken as 1.

2.7.4 Foundation damping

Foundation damping can contribute to the total damping and is typically introduced through Equation (2.31).

$$\beta_{tot} = \beta_f + \frac{\beta_i}{\left(\frac{\tilde{T}}{T}\right)^n_{eff}} \quad (2.31)$$

Where β_f is the foundation damping and β_i is the initial viscous damping which is normally assumed as 5% for typical building structures.

The contributions to foundation damping are *soil hysteretic damping*, β_s, and *radiation damping*, β_{rd}.

The soil hysteretic behaviour is conceptually similar to any strain dependent material hysteretic behaviour.

Seismic waves reflecting from the base, back into the ground are called radiation waves and causes *radiation damping*.

Foundation damping is a complex phenomenon. Various researchers present analytical models for foundation damping. The reader is referred to Wolf (1985) for a detailed assessment of this type of damping. This study focusses on the codified guidelines for foundation damping based on these results.

ASCE/SEI 7-16 and ASCE/SEI 41-17 set out the same procedure which is discussed here.

Foundation damping is expressed in Equation (2.32).

$$\beta_f = \left[\frac{\left(\frac{\tilde{T}}{T}\right)^2 - 1}{\left(\frac{\tilde{T}}{T}\right)^2}\right]\beta_s + \beta_{rd} \quad (2.32)$$

The *soil hysteretic damping*, β_s, values obtained from Table 8-6 of ASCE/SEI 41-17 is presented in Table 2-4.

Table 2-4: Soil hysteretic damping as presented by ASCE/SEI 41-17 Table 8-6.

Site Class	Effective Peak Acceleration, $S_{DS}/2.5$[a]			
	$S_{DS}/2.5 = 0$	$S_{DS}/2.5 = 0.1$	$S_{DS}/2.5 = 0.4$	$S_{DS}/2.5 \geq 0.8$
C	0.01	0.01	0.03	0.05
D	0.01	0.02	0.07	0.15
E	0.01	0.05	0.20	[b]
F	[b]	[b]	[b]	[b]

[a] Use straight-line interpolation for intermediate values of $S_{DS}/2.5$.
[b] Site-specific geotechnical investigation and dynamic site response analyses are to be performed.

Where, S_{DS} is the peak spectral design response expressed in gravity acceleration, g as shown in Figure 2-18, adapted from ASCE/SEI 7-16.

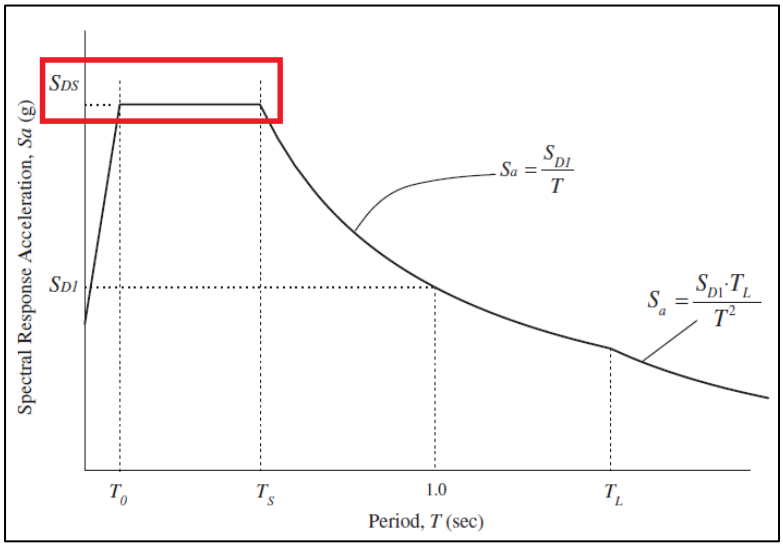

Figure 2-18: Spectral response acceleration (adapted from ASCE/SEI 7-16 Figure 11.4-1)

Radiation damping, β_{rd}, can be determined using Equation (2.33).

$$\beta_{rd} = \frac{1}{\left(\frac{\tilde{T}}{T_y}\right)^2}\beta_y + \frac{1}{\left(\frac{\tilde{T}}{T_{xx}}\right)^2}\beta_{xx} \qquad (2.33)$$

Where T_y and T_{xx} represent the translational and rotational periods, respectively.

$$T_y = 2\pi\sqrt{\frac{m^*}{k_y}} \qquad (2.34)$$

$$T_{xx} = 2\pi\sqrt{\frac{m^* h^*}{\alpha_{xx} k_{xx}}} \qquad (2.35)$$

Where m^* is the effective modal mass of the fundamental period of vibration in the direction considered, and h^* is the effective structural height. The rotational stiffness, k_{xx} and horizontal translational stiffness, k_y are for the motion perpendicular to applied seismic action. Similarly, β_y and β_{xx} are the damping ratios related to the translational and rotational motion; ASCE/SEI 41-17 and ASCE/SEI 7-16 provide empirical formulae to determine these damping values. The approach used for foundation damping in this study is presented in Chapter 7.

2.8 Methods of analysis

The four conventional methods of analysis are summarised in this section. These methods are commonly used in practice, the terminology of which may differ slightly between various design codes of practice. The methods can be grouped into linear (force-based) and nonlinear (displacement-based) methods. The linear methods use design spectra, typically the elastic spectra for 5% damping, reduced by the behaviour factor to account for the nonlinear behaviour of the structure under seismic action. The nonlinear methods do not require a behaviour factor as the nonlinear behaviour is explicitly modelled in the analysis.

The use of linear methods does not imply that the behaviour of the structure under seismic action is expected to be linear elastic. These approaches, together with the correct behaviour factor, are developed to fit into the typical force-based design framework commonly used in the structural engineering environment. (Fardis, et al., 2005, p. 44).

This study utilises all these methods in some form. A brief summary of the procedures is set out in the following subsections.

2.8.1 Linear static analysis procedure

Termed the *lateral force method* in EN 1998-1 or the *equivalent static later force procedure* in SANS 10160-4, whereby a static base shear force is obtained from design spectra using periods calculated from either empirical formulae or more advanced methods. The base shear is then translated to a set of inertial forces in order to represent the first mode shape of a multi degree of freedom (MDOF) system.

The base shear, V_n given in SANS 10160-4 is presented in Equation (2.36).

$$V_n = S_{Ad}(T, a_g, q) \times W_n \qquad (2.36)$$

S_{Ad} is the design acceleration spectra (normalised to gravity acceleration, g) as set out by Equations (2.18) to (2.21). W_n is the nominal sustained vertical load acting on the structure. Some design codes employ an adjustment factor to account for the mass participation of the mode of vibration. Generally, the mass participating in the first mode would not be the full mass.

The lateral force pattern given in Equation (2.37) is used to translate the base shear force to each storey. This should represent the mode shape of the first mode of vibration, given the simplification of the lateral force method that higher modes do not contribute to the response of the structure.

$$F_i = V_n \frac{\Phi_i m_i}{\sum_j \Phi_j m_j} \qquad (2.37)$$

Where F_i is the force per floor *i*. The mode shape, Φ can be seen as the drift pattern of the first mode. Considering the requirements for the lateral force method that there are no abrupt changes in stiffness between floors and that the structure is regular in plan and elevation, the mode shape can be simplified as a function of the height of the storey. The force pattern as given in SANS 10160-4 (2017) is presented in Equation (2.38).

$$F_i = V_n \frac{h_i W_i}{\sum_j h_j W_j} \qquad (2.38)$$

Where h_i is the height of the storey i. The mass (m) is substituted with weight (W), this would not make a difference to the pattern.

2.8.2 Modal response spectrum method

The modal response spectrum method, also referred to as the *linear dynamic analysis method,* is conceptually similar to the linear static analysis where base shear is calculated from the response spectrum, but differs in that the higher modes of vibrations, and their contribution to the response of the structure, is included.

A modal analysis is used to determine the eigenmodes and eigenvalues of the MDOF system.

Equation (2.1) for an undamped free vibration MDOF system with mass matrix [M] and stiffness matrix [K] can be rewritten as Equation (2.39).

$$[\mathrm{M}]\{\ddot{x}\} + [\mathrm{K}]\{x\} = \{0\} \qquad (2.39)$$

The solution of the displacement vector $\{x\}$ and acceleration vector $\{\ddot{x}\}$ can be expressed through Equations (2.40) and (2.41).

$$\{x\} = \{\Phi\} \times Sin(\omega \cdot ti + \vartheta) \qquad (2.40)$$

$$\{\ddot{x}\} = -\omega^2\{\Phi\} \times Sin(\omega \cdot ti + \vartheta) \qquad (2.41)$$

Where, Φ is the displacement shape. Substituting Equations (2.40) and (2.41) into Equation (2.39) results in Equation (2.42).

$$(-\omega^2[\mathrm{M}] + [\mathrm{K}])\{\Phi\} \times Sin(\omega \cdot ti + \vartheta) = \{0\} \qquad (2.42)$$

The solution of interest is given by Equation (2.43).

$$(-\omega^2[\mathrm{M}] + [\mathrm{K}])\{\Phi\} = 0 \qquad (2.43)$$

Where:

$$|-\omega^2[\mathrm{M}] + [\mathrm{K}]| = 0 \qquad (2.44)$$

Rearranging Equation (2.43), Equation (2.45) is obtained.

$$([\mathrm{M}^{-1}][\mathrm{K}])\{\Phi\} = \omega^2\{\Phi\} \qquad (2.45)$$

Where ω^2 is the eigenvalue that defines the modal frequencies and $\{\Phi\}$ is the eigenvector that describes the modal shape.

It is possible to determine a modal participation factor, Γ and subsequent effective modal mass, m^* of each mode shape that represents the mass that will contribute to that mode shape. The base shear of each mode shape is calculated using the response spectrum for each effective modal mass and corresponding period. In simple terms this can be seen as converting a MDOF system into a series of SDOF each with an effective mass and fundamental period. Figure 2-19 sets out the process.

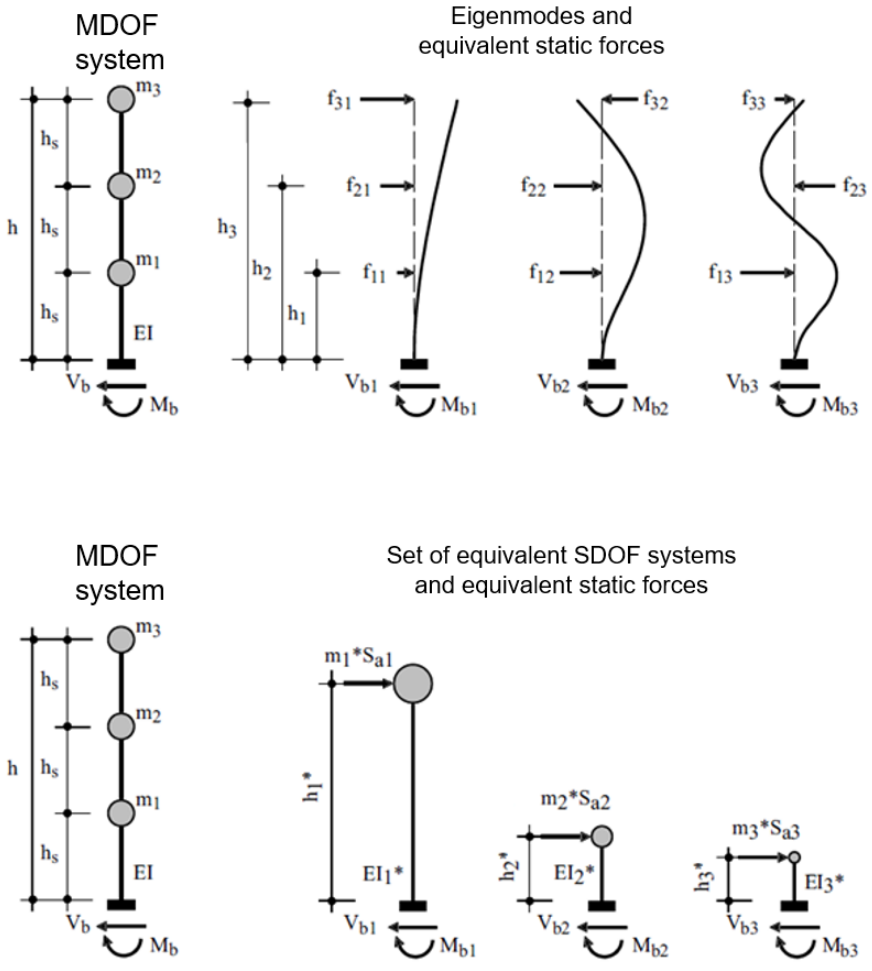

Figure 2-19: Representation of the modal response spectrum method (Monteiro, 2019, p. 5-23)

The modal responses are then combined to determine the total response, E_E. The two most common methods to combine the modal responses are the *square root of the sum of the squares* (SRSS rule) or the more accurate procedure called the *complete quadratic combination* (CQC rule).

Structural wall buildings with regular shapes typically do not have significant higher mode contributions. In this study, eigenvalue analysis is used to determine the first period of vibration and to assess the contribution of the higher modes, which was found to be low.

2.8.3 Nonlinear static analysis

Nonlinear static analysis is also referred to as the pushover analysis. The lateral forces (or displacements) that are applied on each level at the centre of mass is gradually increased to determine the nonlinear force displacement relationship of the structural system. The technique is useful in identifying the plastic hinge mechanisms and the evolution thereof, as well as expected damage at associated horizontal displacement.

The load pattern should represent the expected pattern of inertia forces. EC 1998-1 (2004) prescribes two load patterns:

- A ‘uniform pattern’, corresponding to a uniform unidirectional lateral acceleration.
- A ‘modal pattern’, which represents the mode shape of the first mode of vibration. If the building satisfies the requirements for the application of the lateral force method, a reverse triangular load pattern with load shape similar to Equation (2.37) can be applied.

A newer development for nonlinear analysis is referred to as ‘*adaptive pushover analysis*’ where an eigenvalue analysis is performed after each load step to determine the mode shape after each stiffness update. The load pattern is then adapted according to the new mode shape. (Pinho & Antoniou, 2005).

An initial investigation determined that the output of the adaptive pushover analysis does not vary significantly from the normal pushover analysis with reverse triangular load pattern in structural buildings used in this study. The adaptive pushover analysis is typically used for buildings with vertical irregularities where the higher modes contribute significantly to the response of the structure.

The base shear force-displacement curve as the output of the pushover analysis is termed the *capacity curve*. The capacity curve can be manipulated to convert the

MDOF structure to a SDOF structure with equivalent mass, m^* and fundamental period, T^*. This equivalent SDOF system can then be used, together with the displacement spectrum, to determine the target displacement (or displacement demand). The target displacement for the equivalent SDOF system is in turn converted back to the MDOF system, which will produce the target displacement at a control point of the structure.

The procedure is defined in *Annex B* of EN 1998-1 and is based on the N2 procedure (Fajfar, 2000). The process is briefly described here.

Firstly, the MDOF system is transformed into a SDOF system using a transformation factor, Γ, which is in principle the same as the participation factor mentioned in Section 2.8.2. EC 1998-1 provides Equations (2.46) to (2.49) for the transformation.

$$\Gamma = \frac{\sum m_i \Phi_i}{\sum m_i \Phi_i^2} \qquad (2.46)$$

$$F^* = \frac{\sum F}{\Gamma} \qquad (2.47)$$

$$d^* = \frac{\sum d}{\Gamma} \qquad (2.48)$$

$$m^* = \sum m_i \Phi_i \qquad (2.49)$$

Where the horizontal displacement per floor, Φ_i is normalised so that the displacement at the control node, Φ_n = 1. If the displacement shape represent the shape of the fundamental mode, then Γ will represent the participation factor of that mode, as described in Section 2.8.2. An elastic-perfectly plastic idealisation of the capacity curve

is determined in such a way that the areas under the idealised curve and the capacity curve up to the formation of the plastic mechanism are equal, as shown in Figure 2-20.

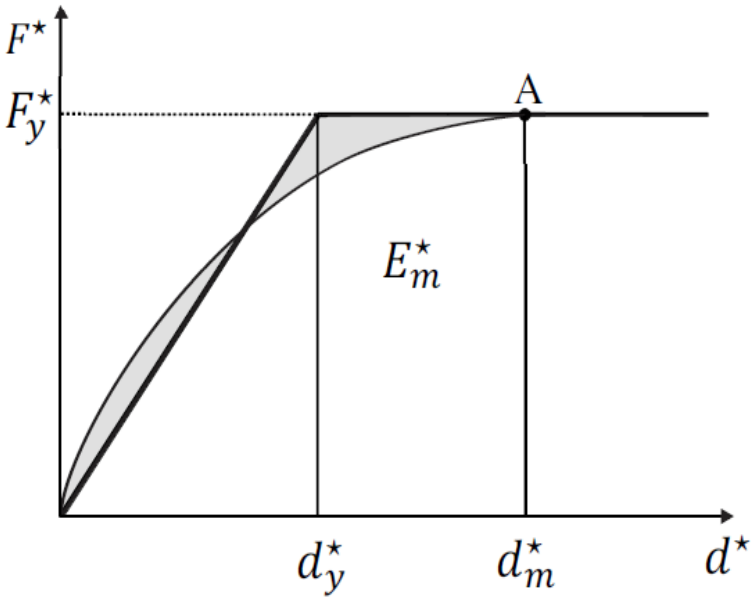

Figure 2-20: Elastic-perfectly plastic idealization of the capacity curve of an equivalent SDOF system (EN 1998-1, 2004, p. 216)

The period of the equivalent SDOF system can then be calculated using Equation (2.50).

$$T^* = 2\pi\sqrt{\frac{m^* d_y^*}{F_y^*}} \qquad (2.50)$$

The displacement of the SDOF under seismic action is determined using displacement spectra and the equivalent period. The displacement demand for MDOF system or *target displacement,* d_t is determined by multiplying the displacement demand of the SDOF by the transformation factor, Γ.

Important guidance documents for the nonlinear static procedure were developed in the US in response to a need to assess and retrofit existing buildings in a practical and cost-efficient procedure (Fardis, et al., 2005, p. 53). FEMA 440: *An improvement of Nonlinear Static Seismic Analysis Procedure* (2005) is one such document that lays out several methods to determine the target displacement when SSI is incorporated in the analysis.

To allow for SSI in this study, the guidelines of FEMA 440 and ASCE/SEI 41-17 are followed in applying nonlinear static procedure, within the framework of the procedure set out by *EC 1998-1 Annex B*. Chapter 7 discusses and compares these methods in more detail.

2.8.4 Nonlinear dynamic (time-history analysis)

Historically, time-history analyses (THA) were used and developed for research and special purposes. However, with the development of more numerically stable computer software and stronger processing power, the method has become more popular.

Unlike other methods where the seismic demand is determined by approximation, typically using response spectra, the demand is determined in the course of the analysis of the response. The method does, however, require some sophistication in the selection of ground motion, material behaviour and damping. (Fardis, et al., 2005, p. 58).

Most codes define two alternatives for the selection of records:

- Maximum response from three spectrum-compatible records.
- Mean response from seven spectrum-compatible records.

Typical methods used to obtain spectrum-compatible records are:

- Selecting the right natural records to provide the best fit to the design spectrum or amplitude scaling of records with similar characteristics.
- Mathematically sourced models to generate artificial records with special purpose software.
- Matching (not just scaling) records to fit the design record.

It is seen that the method still requires the use of response spectra, although indirectly, for practical design applications.

This study uses THA as a supplementary response verification. The models are subjected to 3 suitably matched ground acceleration records. Response reduction due to kinematic effects is not incorporated in the selection of the ground motion.

Chapter 8 addresses the incorporation of SSI, selection of ground motions, spectral matching, and damping.

2.9 Assessing the behaviour factor

The relationship between ductility and force reduction is introduced in Section 2.5 where it is concluded that the relationships are approximations, and that they hold on average, but are rather irregular in some cases (Figure 2-12). Even if it is assumed that the equal displacement relationship holds, there is still a lack of consensus as to the appropriate definition for yield and ultimate displacement when a bilinear approximation of the force-displacement relationship is produced. With reference to Figure 2-21, Priestley, et al. (2007, pp. 12-13) explain this problem. Point 1 in Figure 2-21 b) is the intersection between the line of initial stiffness and nominal strength. Point 3 is the yield displacement when using the intersection of the line through the origin of secant stiffness to first yield (point 2) with the nominal strength. The displacement at point 1 can differ significantly from the displacement at point 3. Displacement capacity is typically defined as displacement at peak strength (point 4), or at some percentage reduction of peak strength (point 5) or ultimate displacement (point 6).

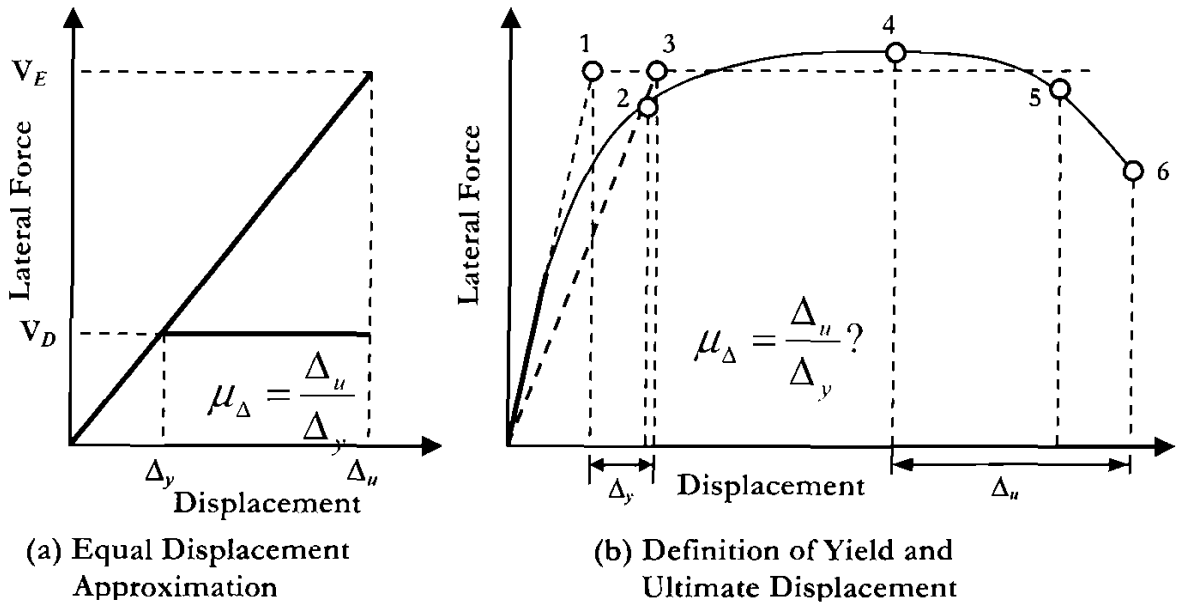

Figure 2-21: Defining ductility capacity (Priestley, et al., 2007)

Given the various definitions of ductility capacity and the uncertainty regarding the R-μ-T approximations, it is not surprising that there is such a variation in the codes with respect to force reduction (behaviour factor or force-reduction factor).

A further complication is that the codes often consider additional *redundancies* within the behaviour factor. EC 1998-1: 3.2.2.5, referred to in Section 2.5, also states that the values of the behaviour factor account for the influence of the viscous damping being different from 5%.

SSI will influence the damping and ductility of a structure and, therefore, will influence the behaviour factor. Figure 2-22 illustrates the influence of SSI on ductility with a simple standalone concrete wall on a flexible foundation. The yield displacement, Δ_y at the effective height of the wall will increase with the displacement due to foundation flexibility, Δ_F to Δ'_y.

If the design displacement, Δ_D is strain limited it will increase by essentially the same amount. The ductility capacity can then be expressed through Equation (2.51).

$$\mu = \frac{\Delta_D + \Delta_F}{\Delta_y + \Delta_F} \qquad (2.51)$$

If the design displacement is limited by codified maximum drift, then the ductility capacity can be expressed in Equation (2.52).

$$\mu = \frac{\Delta_D}{\Delta_y + \Delta_F} \qquad (2.52)$$

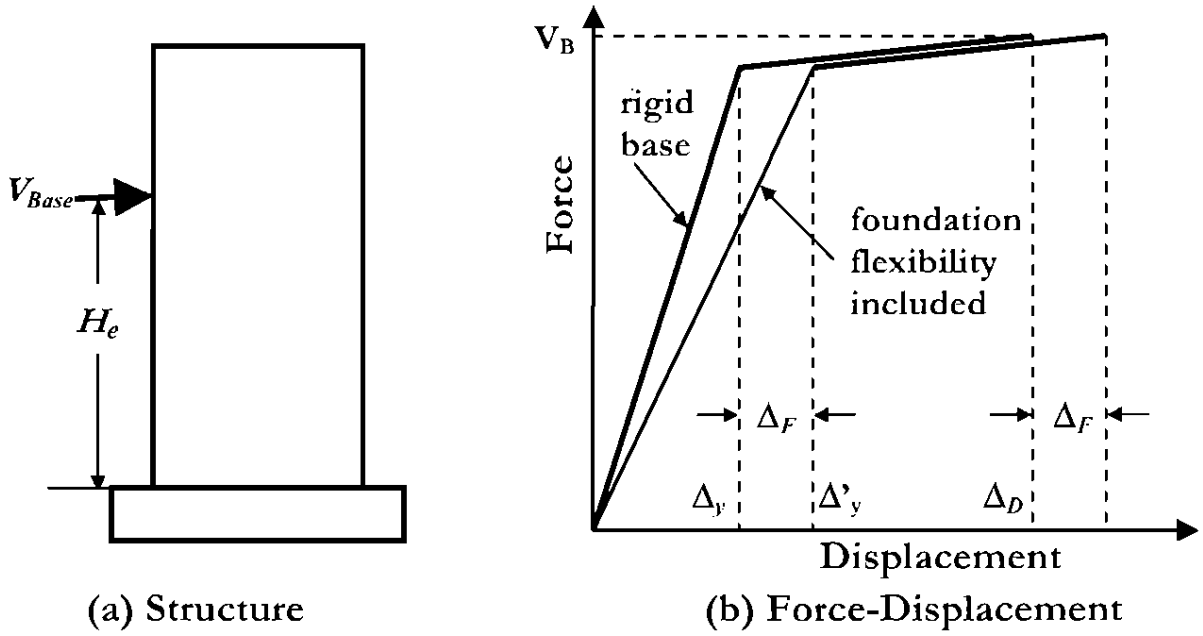

Figure 2-22: Influence of foundation flexibility on ductility (Priestley, et al., 2007, p. 354)

With the likely reduction in ductility capacity, a similar reduction in behaviour factor would be expected. However, it is observed in Section 2.7 that, amongst other effects, SSI will contribute to the total damping of a structure. This, according to EC 1998-1, will also influence the behaviour factor.

As a commentary on the potential shortcomings of existing design guidelines on SSI, NIST GCR 12-917-21 (2012, p. 4-3) points out that there is no link prescribed between behaviour factors intended to represent structural ductility and soil-structure interaction. Crouse (2001) notes that the existing force reduction factors could already include the beneficial effects of SSI and that including these effects might be unconservative in some cases.

3 Foundation behaviour

The objective of this chapter is to establish a moment-rotation relationship for foundation behaviour. The principle of this relationship is used for foundation modelling in the various structures considered in this study.

3.1 Beam-on-nonlinear Winkler foundation (BNWF)

A horizontal member distributed over a set of springs and/or dashpots can represent foundation behaviour with sufficient accuracy. The supporting springs typically would not have tension resistance, therefore simulating foundation uplift and separation between the foundation and the soil. Figure 3-1 illustrates an SDOF oscillator attached to a Winkler soil model.

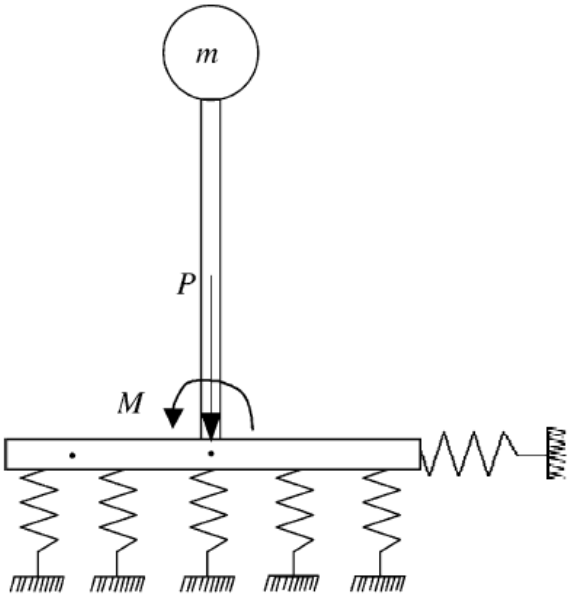

Figure 3-1: Winkler soil model

The BNWF is widely used in practice because of the simplicity of the model and the ability to simulate nonlinear behaviour (NIST GCR 12-917-21, 2012, p. 2-35).

3.2 Moment-rotation relationship

Allotey & Naggar (2003) developed analytical expressions for the moment-rotation relationship based on a Winkler Model. Consider a Winkler soil model with rigid horizontal support, vertical spring stiffness of k_v, bearing capacity q_u, base length, L

and base width, B. The nondimensional variables are introduced as Equations (3.1) to (3.3) for ease of comparison.

$$\psi = \frac{k_v L}{q_u} \qquad (3.1)$$

$$\chi = \frac{P}{q_u L} \qquad (3.2)$$

$$M_{qL} = \frac{M}{q_u L^2 B} \qquad (3.3)$$

Where ψ represents the soil stiffness to its strength; χ is the inverse of the foundation bearing capacity safety factor under vertical load and M_{qL} the normalised moment.

Equation (3.4) present expressions for moment-rotation when $\chi \leq 0.5$.

$$M_{qL} = \begin{cases} \dfrac{\psi\theta}{12} & 0 \leq \theta \leq \dfrac{2\chi}{\psi} \\ \dfrac{\chi}{6}\left(3 - 2\sqrt{\dfrac{2\chi}{\psi\theta}}\right) & \dfrac{2\chi}{\psi} \leq \theta \leq \dfrac{1}{2\psi\chi} \\ 0.5(\chi - \chi^2) - \dfrac{1}{24\psi^2\theta^2} & \dfrac{1}{2\psi\chi} \leq \theta \end{cases} \qquad (3.4)$$

Equation (3.5) present expressions for moment-rotation when $\chi \geq 0.5$.

$$M_{qL} = \begin{cases} \dfrac{\psi\theta}{12} & 0 \leq \theta \leq \dfrac{2(1-\chi)}{\psi} \\ \dfrac{(1-\chi)}{6}\left(3 - 2\sqrt{\dfrac{2(1-\chi)}{\psi\theta}}\right) & \dfrac{2(1-\chi)}{\psi} \leq \theta \leq \dfrac{1}{2\psi(1-\chi)} \\ 0.5(\chi - \chi^2) - \dfrac{1}{24\psi^2\theta^2} & \dfrac{1}{2\psi(1-\chi)} \leq \theta \end{cases} \qquad (3.5)$$

For $\chi < 0.5$, foundation uplift will occur before soil yielding, while for $\chi > 0.5$, soil will yield before foundation uplift and for $\chi = 0.5$, uplift and yield will occur simultaneously. Figure 3-2 illustrates the foundation behaviour with reference to χ.

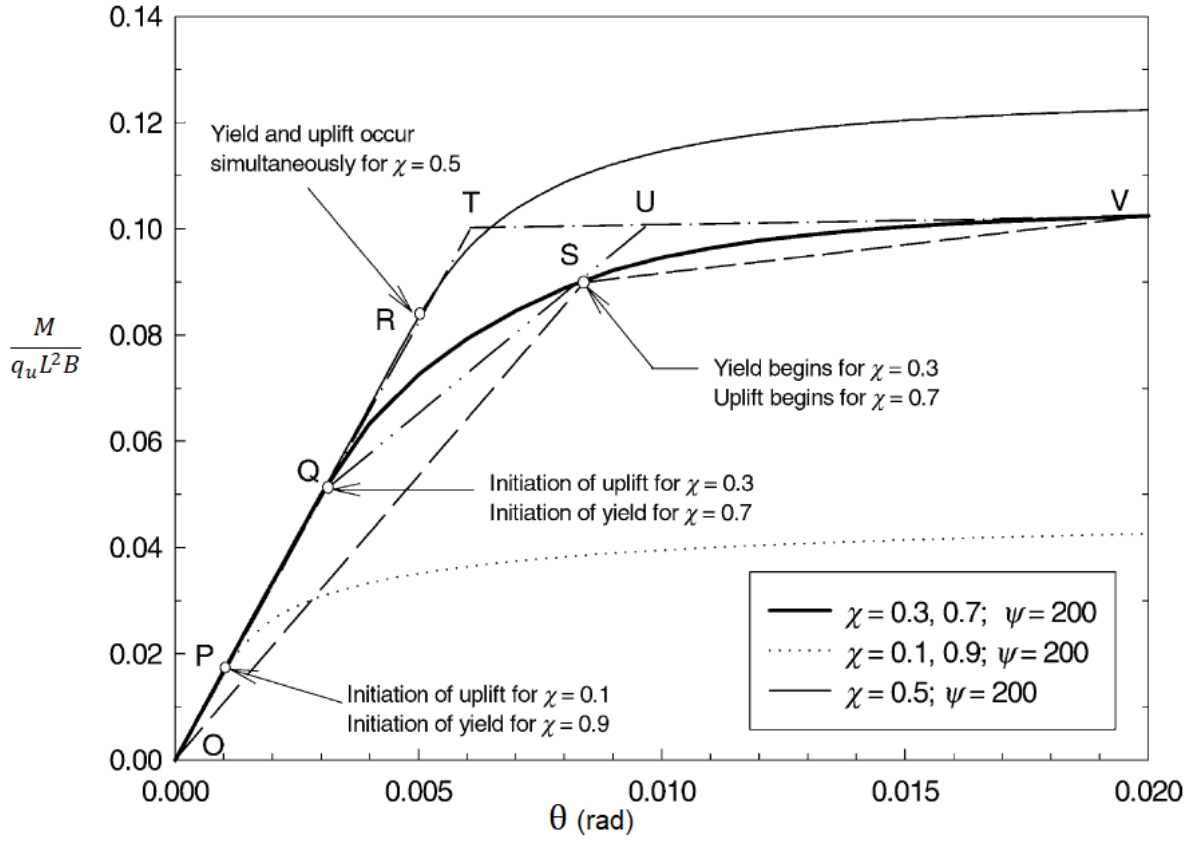

Figure 3-2: Moment-rotation relationship (Allotey & Naggar, 2003)

Furthermore, with the assumption that the structure can accommodate large foundation rotations, Allotey and Naggar (2003) present the ultimate moment capacity for a base, M_{ub} as shown in Equations (3.6) and (3.7):

$$M_{ub} = \frac{PLB}{2} - \frac{P^2 B}{2q_u} - \frac{q_u^3 B}{24(k_v \theta)^2} \qquad (3.6)$$

$$\lim_{\theta \to \infty} M_{ub} = \frac{PLB}{2} - \frac{P^2 B}{2q_u} \qquad (3.7)$$

Equation (3.7) is presented in various design guides to express the ultimate moment capacity for rectangular foundations, where it is observed that the capacity is independent of the soil stiffness.

3.3 Soil parameters

There is a level of uncertainty and variability related to the exact soil properties of a given site. Modelling considerations such as the bilinear approximation for nonlinear soil response and idealised assumption for cyclic loading effect on strength and stiffness adds to this uncertainty. These factors will influence the response of the structure. To account for the variability, most US standards recommend an upper- and lower-bound approach to evaluate the sensitivity of the structural response. Typically, the upper-bound is double the expected value, and the lower-bound is half of the expected value. Figure 3-3 illustrates this principle as prescribed by FEMA 356 and ASCE/SEI 41-17.

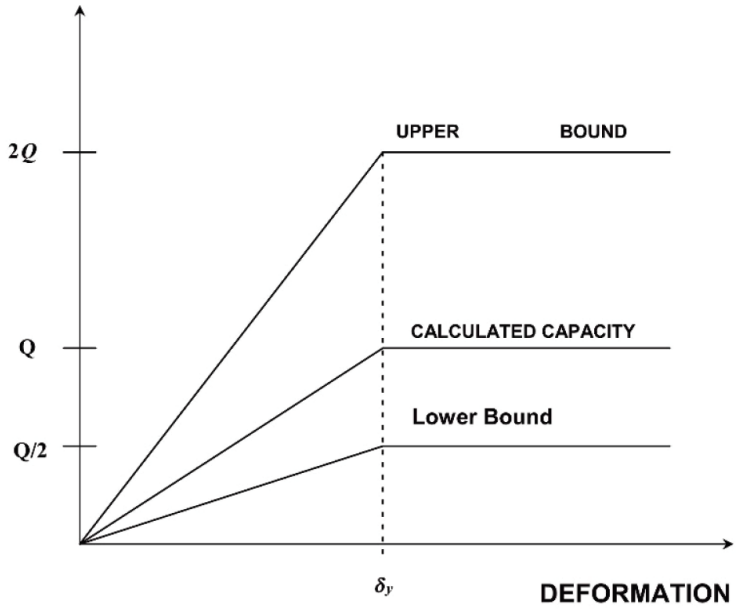

Figure 3-3: Idealised elastoplastic soil behaviour (ASCE/SEI 41-17, 2017)

As a commentary on the expected capacity, ASCE/SEI 41-17 notes that in many cases allowable pressure is determined by long-term settlement, not capacity. Traditionally, geotechnical reports already include a safety factor for gravity loads under long-term loads. The expected short-term capacity appropriate for seismic loads should not include these safety factors.

US codes and technical reports allow three basic analysis methods for SSI of shallow foundations. The methods, as set out by ASCE/SEI 41-17, are discussed here.

Method 1 - Footings considered rigid, uncoupled spring model: The expected nonlinear sliding, bearing, and rocking behaviour shall be represented by uncoupled springs. The stiffnesses are typically represented by an idealised bilinear or trilinear load-deformation relationship. Figure 3-4 illustrated the model, where k_{sv}, k_{sh} and k_{sr} represents the vertical-, horizontal- and rotational stiffnesses, respectively.

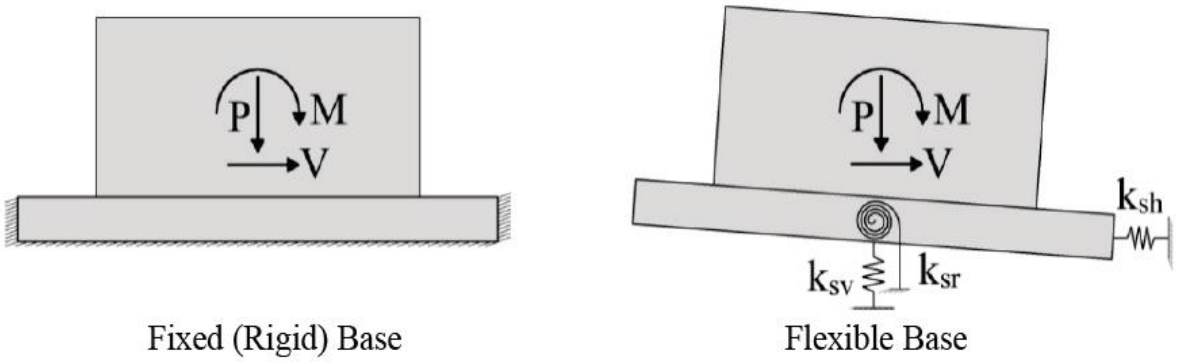

Figure 3-4: ASCE 41-17 Method 1 representation (FEMA P-2006, 2018, Figure 5-11)

The values for the respective spring stiffnesses are based on Gazetas (1991). The stiffnesses are indicated in Table 3-1, as obtained from ASCE/SEI 41-17 and FEMA 356:

Table 3-1: Foundation stiffness for ASCE 41-17 method 1 (adapted from ASCE 41-17 Figure 8-2)

Degree of Freedom	Stiffness of Foundation at Surface	Note
Translation along x-axis	$K_{x,sur} = \frac{GB}{2-\nu}\left[3.4\left(\frac{L}{B}\right)^{0.65} + 1.2\right]$	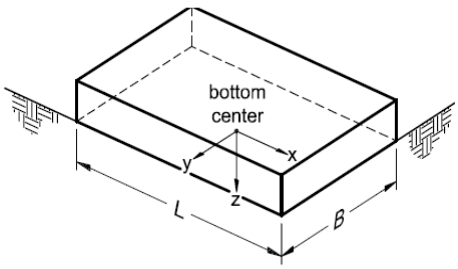
Translation along y-axis	$K_{y,sur} = \frac{GB}{2-\nu}\left[3.4\left(\frac{L}{B}\right)^{0.65} + 0.4\frac{L}{B} + 0.8\right]$	
Translation along z-axis	$K_{z,sur} = \frac{GB}{1-\nu}\left[1.55\left(\frac{L}{B}\right)^{0.75} + 0.8\right]$	
Rocking about x-axis	$K_{xx,sur} = \frac{GB^3}{1-\nu}\left[0.4\left(\frac{L}{B}\right) + 0.1\right]$	
Rocking about y-axis	$K_{yy,sur} = \frac{GB^3}{1-\nu}\left[0.47\left(\frac{L}{B}\right)^{2.4} + 0.034\right]$	Orient axes such that $L \geq B$
Torsion about z-axis	$K_{zz,sur} = GB^3\left[0.53\left(\frac{L}{B}\right)^{2.45} + 0.51\right]$	

G is the effective shear modulus and υ the Poisson's ratio of the soil.

NIST GCR 12-917-21 (2012) Table 2.2 shows similar expressions for foundation stiffnesses.

Method 2 - Footings considered rigid, Winkler type model: A Winkler type model similar to what is discussed in Section 3.1, but with end stiffness adapted to simulate the moment-rotation (rocking) stiffness of Method 1.

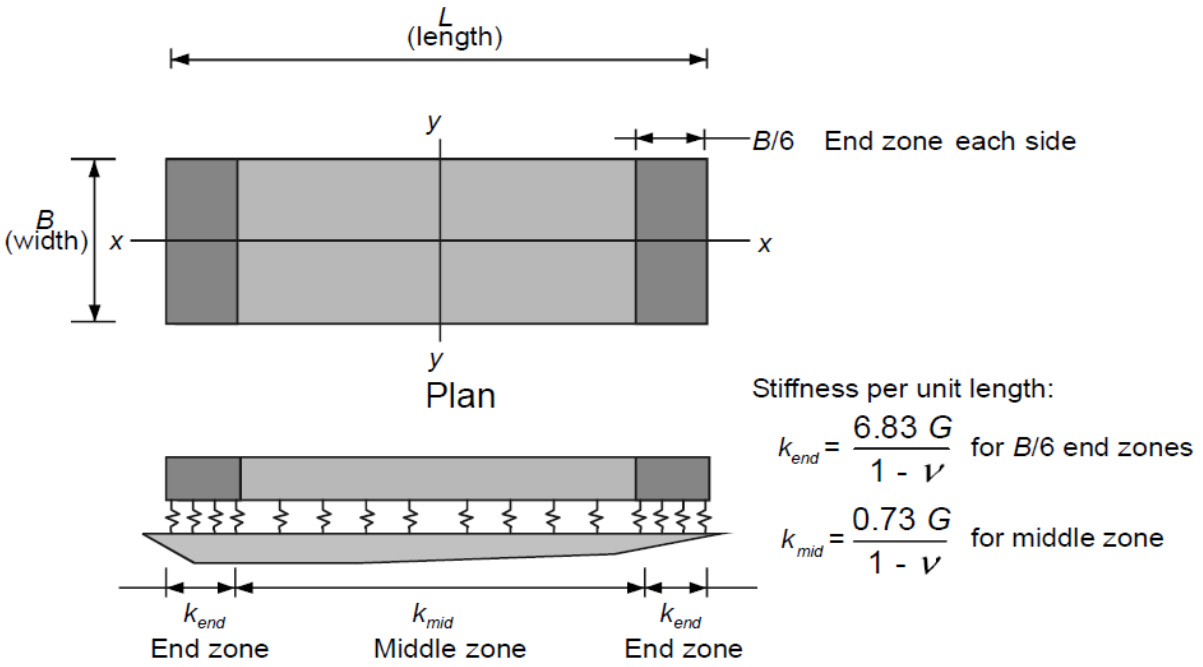

Figure 3-5: ASCE/SEI 41-17 Method 2 illustration

Commentary on ASCE/SEI 41-17 suggests that the stiffnesses should be adjusted to represent the same moment-rotation behaviour as Method 1 above, but does not present specific details on this.

Method 3 – Footings not rigid relative to soil, Winkler type model. This approach is similar to Method 2, except a flexible footing is modelled and the soil stiffnesses are adapted. Method 3 is not considered in this investigation as incorporating non-rigid foundations introduces additional variables.

Modulus of subgrade Reaction:

It is known that the modulus of subgrade reaction, k_v is not explicitly a property of the soil, but rather a representation of the load-deformation behaviour and is a function of foundation shape. The modulus of subgrade reaction will therefore change with a

change in the shape of the foundation. FEMA 274 (1997b) states that the conversion to Winkler springs requires consideration that the rotational stiffness may differ from vertical stiffness, FEMA 274 references Bowles (1982) in order to consider these changes.

3.4 Moment-rotation relationship comparison

An initial investigation is performed to compare the moment-rotation relationship of a Winkler soil model with stiffnesses proposed by Bowles (1996) against the methods described in Section 3.3. The foundations are modelled using SeismoStruct analysis software, each modelled with soil stiffness according to the respective methods. The results are compared with the predicted moment-rotation behaviour from the expression of Allotey & Naggar (2003), using the spring stiffnesses proposed by Bowles (1996). The model is based on 5M60AR3 model. The model notation is described Chapter 4. The relevant properties are provided in Table 3-2.

Table 3-2: Soil parameters

Soil Properties:		**Foundation:**
Ground Type 3 (SANS 10160-4)		Length, *L*: 10.2 m
Shear wave velocity, v_{s0}:	180 m/s	Breadth, *B*: 1.6 m
Expected Bearing Capacity, q_u:	400 kPa	Thickness, *t*: 0.6 m
Stress Strain Modulus, E_s:	50 MPa	Depth, *d*: 0.6 m
Poisson's Ratio, υ:	0.4	Density, γ_{conc}: 24 kN/m^3
Soil Density, γ_{soil}:	18 kN/m^3	Axial Load (including base), *P*: 3535 kN

Method 1:

The shear strain modulus is calculated using Equation (3.8), as prescribed by ASCE/41-17 as:

$$G_0 = \frac{\gamma_{soil} v_{s0}^2}{g} = \frac{18 \times 180^2}{9.81} = 59.45\ MPa \qquad (3.8)$$

The shear modulus is adjusted to account for the nonlinearity associated with ground shaking. Table 3-3 presents the values obtained from ASCE/SEI 41-17 (Table 8-2):

Table 3-3: Effective shear modulus ration (G/G_0) adapted from ASCE 41-17 Table 8-2.

Effective Shear Modulus Ratio (G/G_0)				
	Effective Peak Acceleration, $S_{XS}/2.5$[a]			
Site Class	$S_{XS}/2.5 = 0$	$S_{XS}/2.5 = 0.1$	$S_{XS}/2.5 = 0.4$	$S_{XS}/2.5 = 0.8$
A	1.00	1.00	1.00	1.00
B	1.00	1.00	0.95	0.90
C	1.00	0.95	0.75	0.60
D	1.00	0.90	0.50	0.10
E	1.00	0.60	0.05	[b]
F	[b]	[b]	[b]	[b]

[a] Use straight-line interpolation for intermediate values of $S_{XS}/2.5$.
[b] Site-specific geotechnical investigation and dynamic site response analyses shall be performed.

Ground Type 3 of SANS 10160-4 (2017) have similar properties as Site Class D of ASCE/SEI 41-17 and ASCE/SEI 7-16. *Sxs* is the effective peak spectral acceleration similar to what is indicated in Figure 2-18. This will equate to the ground acceleration, a_g x S (refer to Equation (2.19)). Table 2 of SANS 10160-4 (2017) presents the same spectral parameters of EC 1998-1 that are shown in Table 2-1, but with a slight variation in the Ground Type name. Ground Type 3 in SANS 10160-4 (2017) is Ground Type C in EC 1998-1 (2004). The soil factor, S used is shown in Table 3-4.

Table 3-4: Spectral parameters as described in SANS 10160-4 (2017) Table 2

Ground type	Parameters			
	S	T_B	T_C	T_D
1	1.0	0.15	0.4	2.0
2	1.2	0.15	0.5	2.0
3	1.15	0.20	0.6	2.0
4	1.35	0.20	0.8	2.0

The value *Sxs/2.5* is then 0.15x1.15 = 0.1725. Using interpolation, the effective shear ratio G/G_0 = 0.803, which leads the effective shear strain modulus, G = 47.73 MPa.

The rotational stiffness can now be calculated using Table 3-1 above, k_{yy} (rocking about y-axis). For consistency, no allowance is made for embedment effects.

k_{yy} = 13 070 475.44 kNm/rad

The ultimate moment capacity, M_{ub} as given in equation 8-10 of ASCE 41-17 is presented through Equation (3.9).

$$M_{ub} = \frac{LP}{2}\left(1 - \frac{P}{BLq_u}\right) = 8265\ kNm \qquad (3.9)$$

Method 2:

The same effective shear strain modulus is used together with Figure 3-5 to calculate the spring stiffnesses. Note that the edge stiffness is more than nine times stiffer than the internal stiffness.

Winkler model using stiffness according to Bowles (1996):

Bowles (1996) gives an expression for the plane strain modulus calculated from the static stress strain modulus as:

$$E_s' = \frac{E}{1 - \upsilon^2} = 59.524\ MPa \qquad (3.10)$$

The modulus of subgrade reaction, k_v is calculated using strain modulus with influence factors I_1, I_2 and I_s presented in Equations (3.11), (3.12), (3.13) and (3.14).

$$I_1 = \frac{1}{\pi}\left[\left(\frac{L}{B}\right)\ln\frac{\left(1+\sqrt{\left(\frac{L}{B}\right)^2+1}\right)\sqrt{\left(\frac{L}{B}\right)^2+\left(\frac{2H}{B}\right)^2}}{\left(\frac{L}{B}\right)\left(1+\sqrt{\left(\frac{L}{B}\right)^2+\left(\frac{2H}{B}\right)^2+1}\right)} + \ln\frac{\left(\left(\frac{L}{B}\right)+\sqrt{\left(\frac{L}{B}\right)^2+1}\right)\sqrt{1+\left(\frac{2H}{B}\right)^2}}{\left(\frac{L}{B}\right)+\sqrt{\left(\frac{L}{B}\right)^2+\left(\frac{2H}{B}\right)^2+1}}\right] \qquad (3.11)$$

$$I_2 = \frac{H_s}{B\pi}\tan^{-1}\left(\frac{\left(\frac{L}{B}\right)}{\left(\frac{2H_s}{B}\right)\sqrt{\left(\frac{L}{B}\right)^2+\left(\frac{2H_s}{B}\right)^2+1}}\right) \qquad (3.12)$$

$$I_s = I_1 + \frac{1-2v}{1-v} I_2 \qquad (3.13)$$

$$k_v = \frac{E'}{B I_s I_F} = 63\,796\ kN/m^3 \qquad (3.14)$$

H_s is defined as the depth of stratum and is taken as 10m. I_F is the influence factor related to embedment depth (Bowles, 1996, p. 306). Factors associated with embedment depth is taken as 1 for this investigation.

Figure 3-6 shows the comparison between the various methods:

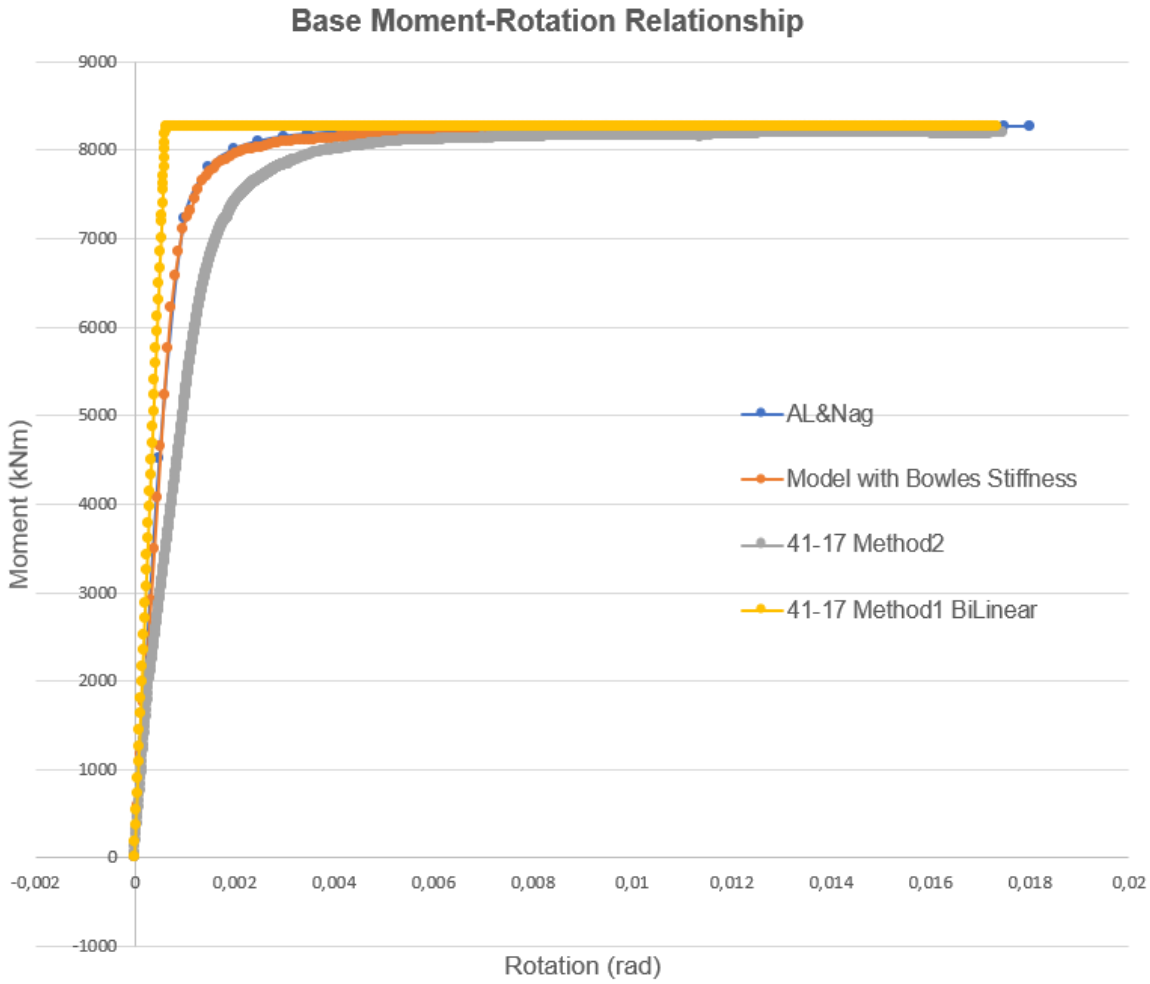

Figure 3-6: Moment-rotation comparison between methods

The model with spring stiffness according to Bowles (1996) compares well with predictions of Allotey & Naggar (2003). Although the arbitrary influence functions might make it difficult to compare directly, the Bowles model is a good average between Method 1 and Method 2. The ultimate moment capacities for all methods are

essentially the same. This is expected, as previously noted, the ultimate moment capacity is not dependent on soil stiffness.

This study uses Winkler foundation models with spring stiffnesses proposed by Bowles (1996) for reasons explained and for ease of comparison with predictions.

4 Methodology and buildings investigated

4.1 Structural type

Building layout:

The purpose of the investigation is to assess building models that can be analysed with any of the methods explored in Chapter 2.8. The principal building is regular in plan and elevation, so to comply with the requirements for the use of the linear static procedure. The lateral load resisting systems must run without interruption from the base to the top of the building. The structural walls are arranged to achieve torsional stability in the direction of seismic loading. Arrangements for stable and unstable systems in torsion are shown in Figure 4-1.

The reference layout with load direction is presented in Figure 4-2. It is assumed that the building is sufficiently protected against seismic loading for the direction perpendicular to what is the applied loading.

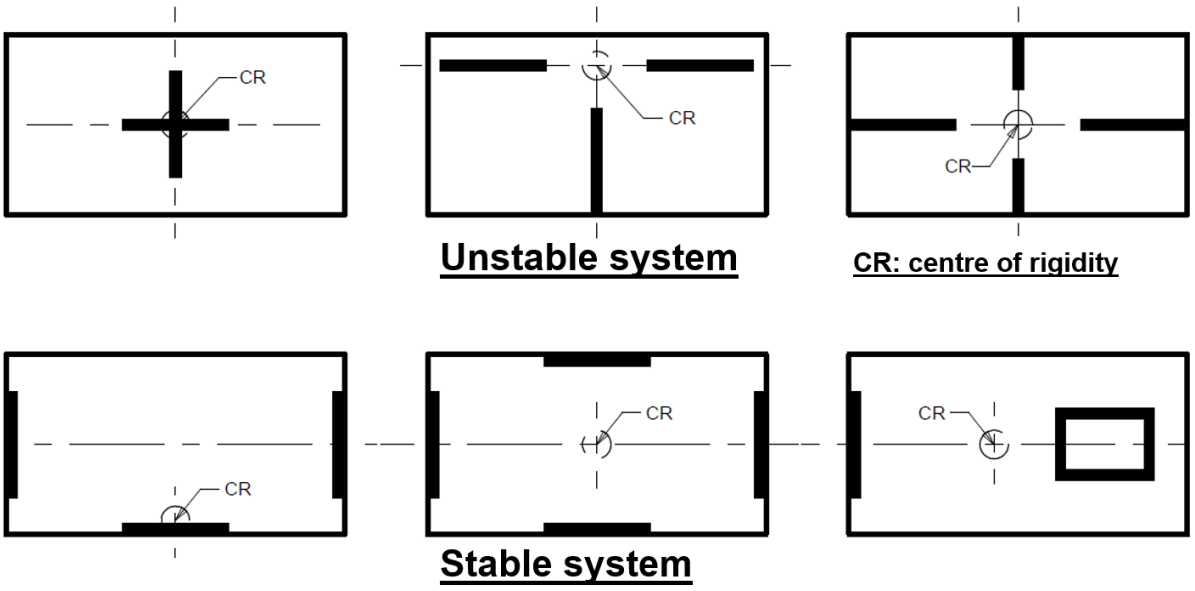

Figure 4-1: Stable vs unstable wall arrangement (adapted from Fig 5.2 Pauley & Priestley (1992))

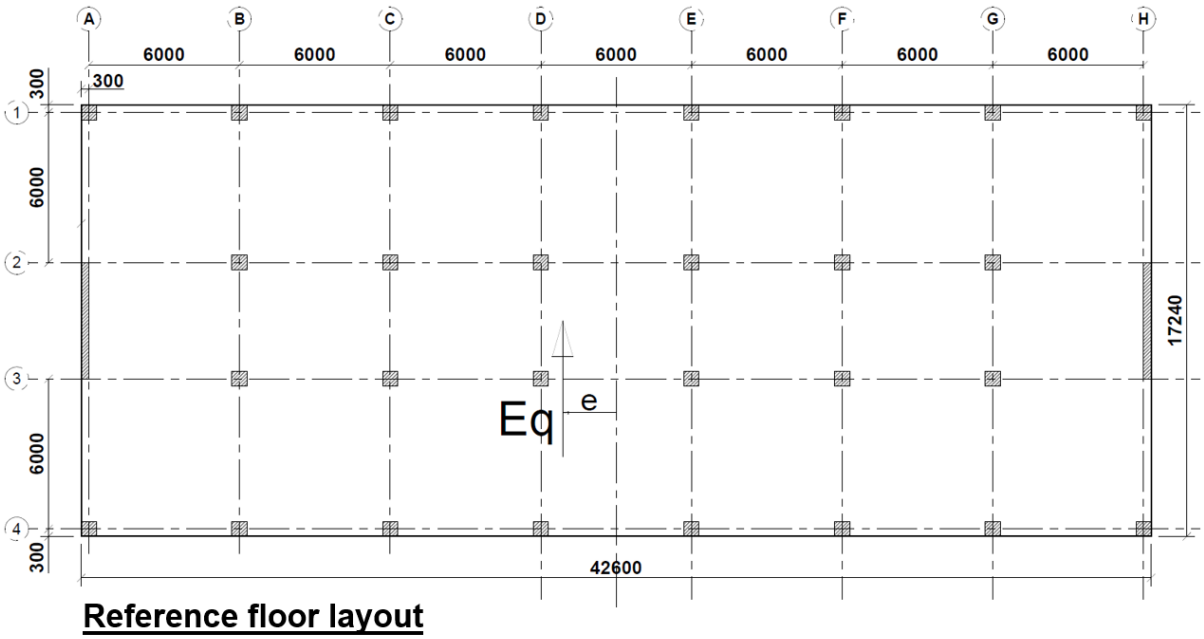

Figure 4-2: Reference floor layout

Importance class:

Code philosophy recognises that different building occupations should be associated with unique reliability. Buildings like hospitals, fire stations, power plants; buildings that should remain fully operational in an emergency, must be designed for higher reliability than structures associated with minor importance. The factor is taken as unity for this investigation. This corresponds to the importance class 2 of "*ordinary buildings*" in SANS 10160-4 (2017), which would be typical for office buildings.

4.2 Foundation parameters

Ground type:

From Section 2.7 and Chapter 3, it is observed that different soil types influence the seismic demand as well as the seismic response. Table 4-1 describes the soil types as presented in Table 1 of SANS 10160-4 (2017), which is similar to EN 1998-1 (2004) Table 3-1.

Table 4-1: Ground Types to SANS 10160-4 (2017) Table 1

1	2	3		
Ground type	**Description of stratigraphic profile**	**Parameters**[a]		
		$v_{s,30}$ m/s	N_{SPT} blows/30 cm	c_u kPa
1	Rock or other rock-like geological formation, including at most 5 m of weaker material at the surface	> 800	–	–
2	Deposits of very dense sand, gravel, or very stiff clay, at least several tens of metres in thickness, characterised by a gradual increase of mechanical properties with depth	360 – 800	>50	>250
3	Deep deposits of dense or medium dense sand, gravel or stiff clay with thickness from several tens to many hundreds of metres	180 – 360	15 – 50	70 – 250
4	Deposits of loose-to-medium cohesion-less soil (with or without some soft cohesive layers), or of predominantly soft-to-firm cohesive soil	< 180	<15	<70
[a] $v_{s,30}$ = average value of propagation of S-waves in the upper 30 m of the soil profile at shear strains of 10^{-5}, or less; N_{SPT} = standard penetration test blow-count; c_u = un-drained shear strength of soil, expressed in kilopascals (kPa).				

This investigation focusses on Ground Type 3 (EN 1998-1 Ground Type C), which is consistent with soil conditions commonly found in the Western Cape region, an area under the highest risk associated with natural seismic activity in South Africa.

It can be observed from Figure 2-6 that Ground Type 3 represents a reasonable average response for all 4 ground types.

<u>The relevant soil parameters that are used in this investigation are:</u>

Shear wave velocity, $v_{s,30}$: 180 m/s

Expected Bearing Capacity, q_u: 400 kPa

Stress Strain Modulus, E_s: 50 MPa

Poisson's Ratio, υ: 0.4

Soil Density, γ_{soil}: 18 kN/m^3

It is noted in Chapter 3.3 that to account for the variability in soil properties, design standards like ASCE/SEI 41-17, propose an upper- and lower-bound for stiffness and

capacity. To investigate the effects of SSI, the soil parameters were kept constant throughout the study, for direct comparison.

Foundation type:

The foundation shape will influence the modulus of subgrade reaction and, therefore, the response of the structure. As seen in Chapter 2.7, the foundation depth adds to the kinematic effects as well as foundation stiffness and damping. This investigation focuses on freestanding shallow structural wall foundations, thus no adjustment factors associated with foundation depth are considered.

4.3 Structural walls

Wall shape:

Structural walls exist in various forms in building structures. Figure 4-3 illustrates the general structural wall shapes in buildings.

Figure 4-3: Common section of structural walls

Two walls intersecting at right angles will result in an effective flanged compression or tension wall section. The structural strength of the wall is insensitive to the assumed compression flange width, but with load reversal under large ductility demand and subsequent cracking of concrete and yielding of reinforcement, the effective flange width estimation becomes more complex. (Pauley & Priestley, 1992, pp. 368-370).

This study focuses on rectangular walls only. In principle, any wall shape can be used, as the effects of SSI on the wall will be similar, however rectangular wall shapes allow for simple integration with code definitions of boundary elements and confinement reinforcement.

Aspect ratio:

The wall aspect ratio is defined as the total height, H_w to wall length, L_w. For a given global displacement ductility, μ_Δ the local curvature ductility demand, μ_Φ will increase with increasing wall aspect ratio, H_w/L_w (Pauley & Priestley, 1992, p. 400). Figure 4-4 illustrates the approximate relationship.

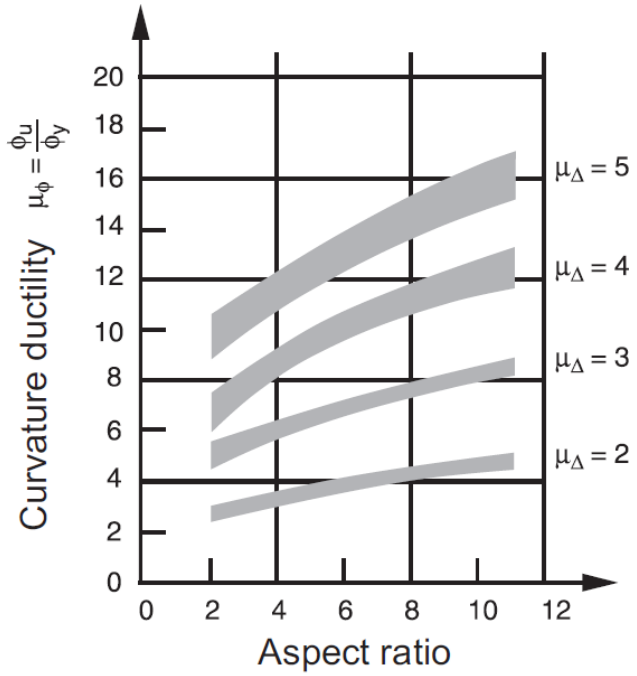

Figure 4-4: Relationship between curvature ductility, displacement ductility, and aspect ratio (Monteiro, 2019, p. 3-19)

Squat walls with small aspect ratios are more likely to be dominated by shear behaviour. To ensure ductile, flexure dominated behaviour, rather than the more brittle, shear dominated behaviour, it would make sense to limit the aspect ratio to some extent. SANS 10160-4 (2017) does not explicitly limit this ratio. EN 1998-1 (2004) makes use of a factor, k_w to adjust the behaviour factor according to the prevailing mode of failure. This factor is a function of the aspect ratio. The expression for k_w reduces the behaviour factor for aspect ratios lower than two.

As the aspect ratio increases, the lateral drift limits play a bigger role in the allowable displacement limits. This means that for slender walls, with large aspect ratios, the member would not reach its full ductility capacity associated with strain limits but would rather reach drift limits associated with secondary damage of non-structural infill panels. Priestley, et al. (2007, pp. 325-327) suggest that for aspects ratios

approximately 9 and larger, a structural wall is expected to reach storey drift limits while still behaving elastically.

This study investigates rectangular walls with aspect ratios of 3 and 5. These ratios fall within the practical range for structural walls associated with ductile, flexure dominated behaviour.

It can be argued that for the sake of compatibility, SSI should always be considered. However, the advantages of SSI on taller buildings become less pronounced (PEER Report 2017/06, 2017, p. 4-16). For this reason, only medium- to low-rise buildings were investigated; namely 3, 5 and 7 storey buildings.

Lateral stability:

To prevent lateral out-of-plane buckling of the compression flange in the wall sections, Pauley & Priestley (1992, p. 403) suggest a limit to the width of the section. Figure 4-5 illustrates these proposed limits.

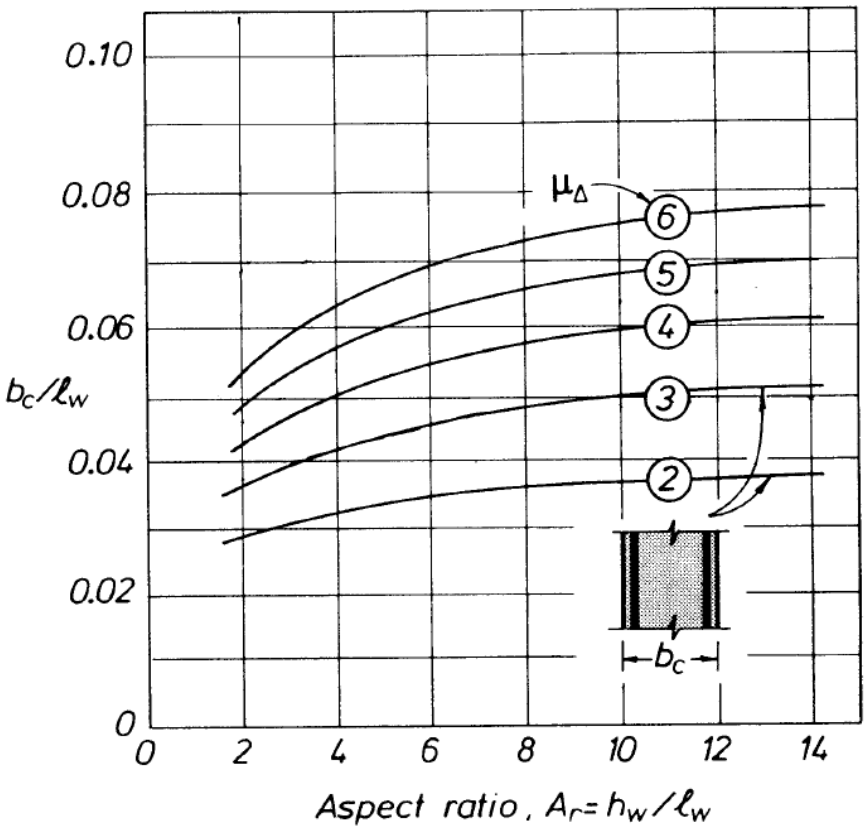

Figure 4-5: Critical wall thickness- displacement ductility relationship (Pauley & Priestley, 1992, p. 403)

With the behaviour factor of 5, assuming the equal displacement approximation and taking an approximate value of 1.5 for overstrength, the displacement ductility is expected to be around 3.3. The wall width is taken as 300 mm which is above the limits for all ranges of wall lengths and aspect ratios chosen, with the exception of the 7 storey wall with an aspect ratio of 3 where the ratio of wall width to length, b_c/Lw is 0.038 and the approximate limit from Figure 4-5 is around 0.04. As this mode of failure is not investigated in this study and considering that for the interests of this study it is more important to keep the width constant, the width of 300 mm is assumed to be within the reasonable range.

4.4 Frame contribution

The contribution of the frame to the stability of the structure will increase with an increase in the foundation rotation. Consider the simplified structural wall frame shown in Figure 4-6. Assuming that the vertical members are rigid, it is expected that for a foundation rotation of θ, a similar additional rotation would occur in the horizontal frame elements at the wall face, resulting in the frame contributing more to the stability of the structure.

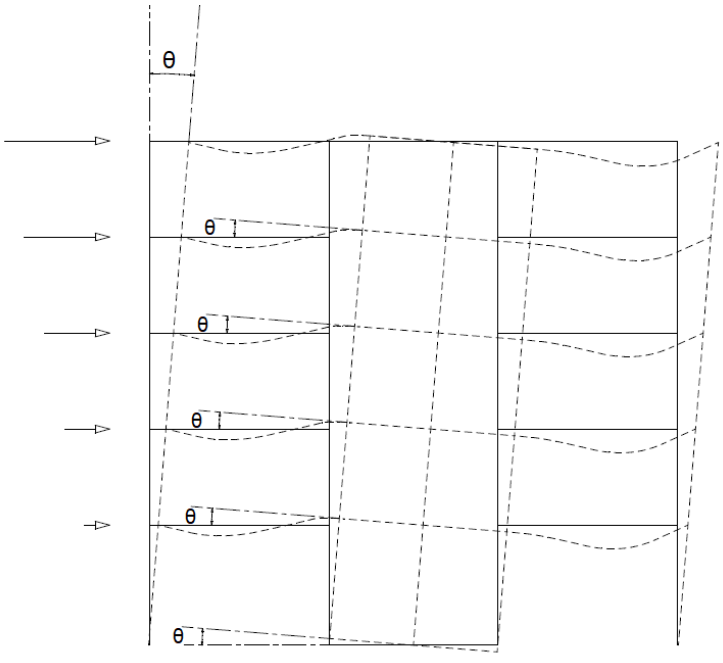

Figure 4-6: Simplified frame rotation

Relatively slender horizontal members are chosen to minimise the contribution of the frame. This study investigates concrete wall buildings with reinforced concrete flat

slabs as diaphragms. The principle can be extended to reinforced concrete beams or post-tensioned elements. The span of the horizontal elements is kept constant at 6 m, with slab thicknesses of 250 mm. This falls within the typical panel width for residential buildings under gravity loads.

The equivalent frame width is taken as the panel width between spans. Strictly speaking this should be taken as the width between points of zero shear. As the contributing slab is already relatively slender and would depend on the structural layout, the width is rather arbitrary. Therefore, the simplistic approach of width equal to half the span is followed as shown in Figure 4-7.

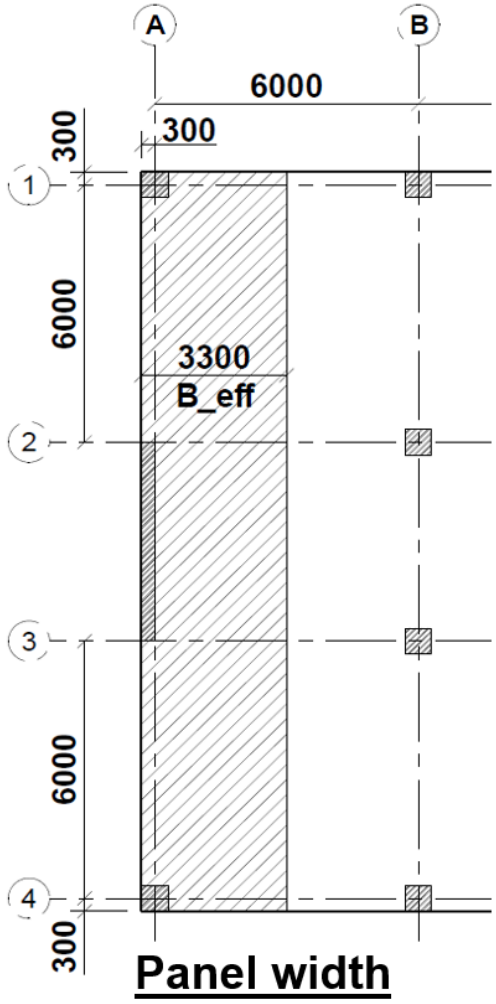

Figure 4-7: Assumed effective slab width

4.5 Loading

Self-weight: The concrete density, γ_{conc} is taken as 24 kN/m^3. With a 250 mm slab thickness, the slab self-weight is obtained as 6 kN/m^2.

Permanent load: For office building with masonry as infill panels with a typical arrangement of internal brickwork together with tiling, services and screed, an additional Dead Load (DL) of 5.5 kN/m^2 was assumed.

Imposed load: SANS 10160-2 (2011) Table 1 prescribes a 2.5 kN/m^2 imposed load for offices, as presented by Table 4-2:

Table 4-2: Imposed loads on office buildings according to SANS 10160-2 (2011) Table 1

Category	Specific Use	Subcategory	Example	Qk (kN/m^2)	Qk (kN)
B	Public areas (not susceptible to crowding)	B1	Office areas for general use	2.5	4.5

4.6 Summary of scope

A total of 24 models are investigated, which is summarised in Table 4-3.

Table 4-3: Structural models investigated

	Aspect Ratio 5			Aspect Ratio 3		
	3 Storey	5 Storey	7 Storey	3 Storey	5 Storey	7 Storey
M100 Base	3M100AR5	5M100AR5	7M100AR5	3M100AR3	5M100AR3	7M100AR3
M80 Base	3M80AR5	5M80AR5	7M80AR5	3M80AR3	5M80AR3	7M80AR3
M60 Base	3M60AR5	5M60AR5	7M60AR5	3M60AR3	5M60AR3	7M60AR3
M40 Base	3M40AR5	5M40AR5	7M40AR5	3M40AR3	5M40AR3	7M40AR3

M100 refers to the original base size with the capacity to resist the total fixed moment condition whereas M60 is the base size with the capacity to resist 60% of the fixed moment. Figure 4-8 explains the model notation.

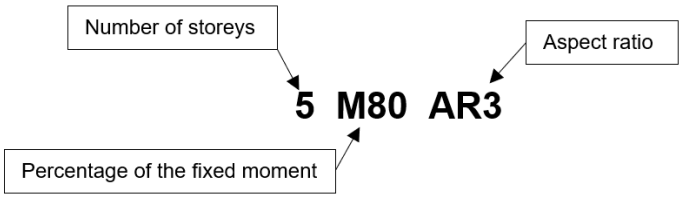

Figure 4-8: Model notation

The foundation sizes are summarised in Table 4-4.

Table 4-4: Foundation sizes investigated

	Aspect Ratio 5			Aspect Ratio 3		
	Foundation Size L x B x t (m)			Foundation Size L x B x t (m)		
	3 Storey	5 Storey	7 Storey	3 Storey	5 Storey	7 Storey
M100 Base	Fixed	Fixed	Fixed	Fixed	Fixed	Fixed
M80 Base	6.3x1.5x0.6	7.9x2x0.7	10x2.2x1.1	8.8x2.2x0.6	11.1x1.8x0.7	12.2x2.4x1
M60 Base	5.7x1.3x0.5	7x1.9x0.6	8.8x2.2x1	7.9x1.7x0.5	10.2x1.6x0.6	11.3x2.2x0.9
M40 Base	4.9x1.2x0.4	6.3x1.7x0.5	8.1x2x0.9	6.5x1.5x0.5	9x1.5x0.6	10.5x2x0.9

The wall buildings height and storey heights are given in Table 4-5.

Table 4-5: Storey heights investigated

	Storey Height (m)		
	7 Storey	5 Storey	3 Storey
Foundation	0	0	0
Level 1	4	4	4
Level 2	7.2	7.2	7.2
Level 3	10.4	10.4	10.4
Level 4	13.6	13.6	
Level 5	16.8	16.8	
Level 6	20		
Level 7	23.2		

The wall lengths are shown in Table 4-6:

Table 4-6: Wall lengths investigated

		Length of Wall (m)	
Storeys	Height (m)	Aspect Ratio 3	Aspect Ratio 5
3	10.4	3.47	2.08
5	16.8	5.60	3.36
7	23.2	7.73	4.64

4.7 Methodology

The previous chapters explored the main factors to consider when assessing the behaviour factor. A summary of the considerations for SSI with reinforced structural walls is repeated here for ease of flow:

- SSI influences ductility.
- SSI influences damping.
- SSI lengthens period.
- *R-μ-T* relationships are approximations.
- Code defined behaviour factors can rely on other influences that are not related to the strict definition of *q*.
- Behaviour factors for the same structural system vary significantly for different design codes.

Given the approximate nature of the behaviour factor, this study assesses the current value for the behaviour factor of reinforced structural walls and the influence of SSI, rather than trying to establish an exact value. This section sets out the procedure used in a stepwise manner.

Step 1: Equivalent lateral force procedure

A reinforced structural wall system with a fixed base is analysed using the equivalent later force method as prescribed by SANS 10160-4 (2017). The design base shear is calculated assuming a behaviour factor of 5. Equation (2.36) is repeated here for reference and ease of flow.

$$V_n = S_{Ad}(T, a_g, q) \times W_n$$

Figure 4-9 illustrate the initial step to obtain the base shear, V_n from the response spectrum.

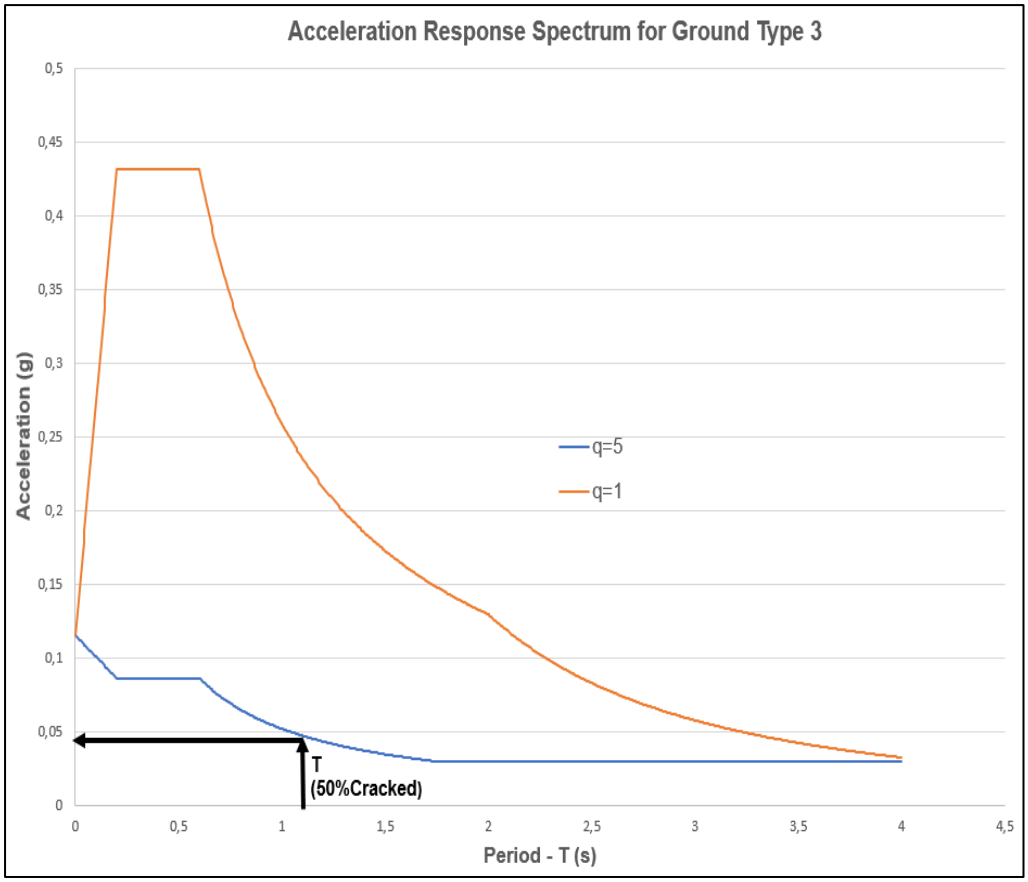

Figure 4-9: Pseudo acceleration from initial period

The fundamental period of vibration is determined using eigenvalue analysis assuming structural wall stiffness as 50% of the elastic stiffness (0.5EI). The iterative procedure described in Section 2.4 is considered more accurate. However, codes intentionally provide formulae to produce short periods and therefore conservatively large design base shears, which is an additional redundancy considered when specifying behaviour factors. The period associated with the 50% elastic stiffness will produce the lowest design base shear allowable within the framework of SANS 10160-4 (2017).

When accounting for SSI, however, as the base size decreases the hinge mechanism moves from the shear wall to base, therefore protecting the structural wall, making the initial prediction of the cracked stiffness more difficult.

Step 2: Code design

The structural wall system is reinforced to resist the total fixed base moment, following capacity design principles. The wall boundary elements are detailed according to SANS 10160-4 (2017) *Annex C*. The structural frame is designed according to SANS 0100-1 (2000).

Step 3: Nonlinear static assessment (pushover analysis)

The nonlinear static procedure is used to produce a capacity curve for the designed building, which is shown in Figure 4-10.

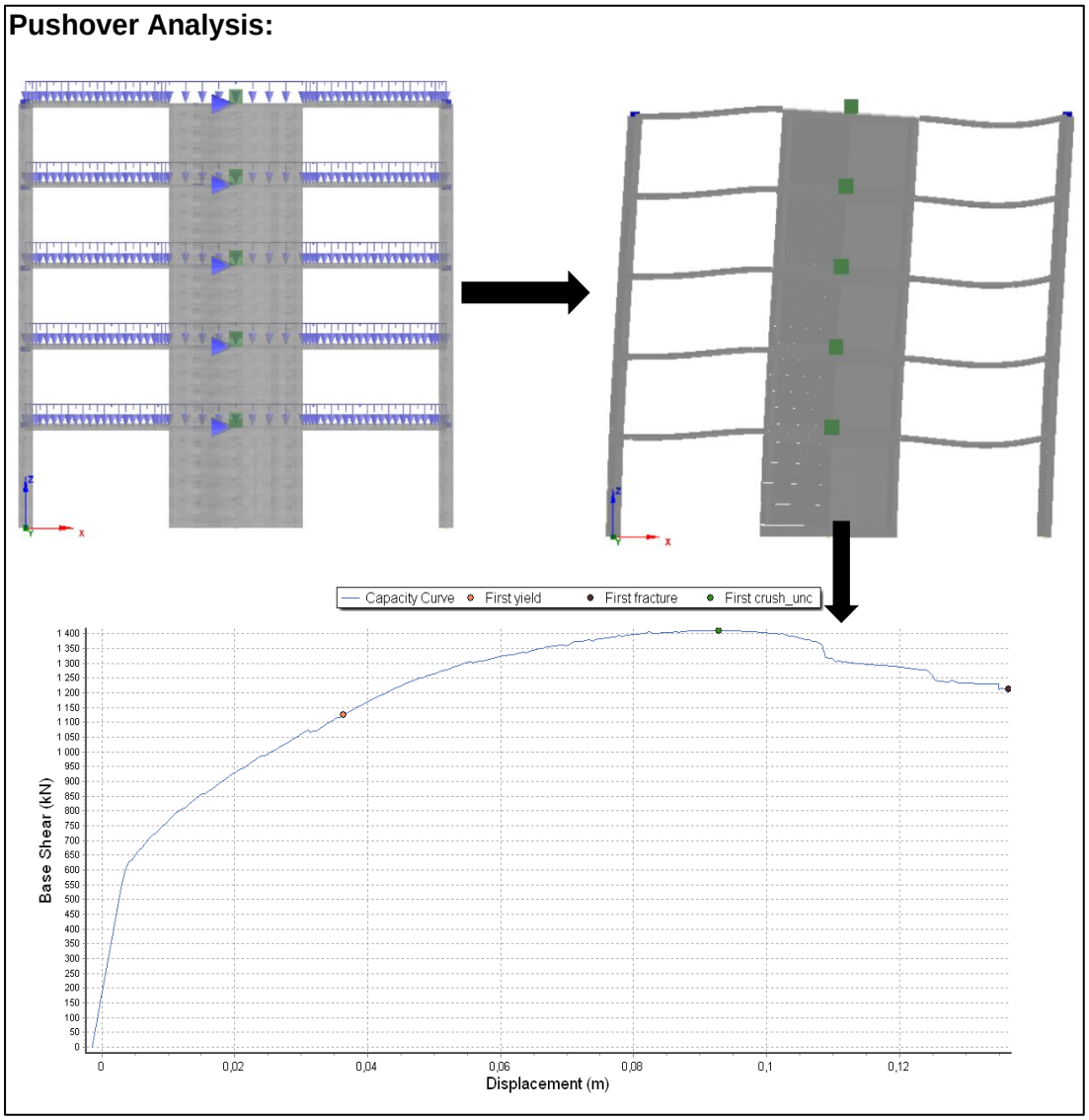

Figure 4-10: Capacity curve from pushover analysis

An idealised bilinear relationship is approximated from the capacity curve and a subsequent target displacement is calculated. As the ductility influences damping, an iterative procedure is used to adjust the equivalent damping and therefore the target displacement. The adjusted target displacement will in turn affect the ductility again, as shown in Figure 4-11. If the structural system reaches the target displacement without exceeding performance criteria, then the behaviour factor of 5 is acceptable. If not, the behaviour factor must be adjusted in step 1. Chapter 7 discusses and compares these methods in more detail.

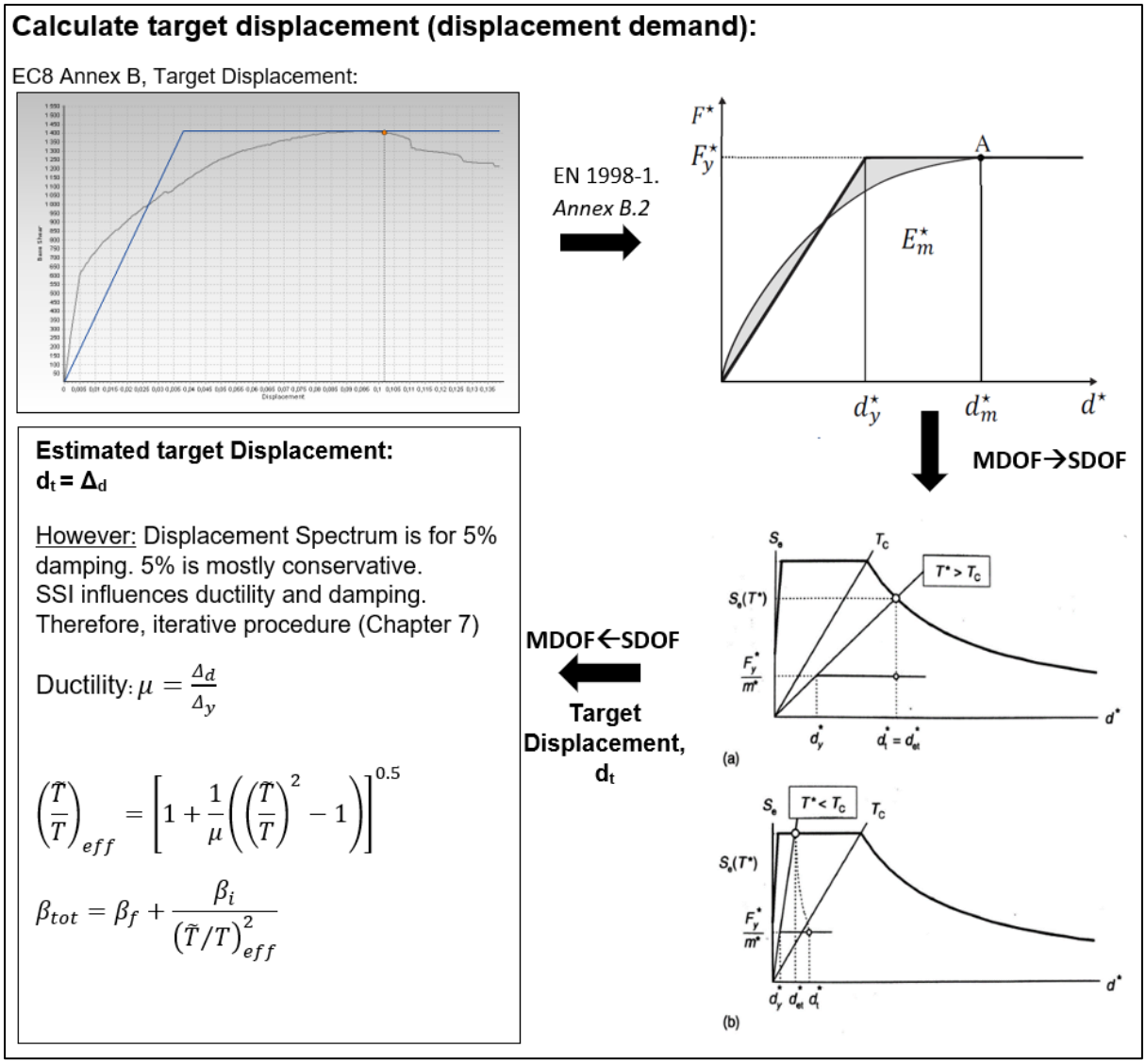

Figure 4-11: Target displacement from capacity curve

The pushover analysis forms the basis of the nonlinear assessment as it allows for a clear assessment of ductility. The capacity curve also indicates certain reliability by showing target displacement against displacements associated with structural failure. In addition to this, there is more consensus in guidelines on the use of SSI with the pushover analysis, as opposed to SSI in THA, where the specifications can involve complex variations in parameters that could detract from the main influences of the study. The THA's are therefore used as displacement response verification of the results from the pushover analyses.

Step 4: Reduce wall foundation size

The foundation size is reduced to resist a percentage of the fixed moment. As the foundation moment reduces, the contribution of the frame for stability will increase.

SSI will also influence the response as discussed in Section 2.7, therefore Steps 1 to 3 are repeated. The effects investigated in this study is defined as:

Step 1*: Longer fundamental period of vibration will produce smaller base shear, but larger displacement. Figure 4-12 and Figure 4-13 illustrate the effects of period lengthening on the response.

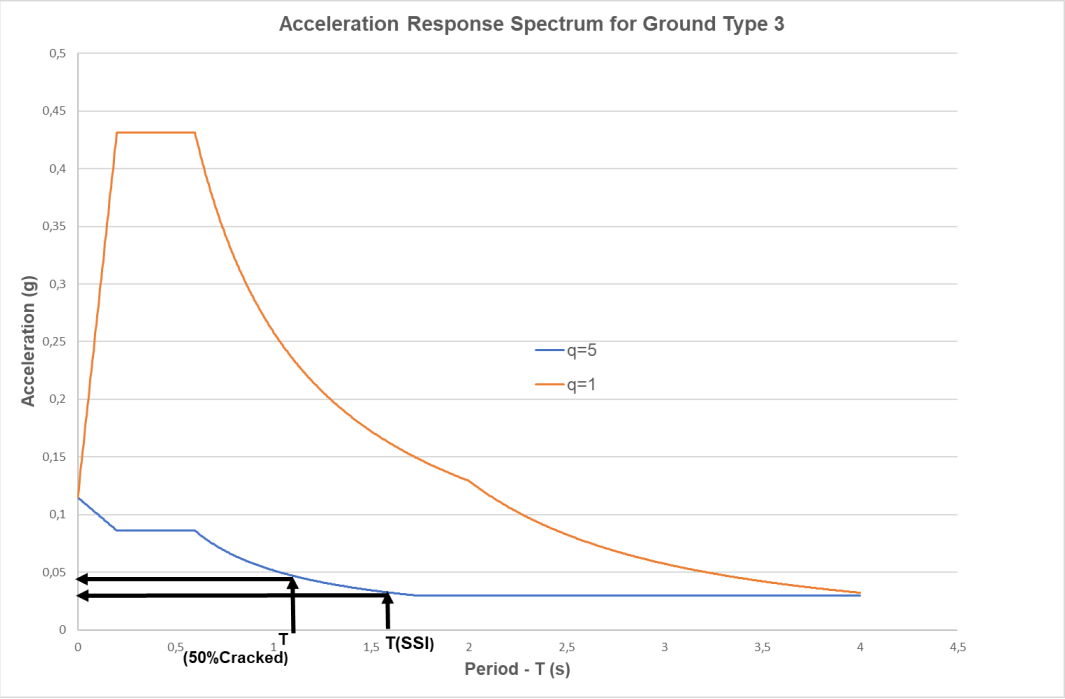

Figure 4-12: Acceleration response spectrum for Ground Type 3

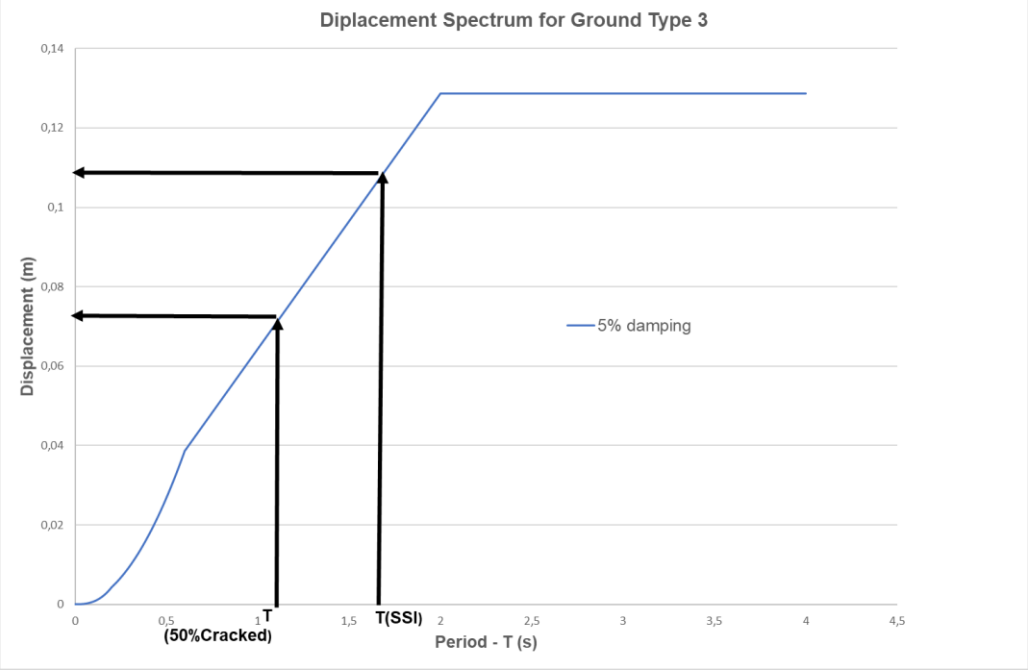

Figure 4-13: Displacement response spectrum for Ground Type 3

Step 2*: Lower design base shear forces will produce smaller foundation overturning moments. Reinforcement requirements for the wall will reduce, while the displacement response should increase.

Step 3*: SSI is incorporated in the models using BNWF models. SSI influences ductility and damping. The target displacement is calculated using the same iterative procedure, but foundation damping is accounted for. Figure 4-14 presents the expected influence of SSI on damping and ductility.

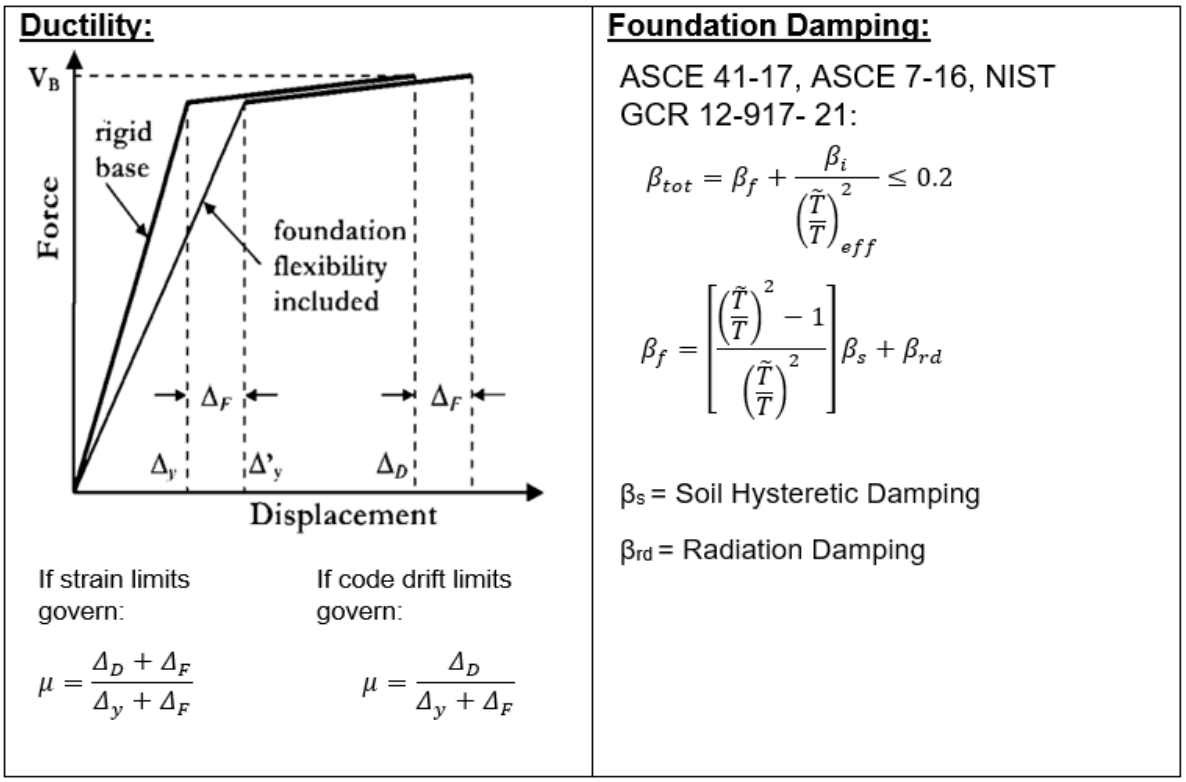

Figure 4-14: SSI effects on ductility and damping

This is repeated for wall foundation sizes with ultimate capacity of 80%,60% and 40% of the fixed moment conditions.

Step 5: Inelastic time-history analysis

Structural systems with reduced base sizes are tested with THA's. The displacement responses are used as an additional verification to determine whether the structures meet required demands. Three accelerograms obtained from PEER strong motion database are matched with South African conditions. Figure 4-15 illustrates typical spectral matching of ground motion records to the response spectrum of Ground Type 3.

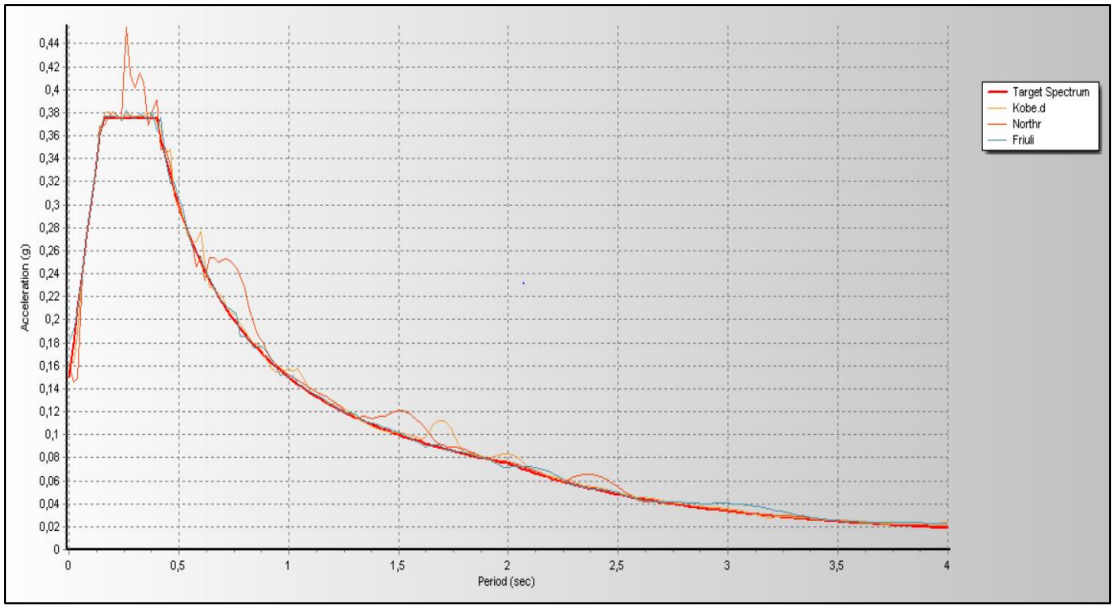

Figure 4-15: Illustration of spectrum matching

The ground acceleration used to calculate the target displacement in Step 3 and for spectrum matching in Step 5 is 0.15g and not 0.1g as recommended by SANS 10160-4 (2017). This is addressed in Chapters 5 and 6.

5 Codified design requirements

This chapter sets out the linear approach followed using standard design requirements and detailing procedures according to South African guidelines. The incorporation of SSI in linear seismic analyses is introduced together with the initial design assumptions.

5.1 Equivalent static lateral force procedure

The equivalent static lateral force procedure is discussed in Section 2.8.1. The expression for base shear as defined in Equation (2.36) is repeated for ease of flow, with the summary of the initial assumption of the parameters.

$$V_n = S_{Ad}(T, q, a_g) \times W_n$$

T Period of vibration is calculated with eigenvalue analysis assuming 50% initial stiffness (0.5EI). Slight iteration is still necessary as the reinforcement affects the initial stiffness. The software program SeismoStruct was used for the eigenvalue analysis for the fixed base condition, as well as for the reduced base sizes taking SSI into account with explicitly modelling of a BNWF as described in Section 3.1.

q Behaviour factor of 5, as presented by SANS 10160-4 (2017) Table 4.

a_g SANS 10160-4 (2017) prescribes a peak ground acceleration (PGA) of 0.1g for all regions experiencing natural seismic activity in South Africa (Zone I regions), despite indicating higher nominal peak ground accelerations with a 10% probability of exceedance in 50 years in Figure A.1 of SANS 10160-4 (2017). The code committee deemed it inappropriate to increase the PGA magnitude, as one of the main motivations for revising the seismic loading code was due to the perception from engineers that the PGA was too conservative. To overcome this concern, the lower limit of the redundancy factor borrowed from Uniform Building Code:1997 (UBC) was rather adjusted to effectively increase the PGA from 0.1g to between 0.12g and 0.15g (Retief & Dunaiski, 2009, pp. 173-174). Remaining consistent with SANS

10160-4 (2017), a PGA of 0.1g together with the redundancy factor are used for design, however, a PGA of 0.15g is used for assessment of the structures utilising nonlinear methods.

Ground Type — SANS 10160-4 (2017) Ground Type 3, corresponding to EN 1998-1 (2004) Ground Type C, was used for all assessments.

W_n — The nominally sustained vertical load is defined by SANS 10160-4 as:

$$W_n = G_n + \sum_i \varphi_i \times Q_{ni} \qquad (5.1)$$

G_n is the permanent load (or Dead Load) and Q_{ni} is the imposed load (or Live Load). The combination factor, $\varphi = 0.3$, as taken from Table 2 of SANS 10160-1 (2011).

The base shear is distributed per floor using Equation (2.38).

ASCE/SEI 7-16 (2016) limits the reduction in design base shear when SSI is considered in the equivalent static lateral force procedure. ASCE/SEI 7-16 equations 19.2-1 and 19.2-3 is repeated as Equations (5.2) and (5.3).

$$\tilde{V} = V - \Delta V \geq \alpha V \qquad (5.2)$$

$$\alpha = \begin{cases} 0.7 & R \leq 3 \\ 0.5 + R/15 & 3 < R < 6 \\ 0.9 & R \geq 6 \end{cases} \qquad (5.3)$$

$$R \; is \; the \; response \; modification \; factor \; (force - reduction \; factor)$$

Interestingly, it is observed that the limits relate to the behaviour factor (or force-reduction factor). The commentary chapters of ASCE/SEI 7-16, section C19.2 states "*the limitation on potential reductions caused by SSI reflects the limited understanding of how the effects of SSI interact with the R factor*".

No limits were placed on the reduction of the base shear for the purposes of this investigation.

The redundancy factor is intended to award designers when more or longer structural walls are used (Retief & Dunaiski, 2009, p. 174). SANS 10160-4 (2017) uses the limits

on the redundancy factor as an arbitrary factor to increase the PGA. The redundancy factor in SANS 10160-4 (2017) equation 6 is repeated as Equation (5.4):

$$\rho = 2 - \frac{6.1}{r_{max}\sqrt{A_B}} \qquad 1.2 \leq \rho \leq 1.5 \qquad (5.4)$$

Where;

A_B Ground floor area of the structure or average floor area where setbacks occur at higher levels

r_{max} Maximum storey shear ratio. For a given direction of loading and for a given storey, I, the storey shear ratio, r_i is the ratio of the design storey shear in the most heavily loaded single element divided by the total design storey shear. The maximum value of, r_i for the lower two-thirds height of the building is, r_{max}.

An increase in the lateral load resisting elements results in a corresponding reduction in the redundancy factor.

Torsional effects are accounted for by complying with SANS 10160-4 (2017), 8.5.4.3: "*The torsional moments, M_{tn} on the structure shall be considered in the design as caused by assumed displacement of the mass each way from its actual location by a distance equal to 5 % of the dimensions of the building perpendicular to the direction of the applied forces".* The eccentricity, *e* indicated in Figure 4-2 is calculated as *0.05 x 42600 = 2130 mm*.

5.2 Capacity design

The principle of capacity design is described in Chapter 1. The hinge position for structural wall buildings, called the critical region, is identified from the base up to, typically, the first storey. The concrete in the critical region is reinforced with confinement reinforcement, called boundary elements, in areas where high strains are expected to occur. The confined concrete can accommodate much higher strains and therefore provides ductility resistance in the critical region in order to protect the brittle

elements of the structure. The principle can be explained with the simple chain analogy shown in Figure 5-1.

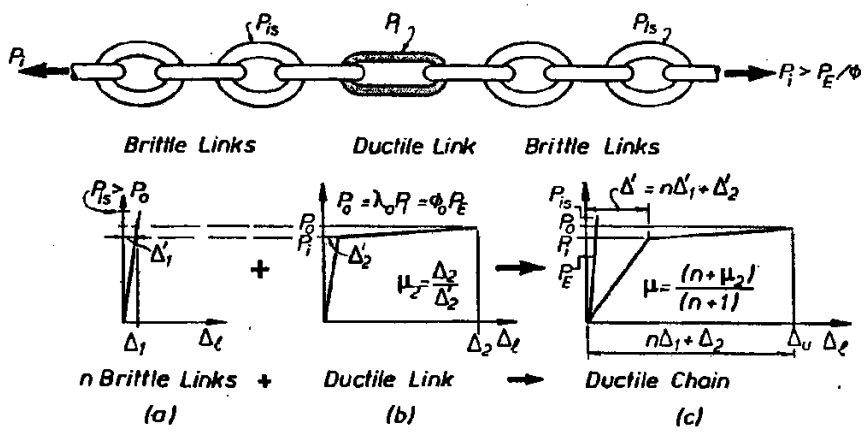

Figure 5-1: Illustration of the capacity design principle (Pauley & Priestley, 1992, p. 40)

The strength of the chain is the strength of the weakest link. Ductility can be achieved for the entire chain by one ductile link. If the brittle links have higher strength than the ductile link, it is protected against failure during large, imposed deformations.

Critical region: SANS 10160-4 (2017) identifies the vertical plastic region, h_{pl} (critical region) with reference to Figure 5-2 as:

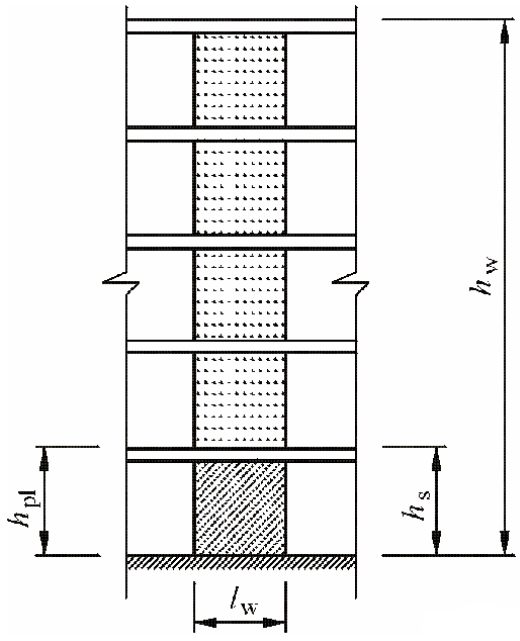

$h_{pl} > l_w \; and \; h_{pl} \geq h_w/6$

If $h_s \geq \frac{2l_w}{3} \; and \; h_s \geq \frac{h_w}{9}$ are both complied with, then $h_{pl} = h_s$.

h_s - height of the storey

h_w - height of the wall

l_w - length of the wall

Figure 5-2: Height of the plastic region at the base of structural walls (SANS 10160-4, 2017, pp. 42-44)

EN 1998-1 (2004, 5.4.3.4.2) similarly defines the critical region (h_{cr}), but also limits the vertical extent to:

$$h_{cr} \leq \begin{cases} 2l_w \\ \begin{cases} h_s \ for\ n \leq 6\ storeys \\ 2h_s \ for\ n \geq 7 storeys \end{cases} \end{cases} \quad (5.5)$$

The requirements of the plastic region according to SANS 10160-4 (2017) are followed in this investigation.

Boundary elements: SANS 10160-4 (2017) defines the boundary elements as the regions where the extreme fibre compressive stress exceeds $0.20f_{cu}$. The boundary element can be discontinued where the compressive stress is less than $0.15f_{cu}$. For this simplification, the stresses are prescribed to be calculated using a linear elastic model and gross cross-sectional properties, where f_{cu} is the concrete characteristic cube compressive strength. For structural walls with critical regions as defined above, clause C.3.1.2.7 of SANS 10160-4 (2017) defines the extent of the boundary element length, l_c as not less than the larger of $x_n - 0.1l_w$ and $x_n/2$. Where x_n is the depth of the neutral axis and can be simplified in accordance with clause C.3.1.2.2 of SANS 10160-4 (2017) as $x_n = l_w/4$.

EN 1998-1 (2004) provides additional limits to the boundary elements regarding wall width, $l_c \geq 1.5b_w$. The width for all structural walls is taken as 300 mm, as addressed in Chapter 4.3, therefore this limit equates to 450 mm. This, together with the specifications of SANS 10160-4 (2017), are adhered to in determining the boundary element length for this study.

The reinforcement requirements for the boundary elements are intended to provide the region with enough confinement to provide sufficient ductility for the structural system. SANS 10160-4 provides the following requirements for the boundary element transverse reinforcement through Equations (5.6) to (5.10):

$$A_{sb} \geq 0.077 \times s_x \times h_c \times \frac{f_{cu}}{f_{yh}} \quad (5.6)$$

$$s_x < 100 + \frac{350 - h_x}{3} \quad (5.7)$$

$$s_x < h_x/4 \quad (5.8)$$

$$s_x \geq 6 \times longitudinal\ bar\ diameter \quad (5.9)$$

$$100\ mm < s_x < 150\ mm \qquad (5.10)$$

Where;

A_{sb} is the area of confinement reinforcement in the boundary zone (mm^2).

s_x is the vertical spacing of confinement reinforcement in the boundary element (mm).

h_c is the dimension of the boundary element in the direction under consideration (mm).

h_x is the maximum horizontal spacing of legs of confinement reinforcement (mm).

f_{cu} is the concrete characteristic strength in megapascals (MPa).

f_{yh} is the specified yield strength of the confining reinforcement in megapascals (MPa).

Figure 5-3 shows the boundary elements as specified for structural walls in SANS 10160-4 (2017).

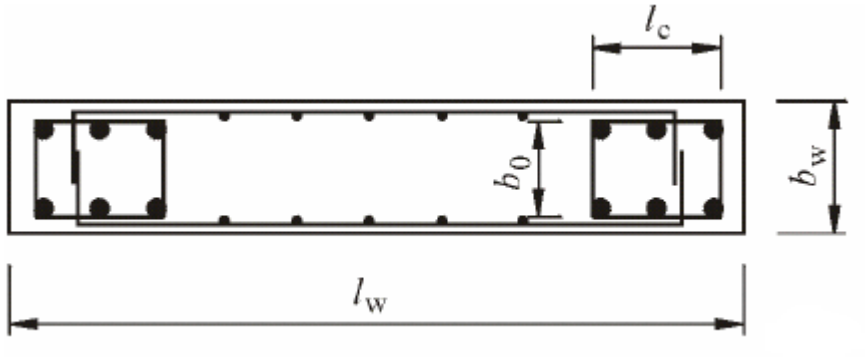

Figure 5-3: Boundary elements in wall section (SANS 10160-4, 2017, Annex C)

SANS 10160-4 (2017) does not provide lower limits on the percentage longitudinal reinforcement in the boundary element. SANS 0100-1 (2000), 4.11.4.2.3, specifies a limit of 0.4% of the gross-sectional area for a wall to be regarded as a structural wall and 1% (clause 4.11.4.2.4) for fire resistance. EN 1998-1 (2004) is more detailed in its specifications for the critical region and prescribes the minimum reinforcement in structural walls as:

$0.2\% \leq \rho_w \leq 4\%$ Reinforcing content in the web, ρ_w (between boundary elements).

$0.5\% \leq \rho_e$	Reinforcing content in the boundary element, ρ_e.
$\rho_t \leq 4\%$	Total reinforcing content, ρ_t.

The specifications of the boundary elements according to SANS 10160-4, together with EN 1998-1 guidelines for the minimum reinforcement are complied with in this investigation. The difference in the stress-strain relationship between confined and unconfined concrete is addressed in Chapter 6.

When SSI is included in the analysis and the foundations are incrementally reduced, the hinge mechanism will move from the wall to the foundation-soil interface and contributing frame. The assumption of the critical/plastic region length may change from the fixed base condition assumed by codes, however, the requirements for the plastic region length as prescribed by SANS 10160-4 (2017) are adhered to for all foundation sizes in this investigation.

Flexural resistance: An approach based on Pauley & Priestley (1992) given in Bachmann, et al. (2002, pp. 137-139) is used to determine the flexural strength of the reinforced concrete walls. This approach is adapted to comply with traditional assumptions regarding the equivalent compressive stress block used in SANS 0100-1 (2000). Figure 5-4 shows the adapted stress block and lever-arms.

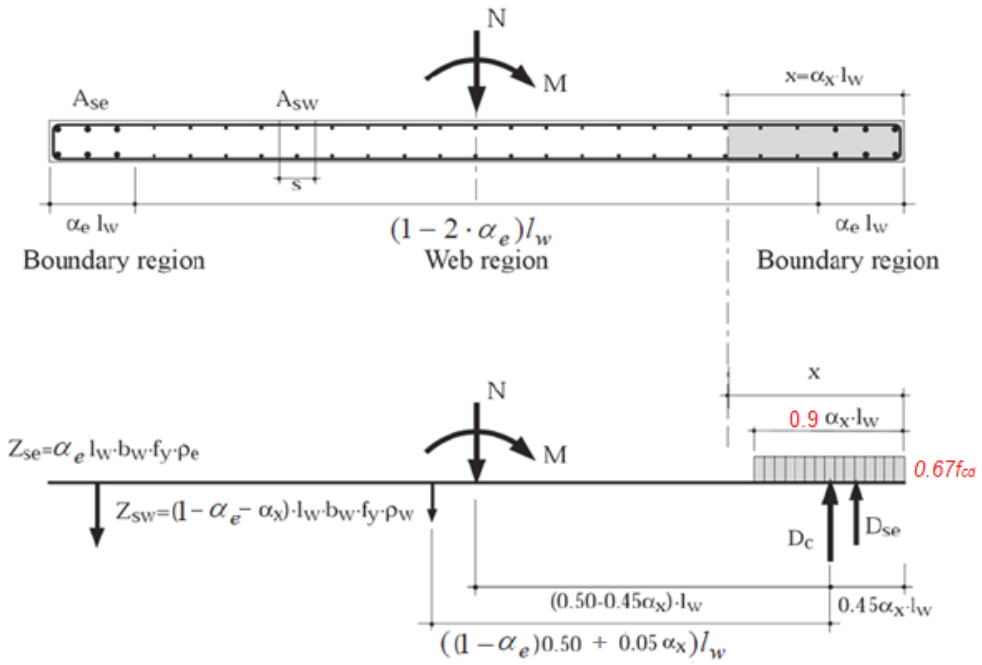

Figure 5-4: Wall flexural strength design procedure (Bachmann, et al., 2002, pp. 137-139) adapted to comply with stress block assumptions used in SANS 0100-1 (2000)

The following idealised assumptions are made (Monteiro, 2019, L6 Ss. 34-35):

- The reinforcing steel has an elastic-perfectly plastic stress-strain relationship.
- The reinforcing in both the boundary elements and the web yield.
- The confined boundary element reinforcement contributes to the compression resistance.
- The unconfined reinforcement in the web does not contribute to the compression resistance.

The notations in Figure 5-4 are defined as:

N	Axial load applied to the wall.
M	Internal bending moment about the strong axis of the wall.
l_w	Wall length.
b_w	Wall width.
f_y	Design steel yield strength.

f_{cd}	Design compressive cube strength.	
x_n	Distance from the extreme compressive fibres to the neutral axis.	
$\alpha_x = \frac{x_n}{l_w}$	Neutral axis length to length of wall.	(5.11)
$\alpha_e = \frac{l_c}{l_w}$	Boundary element length to length of wall.	(5.12)
$\rho_e = \frac{A_{se}}{l_c \cdot b_w}$	Boundary element steel reinforcement ratio.	(5.13)
$\rho_w = \frac{A_{sw}}{s \cdot b_w}$	Web steel reinforcement ratio.	(5.14)
$\rho_t = \frac{A_{st}}{l_w \cdot b_w}$	Total steel reinforcement ratio.	(5.15)
$\omega_e = \rho_e \frac{f_y}{f_{cd}}$	Boundary element reinforcement yield-crush factor.	(5.16)
$\omega_w = \rho_w \frac{f_y}{f_{cd}}$	Web reinforcement yield-crush factor.	(5.17)
$\omega_t = \rho_t \frac{f_y}{f_{cd}}$	Total reinforcement yield-crush factor.	(5.18)
$n = \frac{N}{l_w \cdot b_w \cdot f_{cd}}$	Axial load ratio.	(5.19)
$m_w = \frac{M}{l_w^2 \cdot b_w \cdot f_{cd}}$	Bending moment ratio.	(5.20)

The internal forces are:

$Z_{se} = \alpha_e \cdot l_w \cdot\ b_w \cdot f_y \cdot \rho_e$	Steel tensile force in boundary element.	(5.21)
$Z_{sw} = (1 - \alpha_e - \alpha_w) \cdot l_w \cdot\ b_w \cdot f_y \cdot \rho_w$	Steel tensile force in web.	(5.22)
$D_c = 0.67 \times 0.9 \times l_w \cdot\ b_w \cdot f_{cd}$	Concrete compression force.	(5.23)
$D_{se} = \alpha_e \cdot l_w \cdot\ b_w \cdot f_y \cdot \rho_e$	Steel compression force in boundary element.	(5.24)

Equations (5.25) and (5.26) can be determined from equilibrium.

$$\alpha_x = \frac{n + (1 - \alpha_e) \cdot \omega_w}{0.95 \times 0.67 + \omega_w} \quad (5.25)$$

$$m_w = \left(\frac{1 - \alpha_e}{2}\right) \cdot \omega_t + (0.5 - 0.45 \cdot \alpha_x) \cdot n + \left[\frac{\alpha_e - \alpha_e^2}{2} + 0.45 \cdot (\alpha_e - 1) \cdot \alpha_x - 0.05 \cdot \alpha_x^2\right] \cdot \omega_w \quad (5.26)$$

The bending moment resistance, M can be determined from Equation (5.20) Resulting moment resistance from the above procedure agreed with the moment-curvature analyses performed with Response-2000, reinforced concrete sectional analysis software. Previous comparisons with this procedure adapted to SANS 10100 found it to be sufficiently accurate (Le Roux, 2010, p. 71).

Tension shift: The shear in deep sections can significantly change the direction of the cracks during cyclic loading. This invalidates the initial assumption that plane cross sections remain plane. Figure 5-5 illustrates the tension shift effect.

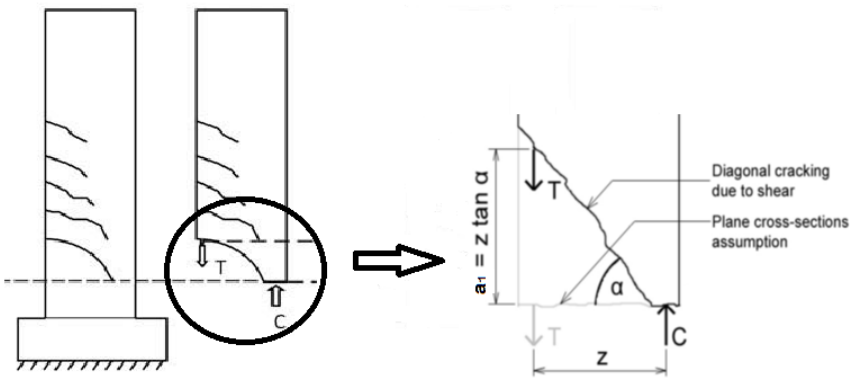

Figure 5-5: Tension shift effect (Feng, et al., 2014)

EN 1998-1 accommodates this effect by moving the moment envelope up by a factor, a_1 as shown in Figure 5-6.

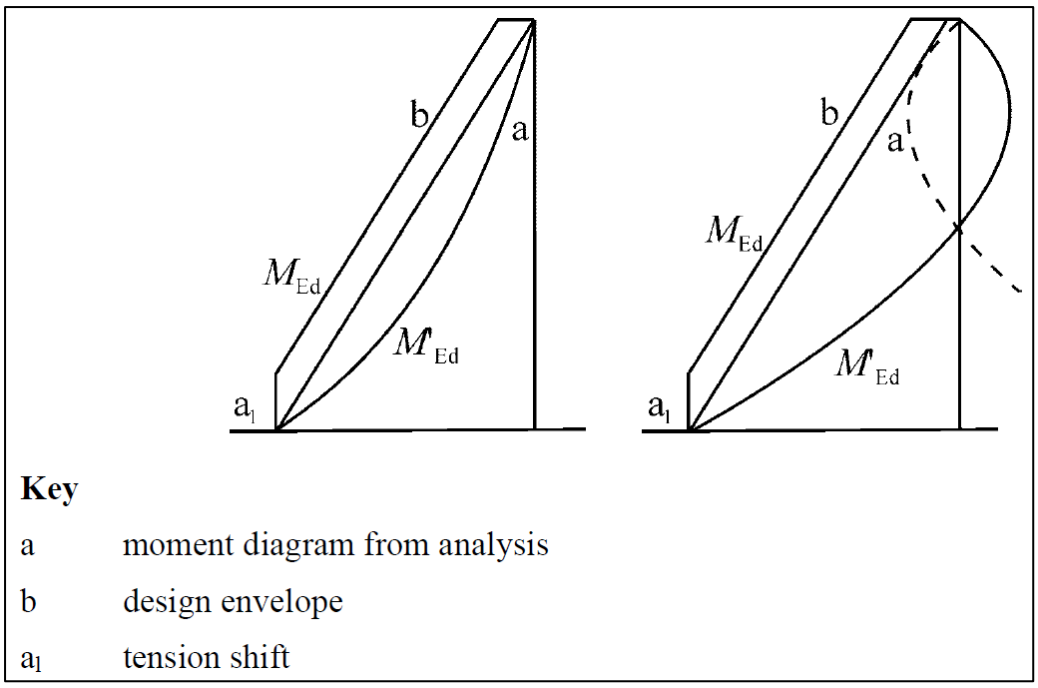

Figure 5-6: Design envelope for bending moments in slender walls (EN 1998-1, 2004, Figure 5.3)

Conservatively, it may be assumed that $\alpha = 45°$ and the lever arm, z = l_w. Then a_1 is equal to the length of the wall, l_w.

Shear resistance: The behaviour factor for structural walls is associated with flexural, ductile response. This study does not investigate the brittle failure associated with shear. It is assumed that the structural walls can adequately resist the shear forces caused by seismic action. As presented in the analogy illustrated in Figure 5-1, the superior strength of the brittle elements remains an important aspect of capacity design. It is therefore essential to design for the correct shear force envelope and the associated overstrength requirements to ensure ductile behaviour. The reader is referred to EN 1998-1, 2004, clauses 5.5.3.4.2 to 5.5.3.4.4 for the design requirements. SSI will, however, reduce the total equivalent base shear forces on the buildings through effects discussed in Section 2.7.

Foundation design: EN 1998-1 (2004) recommends that foundations are designed for overstrength moments to meet the capacity design assumptions about the critical region. The US standards take the opposite approach, which allows for a reduction in overturning moment at the base for uplift by 25% for linear static analysis or up to 10% for a response spectrum analysis (Fardis, et al., 2005, p. 78).

The fixed base condition (where the wall is assumed to be fixed to a rigid support) is used as the reference moment from which to reduce the foundation size to produce a lower percentage moment (for example 80%,60%,40%). The foundation size of the fixed base condition is not of interest, therefore no overstrength moment is used.

5.3 Frame contribution

Consider the typical frame model shown in Figure 5-7.

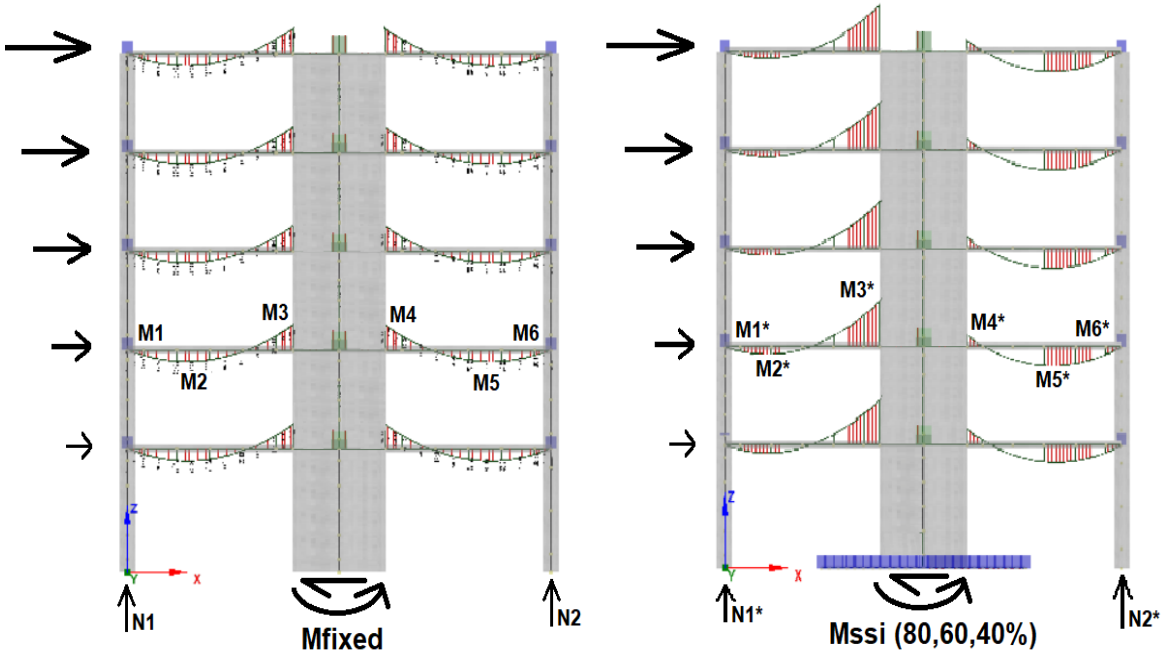

Figure 5-7: Frame contribution (Left: Fixed base condition, Right: Reduced base moment)

With the fixed base condition, the wall is generally stiff enough to attract most of the lateral inertial forces. The horizontal elements will have little contribution to the lateral resistance. The gravity combination dominates the design envelope for the frame. The gravity combination presented in Equation (5.27) is taken from SANS 10160-2 (2011).

$$W_n = 1.2G_n + 1.6Q_n \qquad (5.27)$$

As the wall slenderness increases the seismic load combination contributes more to the design envelope of the horizontal elements.

In the reduced foundation cases with SSI accounted for, the horizontal elements contribute more to the lateral stability. The contribution increases as the foundation sizes are reduced. Table 5-1 and Table 5-2 list the expected change in bending

moment and axial forces in the seismic load combination, with reference to Figure 5-7 for definitions.

Table 5-1: Design moment envelope

Position	Force/Moment Mfixed --> Mssi	Design Envelope considering reverse loading	
	Sagging Moment (+); Hogging Moment (-)	Sagging Moment (+)	Hogging Moment (-)
Support1	M1=M1*=0	Nominal Reinforcement Requirements	
Mid2	M2>M2*	Max(M2,M5,M2*,M5*)	Min(M2,M5,M2*,M5*)
Support3	M3>M3*	Max(M3,M4,M3*,M4*)	Min(M3,M4,M3*,M4*)
Support4	M4<M4*	Max(M3,M4,M3*,M4*)	Min(M3,M4,M3*,M4*)
Mid5	M5<M5*	Max(M2,M5,M2*,M5*)	Min(M2,M5,M2*,M5*)
Support6	M6=M6*=0	Nominal Reinforcement Requirements	

Table 5-2: Column design axial force envelope

Position	Axial Load Nfixed -->Nssi	Design Envelope Considering Reverse Loading
Column1	N1>N1*	Max(N1,N2,N1*,N2*)
Column2	N2<N2*	Max(N1,N2,N1*,N2*)

Note that there is a slight variation in moment diagram per level, due to the change in curvature of the wall. The moments indicated are for illustration purposes.

Reinforced concrete slabs: The slab members are designed with the equivalent frame procedure as set out by SANS 0100-1 (2000), clause 4.6.5. The panel width is taken as an edge panel, as described by Section 4.4. To accommodate the variation in the moment over the width of the panel, SANS 0100 (2000) separates the panel into a column strip and a middle strip. The apportionment of reinforcement between the two strips is prescribed in Table 5-3 below. This arrangement serves to protect the section against excessive cracking in order to achieve the assumed behaviour of an equivalent stress block over the entire panel.

Table 5-3: Distribution of moments in the panels of flat slabs (SANS 0100 (2000))

Moments	Apportionment between column strips and middle strips expressed as a percentage of the reinforcement for the total panel	
	Column Strip	Middle Strip
Negative	75%	25%
Positive	55%	45%

The distribution of reinforcement over the width of the panel would have a minor impact on ultimate flexural capacity and was not investigated in this study.

For an unbraced frame, SANS 0100-1 (2000) recommends that the sectional properties used to analyse moment transfers to columns should be based on half the width of the panel. The frames of this investigation are modelled in such a way that no moment transfer occurs between the slab and the columns and since the structural walls still brace the frame even with the reduced foundations, it is assumed that the full panel width is valid. Regardless, the panel width considered in this investigation is 3.3m, which is relatively small for typical buildings.

Reinforced concrete columns: The columns were designed to remain elastic, therefore not influencing the behaviour factor. Interaction diagrams generated with PROKON design software, together with South African design codes were used for the design of the columns. The assumptions in accordance with the relevant codes are summarised in Table 5-4.

Table 5-4: Column design assumptions

	Design Assumptions	Design Code
Slenderness:	Short Column	SANS 0100-1; 4.7.1.4
Stability:	Braced	SANS 0100-1; 4.7.1.3
End Conditions:	Partially fixed top, pinned bottom	SANS 0100-1; 4.7.1.6
Design concrete strength, *fcu*:	30MPa	
Design yield strength, *fy*:	450MPa	
Column height, bc:	600mm	
Column depth, hc:	600mm	
Required Longitudinal Reinforcement (Nominal)	4Y20 corners, 4Y12 mid (As = 0,04 x hc x bc)	SANS 0100-1; 4.11.4.2
Links:	R8-144	SABS 0144, 9.4
Typical cross section:	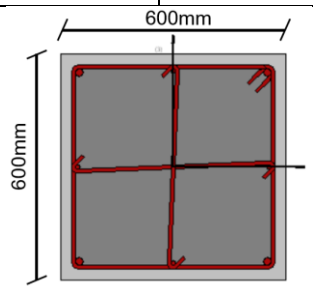	

The columns are still included in the nonlinear analyses, even though they are designed to remain elastic.

Question of compatibility: There is a possible compatibility problem with prescription of linear elastic design approaches. The lateral elastic displacement, d_e produced from linear elastic analyses with applied forces calculated from behaviour factors larger than 1, would not reflect the true deformed shape of the building and could underestimate the frame contribution, as the true deflection is expected to be nonlinear. The true lateral displacement could be much larger, which will affect the contribution of the horizontal elements to the lateral stability. SANS 10160-4 (2017) does not explicitly address this compatibility pitfall, but specifies inelastic displacement, d_s in clause 9.2 as:

$$d_s = 0.7q \times d_e \qquad (5.28)$$

This implies the equal displacement approximation. The full mass of the structure is used to calculate the base shear, instead of the modal mass. The mass participation for the first mode of vibration is likely to be less (approximately 70% of the full mass), therefore an adjustment factor of 0.7 is introduced.

It would make sense to perform additional elastic analyses with base shears applied to the structure as; $V_n = S_{Ad}(T, q = 1, a_g) \times W_n \times 0.7$, to produce more accurate displacement shapes when determining the secondary effects on the elements which are expected to remain elastic.

This investigation follows the typical design procedure for the elastic analyses according to SANS 10160-4 (2017). Updating the deformation profile in the elastic analyses will provide additional resistance to the structure, which is not the purpose of the investigation. The elastic deformations for the SSI models, however, are more realistic because the base rotation is modelled explicitly.

6 Nonlinear modelling

6.1 Component modelling

Figure 6-1 illustrates the typical elements used to model nonlinear behaviour, ranging from uniaxial spring or hinge models to fibre-type models or detailed continuum finite element models. Generally, all models rely on some level of idealised calibration to predict behaviour. The concentrated models, shown in Figure 6-1 (a), (b), (c), are based on calibrations at an overall component level, whereas the fibre and continuum finite elements models, shown in Figure 6-1 (d), (e) are calibrated at the material level (NIST GCR 17-917-46 v1, 2017, p. 2-17).

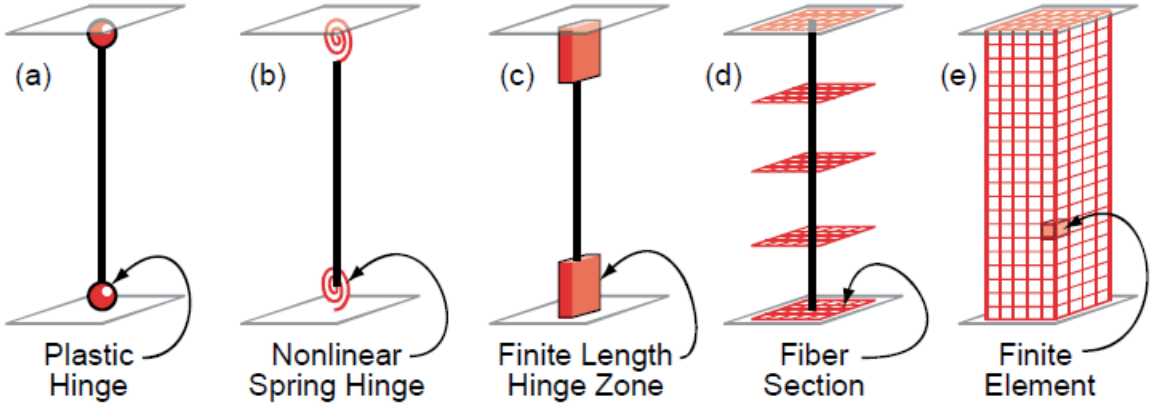

Figure 6-1: Range of structural model types (NIST GCR 17-917-46 v1, 2017)

The computer program SeismoStruct from Seismosoft (2020) is used for all nonlinear modelling. SeismoStruct predominantly uses the fibre section approach, whereby a member is represented by a series of cross-sections that are divided into a number of fibres, separately representing the concrete and the reinforcing steel. Each fibre consists of its own associated uniaxial stress-strain relationship. The fibres are then integrated to obtain the stress-strain state of the section. Separate material rules are used for confined and unconfined concrete. Figure 6-2 shows a typical reinforced concrete cross-section with the fibre element approach.

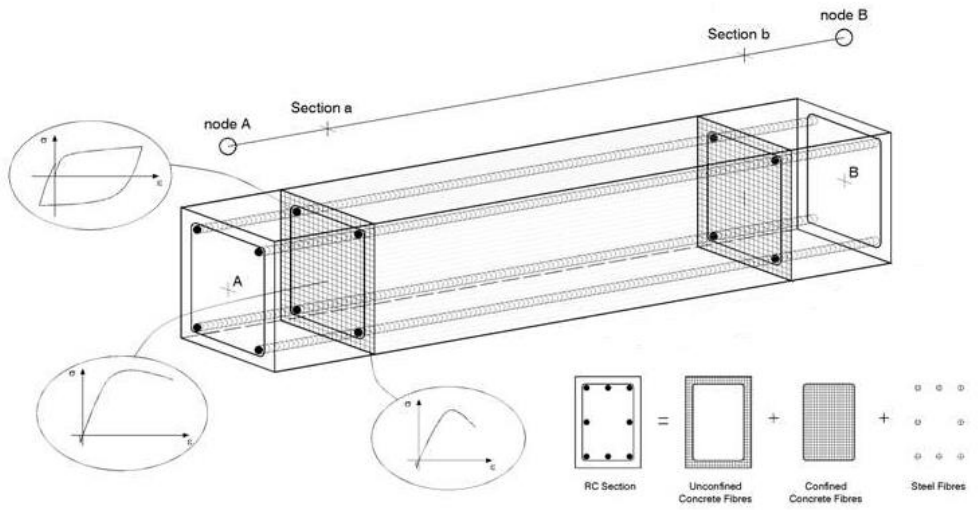

Figure 6-2: Typical reinforced concrete fibre element member (Seismosoft User Manual, 2020, p. 297)

Priestley, et al. (2007, pp. 195-196) and SeismoSoft user manual (2020, p. 297) defines some of the advantages and disadvantages of using fibre elements. The main considerations for this study are described as:

Advantages:

- No prior moment-curvature analysis of members is necessary.
- The hysteretic response is defined by the material properties, there is no need to introduce any element hysteretic responses.
- Direct modelling of axial load-bending moment interaction in both strength and stiffness.
- The member's post-peak strength reduction can be directly modelled.
- Straightforward representation of biaxial loading.
- Structural damping is directly modelled.

Disadvantages:

- Fibre elements model flexural response - shear strength and deformation are not modelled directly.
- The interaction between flexural ductility and shear strength is not modelled directly.
- Strain penetration requires special treatment.
- Excessive computing time for large models.

Nonlinear modelling for shear deformation in cracked reinforced concrete section under dynamic loading falls outside the scope of this study. However, shear deformation will increase the displacement capacity corresponding to strain-based flexural limit states (Priestley, et al., 2007, p. 185). Not considering shear deformation when testing whether the structures meet their corresponding displacement demands is therefore conservative. Furthermore, the additional assessments on ductility are based on the relative change in ductility (see Section 9.2). Shear deformation should not influence these results, provided that the method of analysis is consistent for all models.

Strain penetration into the base was not considered in this study, this simplification implies that the curvature in the base at the wall-foundation interface will immediately drop to zero. However, there will be strains in the wall tensile reinforcement to a depth of the true anchorage depth of the reinforcement into the base. The concrete compression strains will also gradually dissipate with depth into the base. Strain penetration will increase the effective plastic hinge length.

The modelling approach for each member is discussed in the following subsections.

6.1.1 Reinforced concrete slab

Figure 6-3 shows that the slab members are discretised into 6 integrated elements. Each of the individual elements consists of 3 built-in integrated sections as default. SeismoStruct (2020) allows for the variation in reinforcement within these integrated sections, effectively allowing the modeller to change the reinforcing requirements at short lengths. For this study, the reinforcement in the concrete slab can be adjusted at 0.2/3 x L, which equates to 400 mm for the 6m span in this study.

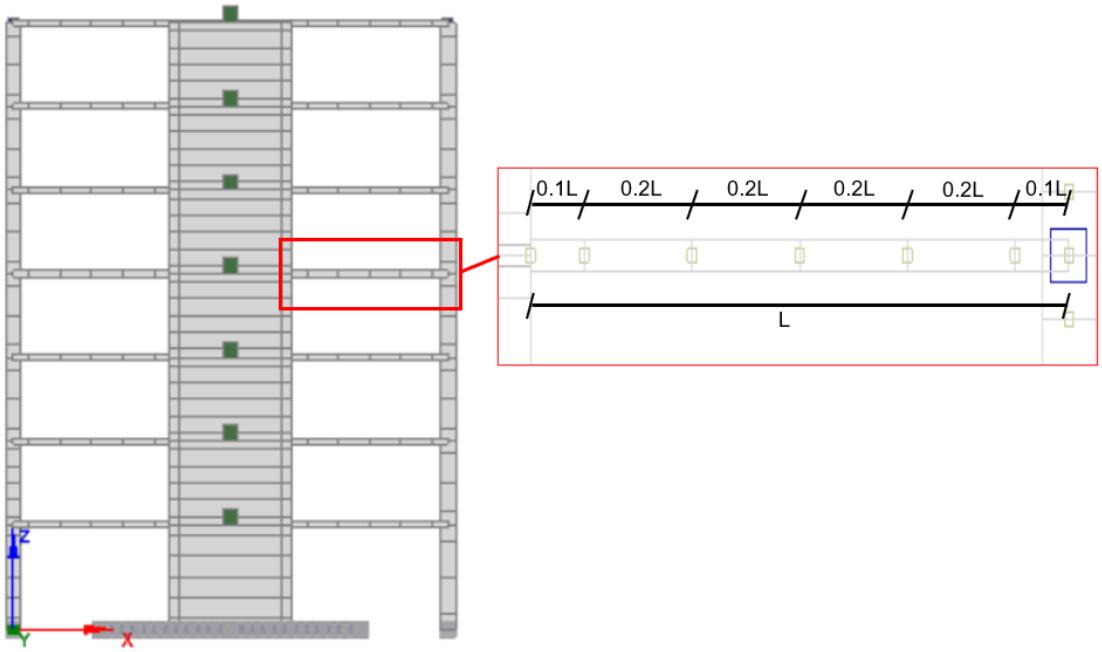

Figure 6-3: Slab element discretisation

This integrated arrangement also conforms with the typical simplified rules for top reinforcement curtailment in slabs under SANS 0100-1 (2000) clause 4.4.4.2.2. The top reinforcement over the continuous edge is extended to *0.3L* from the face of the support. In generally, this arrangement only applies when the dominant combination for the frame is the gravity load combination. The reinforcement is adapted as the bending moment profile changes when the frames contribute more to stability as the foundation size reduce.

The SeismoStruct user manual suggests that 5 to 7 integration elements per member will produce accurate results. Effectively, the member consists of 3x6 integrated elements.

The slab section shape is shown in Figure 6-4.

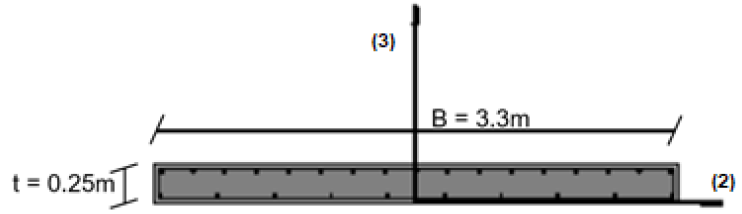

Figure 6-4: Slab cross-sectional shape

The slab width and thickness are discussed in Section 4.4. Note that the stirrup around the reinforcement is only a schematic illustration taken from the model. The concrete in the slab member is modelled as unconfined concrete.

6.1.2 Reinforced concrete structural wall

Figure 6-5 indicates the wall discretisation. The same principle as the slab members is used. Smaller elements close to the joints between wall elements and slab or base elements are used for better accuracy.

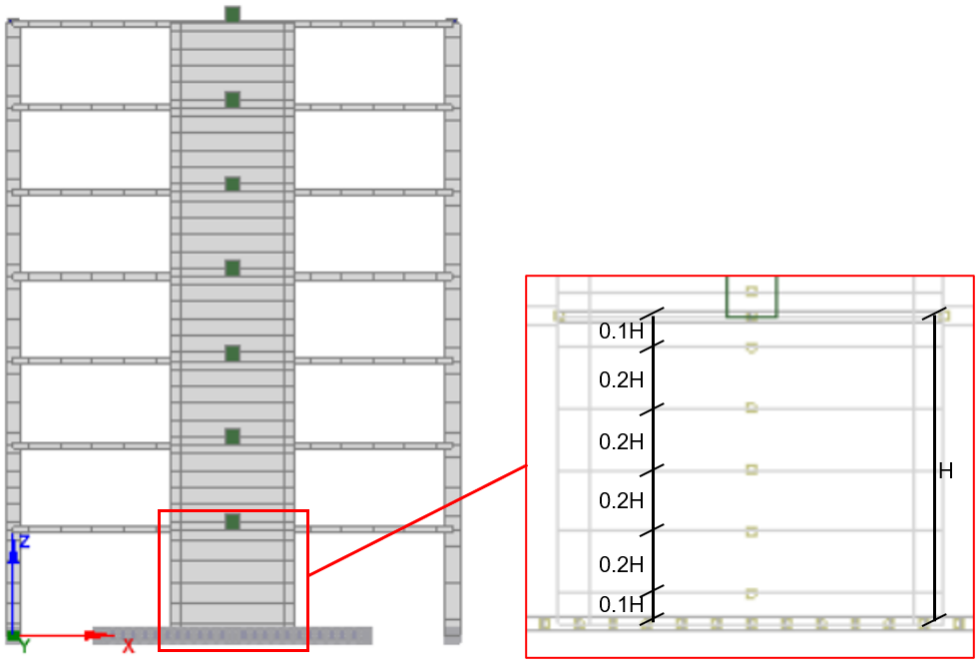

Figure 6-5: Wall element discretisation

Figure 6-6 shows a typical sectional shape. SeismoStruct allows for explicit detailing of the boundary elements. The concrete inside the boundary element is confined, which will enhance the ductility of the wall. The level of confinement and its stress-strain relationship is discussed in Section 6.2.

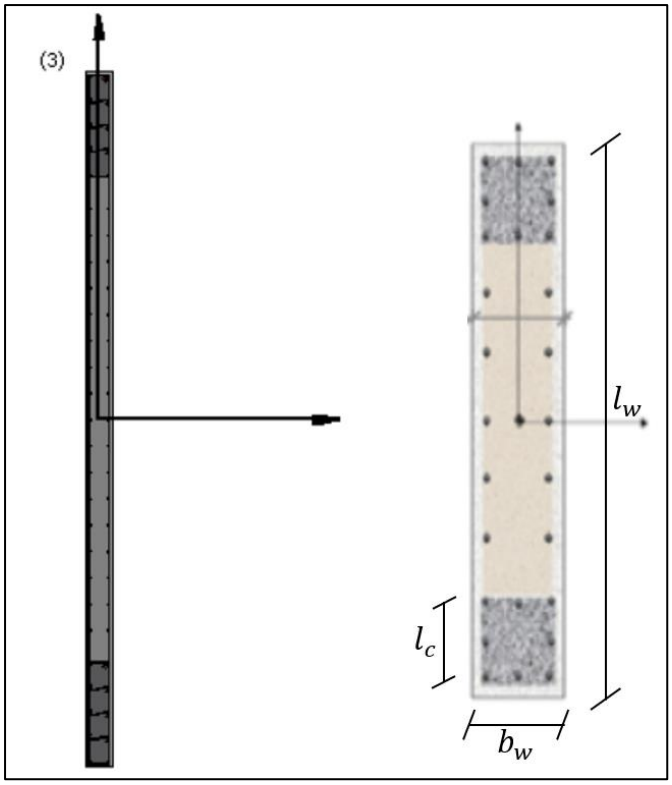

Figure 6-6: Wall cross-section

6.1.3 Foundation elements

Chapter 3 describes the BNWF approach used to model the foundation elements. As indicated in Figure 6-7, a rigid beam distributed over a set of zero-tension spring elements are used to represent the soil-foundation behaviour, each discussed separately here.

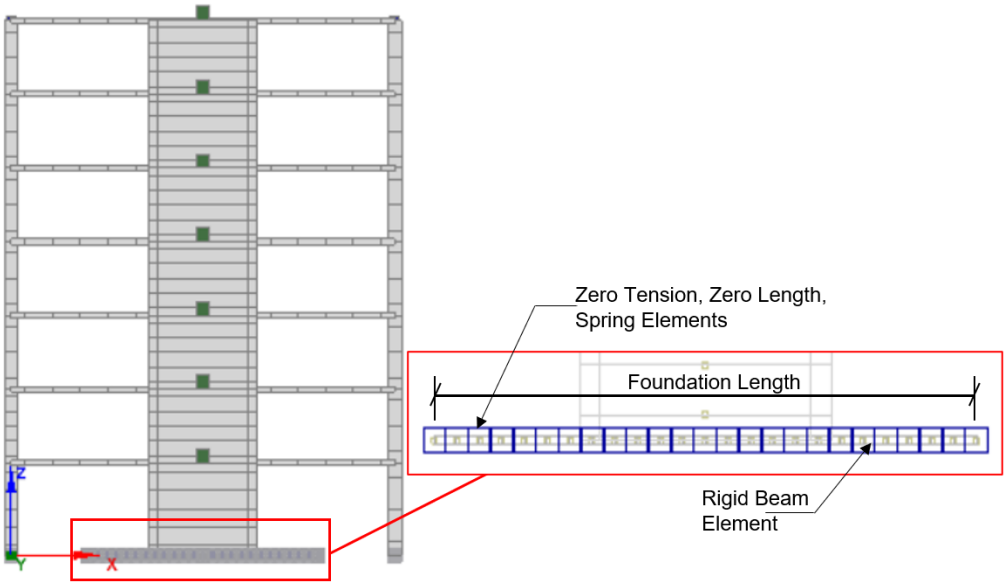

Figure 6-7: Foundation elements

Rigid beam elements: The foundations are modelled with sectional dimensions and density equal to the actual foundation, but with 100 times the elastic stiffness. Elements with larger stiffness cause numerical instability.

Zero-tension spring elements: For numerical stability and acceptable accuracy, NIST GCR 12-917-21 (2012, p. 2-39) recommends a minimum of 25 springs to represents the soil supports.

The stiffness and capacity of each spring element will depend on the spring tributary area and soil parameters. As an example, consider the same soil and foundation parameters provided in Chapter 3 as:

Expected Bearing Capacity, q_u:	$400\ kN/m^2$
Modulus of subgrade reaction, k_v:	$63\ 796.53\ kN/m^3$
Foundation length, *L*:	$10.2\ m$
Foundation width, *B*:	$1.6\ m$
Spring spacing:	$^{10.2}/_{24} = 0.425\ m$
Internal springs tributary area:	$0.425 \times 1.6 = 0.68\ m^2$
Spring capacity:	$0.68 \times 400 = 272\ kN$
Spring stiffness:	$0.68 \times 63\ 796.53 = 43\ 381.64\ kN/m$

Figure 6-8 presents the input table to model the properties in SeismoStruct. To model the zero-tension effects, a negative yield force of 0.0001kN is used, since SeismoStruct does not allow for an absolute zero value.

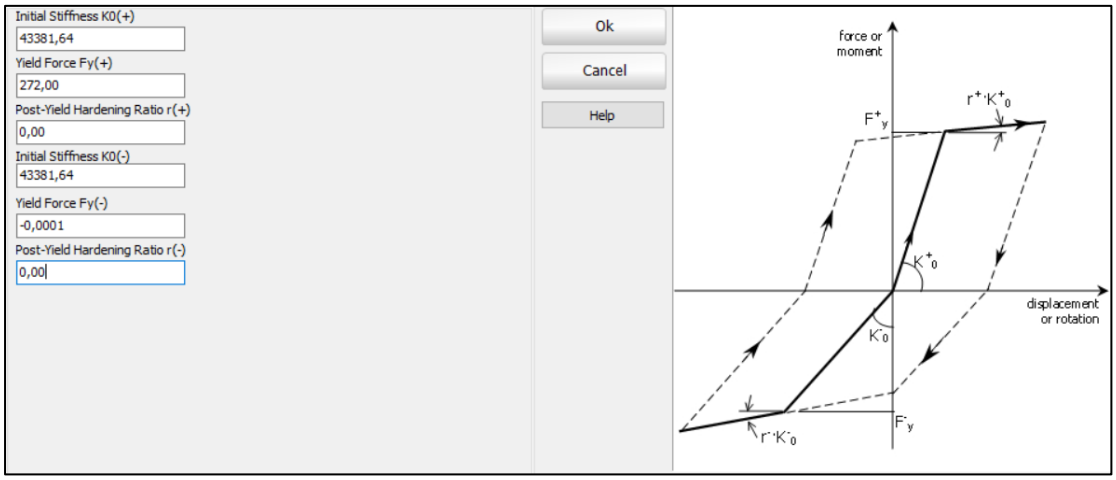

Figure 6-8: Modelled spring stiffness

In Chapter 3 it was shown that an arrangement with 25 springs and rigid elements with 100 times the elastic stiffness compares well with the predicted foundation behaviour.

6.1.4 Reinforced concrete columns

In Section 5.3 it is specified that the columns are designed to remain elastic. Nonlinear behaviour is therefore not expected, even so, the columns are included in the nonlinear assessment, with the discretisation of elements as shown in Figure 6-9. The column stirrups are expected to provide a level of confinement to the concrete core. The factor associated with confinement is discussed in Section 6.2.2.2.

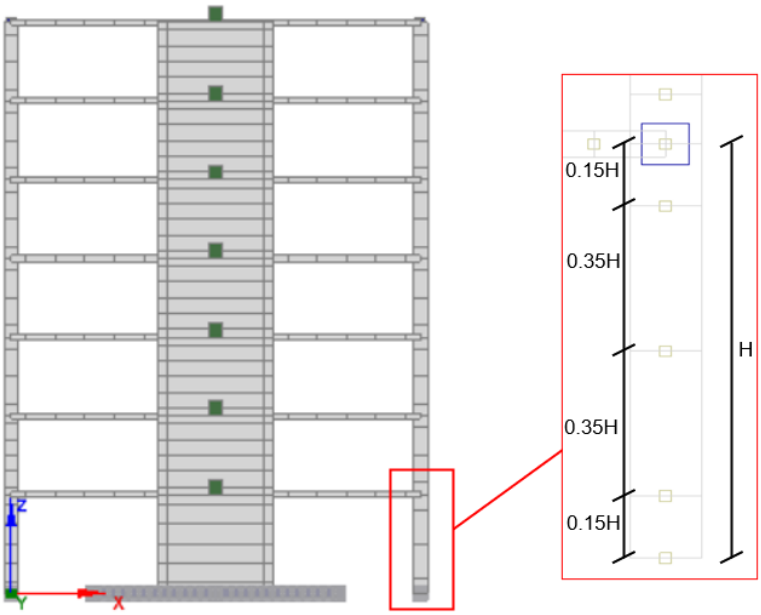

Figure 6-9: Column members

6.1.5 Joint modelling

Figure 6-10 illustrates the various joints modelled between members, each discussed separately below.

Figure 6-10: Joint modelling

Column-slab joint: To simulate bond-slip, a concentrated hinge element can be placed between the beam/slab fibre element and the column fibre element. Alternatively, the reinforced steel should be calibrated at the joint (NIST GCR 17-917-46 v1, 2017, p. 2-21).

Figure 6-11 illustrates the recommended modelling for bond slips in fibre models, according to NIST GCR 17-9147-46 v1 (2017).

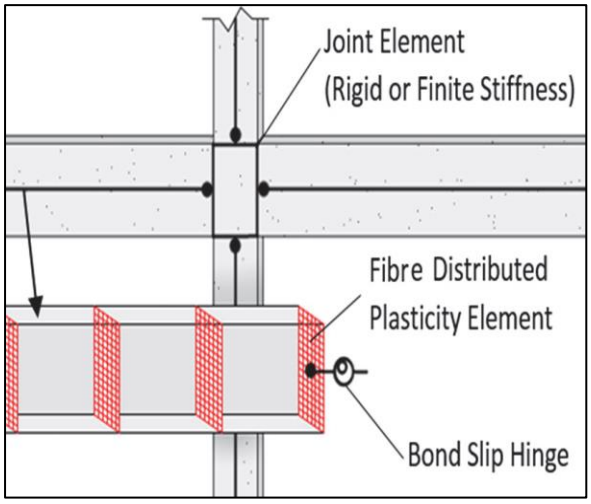

Figure 6-11: Recommended modelling for bond slip (NIST GCR 17-917-46 v1, 2017)

Bond slip occurs when the column-slab/beam joints experience excessive cracking, which causes the reinforcement to lose bondage with the concrete. This results in joint softening and increased frame flexibility. Figure 6-12 illustrates the principle.

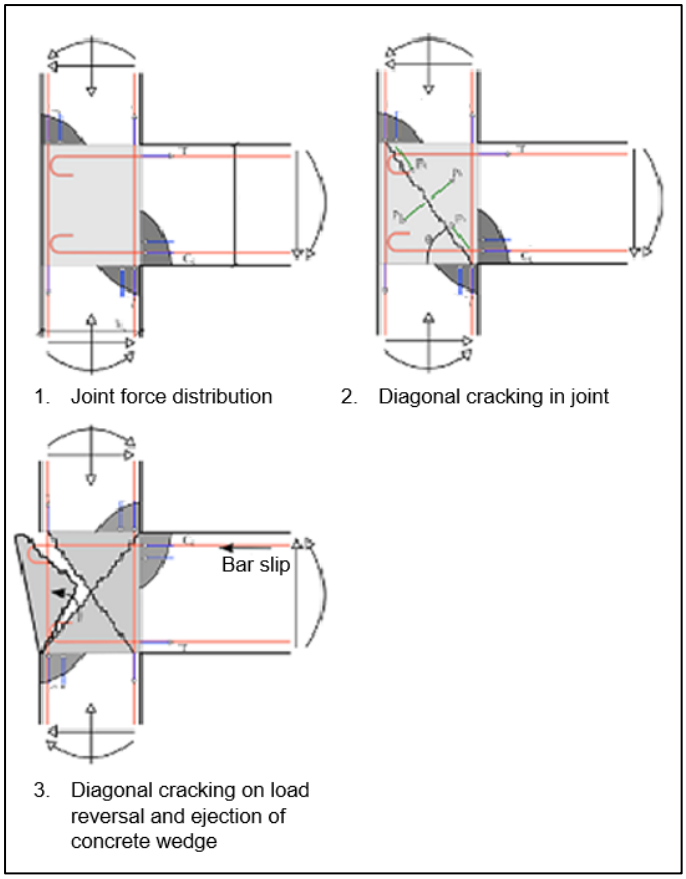

Figure 6-12: Bond slip mechanism (Monteiro & Palmer, 2019, p. 6-166)

The slab to column joint was conservatively modelled as rotationally free about the Y-axis (pinned connection), therefore not transferring any moment to the columns. Note that Figure 6-10 can be misleading in that SeismoSoft models do not graphically show that the *column-to-column* connection is modelled as continuous as in the case of this investigation, it was therefore assumed that the column reinforcement is sufficiently spliced. However, the *column- to-slab* connections are modelled as pinned, therefore not transferring any moment.

Wall-slab joint: As seen in Figure 6-10, rigid elements are used to link the wall elements to the slab elements. The links are rigidly fixed at both ends. Extremely rigid elements cause numerical instability. These links are modelled as elastic elements with stiffness of 100 times the elastic stiffness of the slab elements.

Wall-foundation joint: The wall element is rigidly fixed to the BNWF. Strain penetration was not explicitly modelled in this investigation. It is, however, expected that strain penetration increases the wall hinge length, in turn improving the wall ductility.

6.1.6 Lumped mass

To represent the full mass associated with the seismic response of the equivalent frame, a lumped mass is introduced at every level. The lumped masses do not contribute to the axial load on the structural wall, as this is modelled directly, but will contribute to the mass participation during seismic loading. The lumped masses are shown in Figure 6-13.

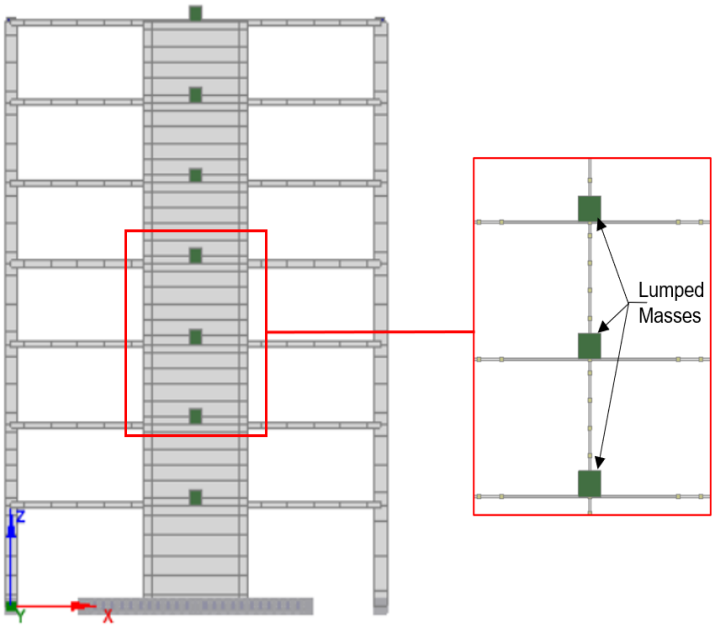

Figure 6-13: Lumped masses

As an example, consider the 5 Storey building with wall aspect ratio 3. With reference to Chapter 4.1 and Figure 4-2 the lumped mass is calculated as:

Total floor area:	$42.6 \times 17.24 = 734.42\ m^2$
Sustained vertical load per floor:	$1DL + 0.3LL = 1 \times (11.5) + 0.3 \times 2.5$ $= 12.25\ kN/m^2$
Total floor mass:	$734.42 \times 12.25/9.81 = 917.089\ ton$
Mass contributing to specific wall:	$917.089 \times 0.55 = 504.399\ ton$
Mass already in equivalent frame:	$12.25\ kN/m^2 \times frame\ area/9.81 =$ $12.25 \times (6 + 5.6 + 6) \times 3.3/9.81 = 72.526\ ton$
Lumped mass:	$504.4 - 72.53 = 431.87\ ton$

6.2 Material properties

6.2.1 Material strength

For the purposes of this investigation, the material strength can be separated into two categories; the design strength associated with linear methods of analysis and mean strength associated with nonlinear methods of analysis. The design strength is typically taken as the characteristic strength adjusted by a partial material factor. For seismic design, SANS 10160-1, 7.3.5 (2019) specifies partial material factors as 1 if sufficient ductility for resistance is provided. The design material strength is then the characteristic strength.

Concrete strength: The characteristic concrete cube strength, f_{cu} is taken as 30 MPa for all members. The associated characteristic cylinder strength, $f_{ck,cyl}$ is 25 MPa. EN 1992-1-1, Table 3.1 (2004) specifies a mean concrete cylinder strength, $f_{cm} = f_{ck,cyl} + 8 = 33$ MPa. The cylinder strength is required in SeismoStruct as input for the nonlinear analysis, and the characteristic cube strength is used in the South African design codes.

Reinforcing steel: The characteristic yield strength, f_{sy} of high-yield steel is taken as 450 MPa (SANS 0100-1, 2000, Table 3). The recommended mean yield strength is taken as $1.1 \times f_{sy} = 495$ MPa (Mirza & MacGregor, 1979, pp. 921-937). SANS 920 (2005), section 3.7, specifies that the ultimate strength should be at least 15% greater than the mean yield strength. Thus, the ultimate steel strength is taken as $1.1 \times 1.15 \times f_{sy} = 569$ MPa.

6.2.2 Stress-strain relationships and material characteristics

6.2.2.1 Reinforcing steel

The typical stress-strain relationship for high yield steel is shown in Figure 6-14.

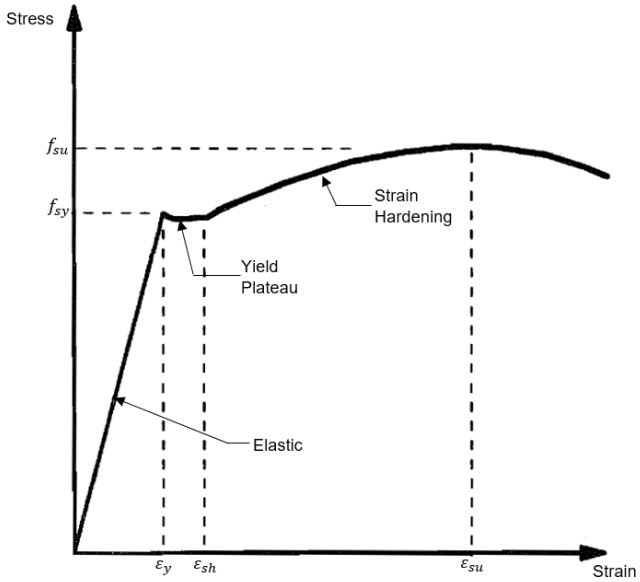

Figure 6-14: Stress-strain relationship for reinforcing steel (EN 1992-1-1, 2004)

EN 1992-1-1, clause 3.2.7 (2004), proposes an idealised bilinear relationship for design purposes, shown in Figure 6-15. Taking the modulus of elasticity for steel reinforcement, E_{stl} as 200 GPa the design-, characteristic- and mean yield strain are calculated using the relationship; $\varepsilon_{sy} = f_{sy}/E_{stl}$. The post yield relationship can be expressed with no strain hardening (elastic-perfectly plastic curve) or with strain hardening (inclining curve is shown in Figure 6-15). SANS 0100-1 (2000, Figure 2) assumes and elastic-perfectly plastic curve for design purposes, which was assumed for the member design in this investigation. For the nonlinear assessment, however, strain hardening was considered with the mean material properties.

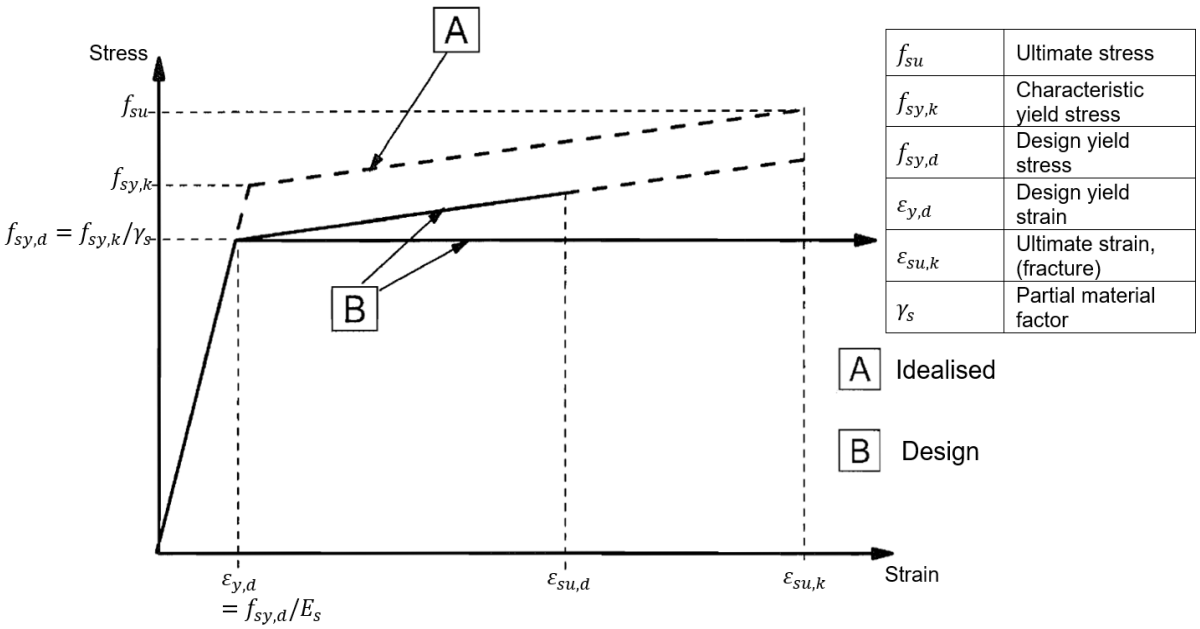

Figure 6-15: Idealised bilinear stress-strain relationship for reinforcing steel (adapted from EN 1992-1-1, 2004)

The ultimate strain at fracture, ε_{su} is expected to be larger than 0.075 for high yield steel (EN 1992-1-1, 2004, *Annex C*), however this is typically reduced for the longitudinal reinforcement under cyclic loading. This is addressed in Section 6.3.

6.2.2.2 Concrete

Transverse reinforcement in the boundary elements confines the inner concrete core and prevents buckling of the longitudinal compression reinforcement. The transverse links together with the longitudinal reinforcement prevent the concrete core from lateral expansion, enabling higher compressive stresses and strains (Pauley & Priestley, 1992, p. 99).

Mander, et al., (1988) proposed stress-strain relationships for confined and unconfined concrete as shown in Figure 6-16.

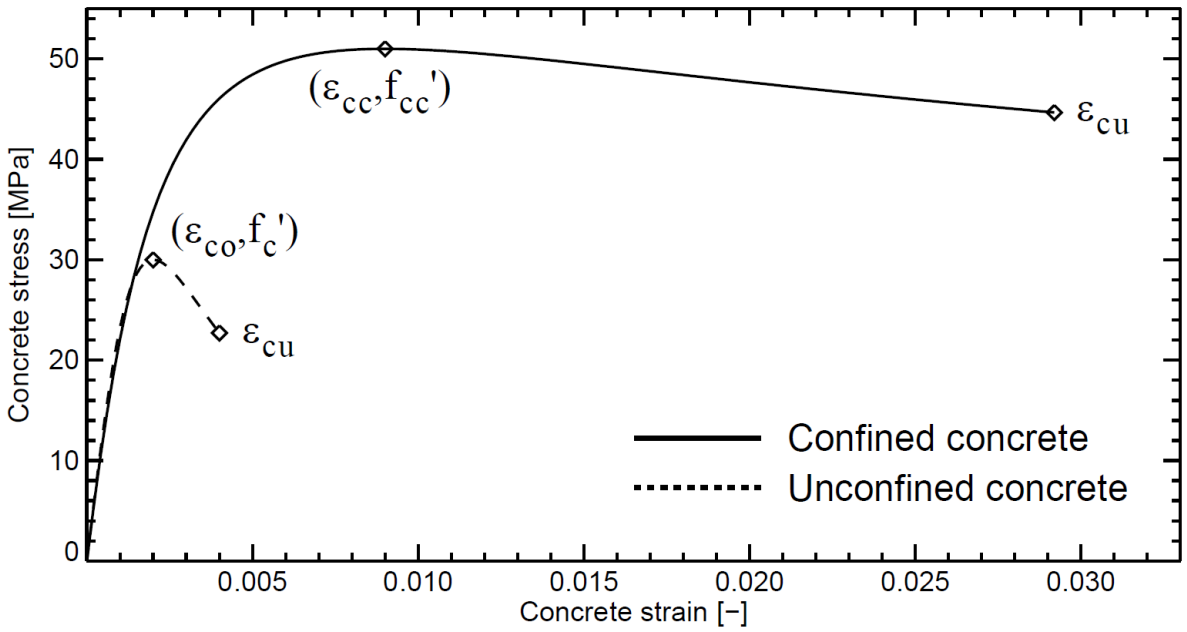

Figure 6-16: Stress-strain relationships for confined and unconfined concrete (Monteiro, 2019, p. 3-3)

The relationship for confined concrete can be expressed through Equations (6.1) to (6.6):

$$f_c = \frac{f'_{cc}}{r - 1 + \alpha^r} \quad (6.1)$$

$$\alpha = \frac{\varepsilon_c}{\varepsilon_{cc}} \quad (6.2)$$

$$\varepsilon_{cc} = \varepsilon_{co}\left[1 + 5\left(\frac{f'_{cc}}{f'_c} - 1\right)\right] \quad (6.3)$$

$$r = \frac{E_c}{E_c - E_{sec}} \quad (6.4)$$

$$E_c = 4700 \times \sqrt{f'_c}\ \text{(MPa)} \quad (6.5)$$

$$E_{sec} = \frac{f'_{cc}}{\varepsilon_{cc}} \quad (6.6)$$

Where;

f_c: Concrete compressive stress.

ε_c: Concrete compressive strain.

f'_c: Unconfined concrete compressive strength (cylinder strength).

ε_{co}: Strain at peak stress for unconfined concrete, generally assumed as 0.002.

f'_{cc}: Confined concrete compressive strength.

ε_{cc}: Strain at peak stress for confined concrete.

E_c: Modulus of elasticity of concrete.

E_{sec}: Tangent modulus of elasticity of the concrete.

The general approach for confined concrete strength is expressed through Equations (6.7) to (6.9).

$$f_l' = f_l \times k_e \qquad (6.7)$$

$$k_e = \frac{A_e}{A_{cc}} \qquad (6.8)$$

$$A_{cc} = A_c(1 - \rho_{cc}) \qquad (6.9)$$

Where;

f_l: Lateral pressure from transverse reinforcement.

f_l': Effective lateral confining pressure.

k_e: Confinement effectiveness ratio.

A_e: Area of effective concrete core midway between two links (Figure 6-17).

ρ_{cc}: Ratio of area of longitudinal reinforcement to area of core of section.

A_c: Area of core of section enclosed by the centre lines of links (Figure 6-17).

With reference to Figure 6-17, the effectiveness of rectangular sections can be calculated with Equation (6.10).

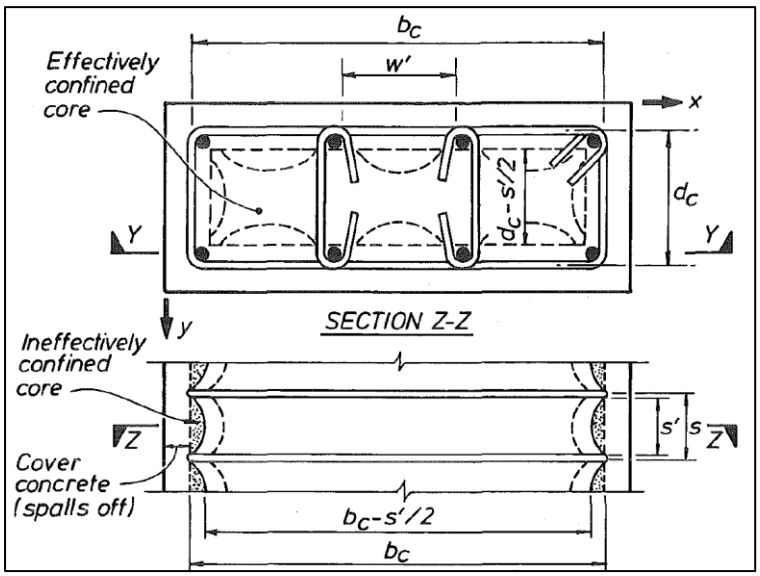

Figure 6-17: Effective area of confinement (Mander, et al., 1988)

$$k_e = \frac{\left(1 - \sum_{i=1}^{n} \frac{(w_i')^2}{6b_c d_c}\right)\left(1 - \frac{s'}{2b_c}\right)\left(1 - \frac{s'}{2d_c}\right)}{(1 - \rho_{cc})} \quad (6.10)$$

The effective lateral confinement for each direction can be obtained from Equations (6.11) through (6.14).

$$\rho_x = \frac{A_{sx}}{sd_c} \quad (6.11)$$

$$\rho_y = \frac{A_{sy}}{sb_c} \quad (6.12)$$

$$f'_{lx} = k_e \rho_x f_{yh} \quad (6.13)$$

$$f'_{ly} = k_e \rho_y f_{yh} \quad (6.14)$$

Where;

$A_{sx}; A_{sy}$: Total area of transverse reinforcement running in the x and y direction.

f_{yh}: Yield strength of the transverse reinforcement (450 MPa conservatively).

$f'_{lx}; f'_{ly}$: Effective lateral confinement pressure in the x and y direction.

The total confined strength ratio, f'_{cc}/f'_c can then be obtained from Figure 6-18, as presented by Mander, et al. (1988, Fig 4).

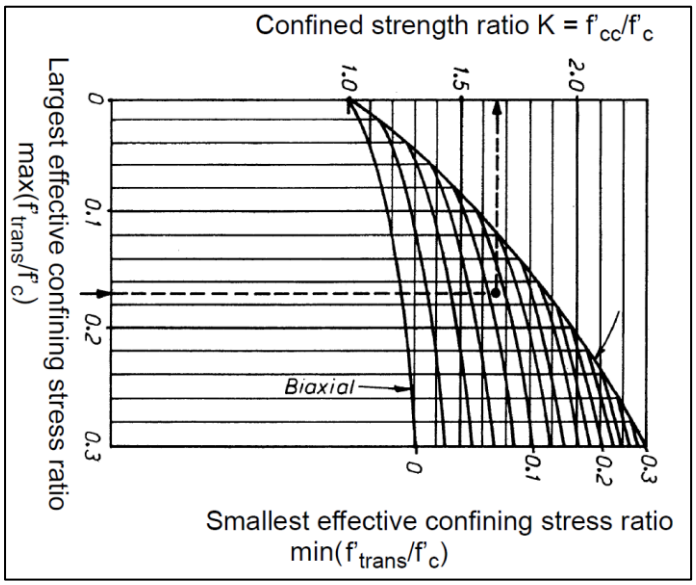

Figure 6-18: Confined strength ratio for rectangular sections (Mander, et al., 1988)

With the confined concrete strength, f'_{cc} obtained, the ultimate strain can be calculated using Equations (6.15) and (6.16).

$$\varepsilon_{cu} = 0.004 + 1.4\rho_s f_{yh}\varepsilon_{sm}/f'_{cc} \quad (6.15)$$

$$\rho_s = \rho_x + \rho_y \quad (6.16)$$

The transverse reinforcing steel strain at maximum stress, ε_{sm} is conservatively taken as 0.075. The ultimate strain for unconfined concrete is specified as 0.0035 (SANS 0100-1, 2000, Figure 1). However, this value is based on experiments on concrete elements subjected to a uniform compression or constant gradient. The critical region is generally subjected to significant moment gradient. Tests have indicated strains well in excess of 0.003 for larger moment gradients (Pauley & Priestley, 1992, p. 98). For such elements, a conservative estimate for ultimate compression strain of 0.004 is recommended. A value of 0.004 is, therefore used in Equation (6.15).

The same procedure can be followed to determine the stress-strain relationship for unconfined concrete by taking the confinement effectivity ratio as, k_e as unity.

SeismoStruct uses the above procedure to determine stress-strain curves for confined and unconfined concrete shown in Figure 6-19. The confinement effectivity ratio is manually calculated for each case.

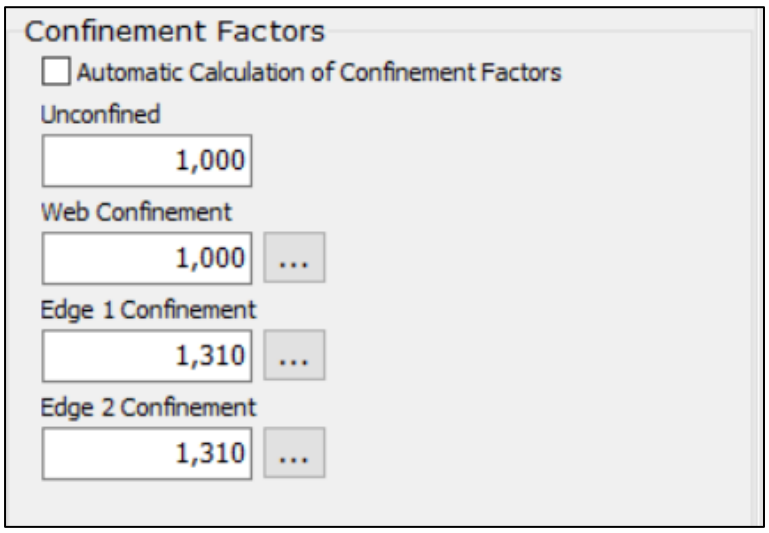

Figure 6-19: Example of confinement factors as input in SeismoStruct

6.3 Performance criteria

6.3.1 Design philosophy

The design seismic action in SANS 10160-4 (2017) is associated with a seismic event of 10% probability of exceedance in 50 years (or a reference return period of 475 years). This relates to the no- (local-) collapse performance requirements in EN 1998-1, clause 2.1.

This requires the protection of life under a rare seismic event by retaining the structural integrity and some residual load capacity of a structure or parts of a structure after the event. A structure can therefore be significantly damaged and may have some permanent drift but should still possess enough strength and stiffness to resist sustained vertical loads and strong aftershocks. The repairs of the structure may be uneconomical (Fardis, et al., 2005, p. 5).

6.3.2 Damage-control limits

Apart from drift limits, there are no explicit requirements in SANS 10160-4 (2017) on what is deemed to be acceptable damage to a structure. The responsibility, therefore, lies with the engineers and developers to ascertain a level of damage that is within the requirements of the design codes and economically acceptable.

This investigation uses guidelines on strain limits as specified by Priestley, et al. (2007), in the development of direct displacement-based design, as the basis of defining the performance criteria.

Four main strain limits, in addition to lateral drift limits, are identified and discussed.

Yielding of reinforcement is a means of energy dissipation and is expected in capacity design approaches. The critical aspect is likely to be the concrete crack widths when yielding occurs. The limits to crack width will depend on the corrosive environment. The steel strain limits can be calculated as described in Section 6.2.2.1, however, this limit is typically associated with serviceability limits for seismic events of a higher probability of exceedance and smaller magnitude.

Crushing of unconfined concrete indicates the onset of cover spalling in confined concrete and spalling/crushing for unconfined concrete. As this limit state indicates failure for unconfined concrete, it is considered significant for slab elements, webs of walls in the critical region and walls outside the critical region in this investigation. A compressive strain of 0.0035 is assumed for crushing of unconfined concrete. This is conservative, as discussed in Section 6.2.2.2.

The spalling of cover does not significantly affect the structural integrity of confined concrete members. This is explicitly modelled with fibre elements, nonetheless.

Crushing of confined concrete signifies the onset of failure. Equation (6.15) is used to define the ultimate compressive strain for a given confined concrete element, this is defined at a material level in SeismoStruct (2020). The equation will predict conservatively low estimates for ultimate strain in members under combined axial compression and flexure (Priestley, et al., 2007, p. 142). For a universal performance criterion, that will generally be conservative for all models, the program default for ultimate compressive strain for confined concrete of 0.02 is used.

Typical values for rectangular sections range for 0.012 to 0.05 (Pauley & Priestley, 1992, p. 103).

Fracture of reinforcement signifies failure. Ultimate tensile strain for high yield steel reinforcement is expected to be in excess of 0.1. However, it is inappropriate to use this as the effective maximum tension strain because the ultimate tensile strain is reduced under load reversal and become susceptible to buckling. A recommended ultimate steel tensile strain of 60% of the mean ultimate strain (found from monotonic testing) is used (Priestley, et al., 2007, p. 143).

It should be noted that the above definitions act as markers for the onset of damage. Performance criteria for crushing of concrete and fracture of reinforcement act to terminate the analysis once these strain limits are reached, but the nonlinear behaviour of the structure is defined at a material level and is explicitly modelled for each element.

Drift limits are typically prescribed to prevent excessive damage to non-structural infill panels and services. In buildings the content and services are typically high, relative

to the structure. Excessive damage is expected for drift levels of larger than 0.025 (Priestley, et al., 2007, p. 71).

SANS 10160-4 (2017) clause 9.3.1 limits inter storey drift to:

$$d_{r\,i-j} \leq 0.025 h_s \qquad if \qquad T < 0.7\ s \tag{6.17}$$

$$d_{r\,i-j} \leq 0.02 h_s \qquad if \qquad T > 0.7\ s \tag{6.18}$$

Where $d_{r\,i-j}$ is the relative drift between two storeys and h_s is the storey height.

The structures in this investigation have fundamental periods larger than 0.7 seconds. Equation (6.18) therefore applies to this investigation.

7 Displacement demand

Design standards use various methods to determine the displacement demand from capacity curves produced by pushover analyses. Section 2.8.3 introduces the approach used by EN 1998-1 (2004) that is based on the N2 method. US guidelines clearly set out procedures to incorporate SSI in determining target displacements (displacement demand) from pushover analyses. In order to implement the procedure for SSI from US standards, the target displacement prescribed by EN 1998 (2004) must compare well with the target displacement of US standards. This chapter first compares the target displacements from these methods, with displacement responses produced from THA for the fixed base models (M100 models), where SSI is not incorporated. A suitable method is then selected to determine the target displacements for the pushover analyses of the reduced bases. If the target displacement is achieved or surpassed without failure (Section 6.3), then the assumption of the behaviour factor for the linear methods is acceptable. If a structure fails before the target displacement is reached, then a reassessment of the behaviour factor is necessary.

7.1 Target displacement comparison

The various methods considered for determining target displacement are described below.

N2 method by EC 1998-1:

The method was briefly described in Section 2.8.3. The process is repeated here in more detail.

A bilinear elastic-perfectly plastic approximation of the capacity curve is determined through ensuring that the area under the bilinear curve is equal to the area under the capacity curve, up until the formation of the plastic mechanism. This implies that the energy of the equivalent system is equal to that of the original, which is illustrated in Figure 2-20. The yield force, F_y is initially taken as the ultimate force on the capacity curve. The yield displacement, d_y is determined as:

$$d_y = 2(d_m - \frac{E_m}{F_y}) \qquad (7.1)$$

Where E_m is the area under the curve and d_m is the displacement at the formation of the plastic hinge mechanism.

The MDOF system is transformed into an equivalent SDOF through Equation (2.46), which is repeated here:

$$\Gamma = \frac{\sum m_i \Phi_i}{\sum m_i \Phi_i^2}$$

The normalised shape vector, Φ_i, represents the lateral deformed shape. A simple example of calculating the transformation factor is shown in Figure 7-1.

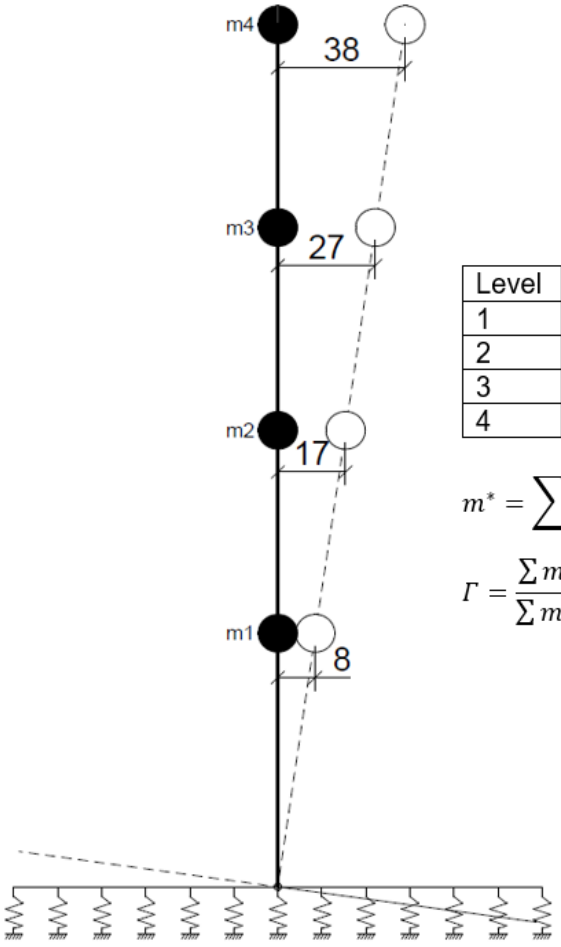

Level	Deflection	Mass	Φ	mΦ	mΦ²
1	8	20	0.21	4.2	0.88
2	17	20	0.447	8.94	4
3	27	20	0.711	14.22	10.11
4	38	20	1	20	20
			Sum:	47.36	34.99

$$m^* = \sum m_i \Phi_i = 47.36$$

$$\Gamma = \frac{\sum m_i \Phi_i}{\sum m_i \Phi_i^2} = \frac{47.36}{34.99} = 1.354$$

Figure 7-1: Example for calculating the transformation factor, Γ.

The equivalent SDOF system can be calculated using Equations (2.47) and (2.48). The effective period, T^* is calculated using Equation (2.50). The displacement of the SDOF system, d_t^* can then be determined using 5%-damped elastic spectra and Equations (7.2), (7.3) and (7.4), with an adjustment for shorter periods where the equal displacement approximation does not apply.

$$d_t^* = d_{et}^* = S_e(T^*)\left(\frac{T^*}{2\pi}\right)^2 \qquad if\ T \geq T_c \qquad (7.2)$$

$$d_t^* = \frac{d_{et}^*}{q_u}\left[1 + (q_0 - 1)\frac{T_c}{T^*}\right] \geq d_{et}^* \qquad if\ T < T_c \qquad (7.3)$$

$$q_0 = \frac{m^* S_e(T^*)}{F_y^*} \qquad (7.4)$$

The target displacement for the MDOF system, d_t is calculated as:

$$d_t = d_t^* \times \Gamma \qquad (7.5)$$

The use of a 5% damped elastic displacement spectrum is expected to produce conservative results. Since ductility influences damping, damping will increase as the structure deforms nonlinearly to reach the displacement demand.

Capacity spectrum method (CSM):

This method applies an iterative approach where the response spectrum is adjusted for damping values greater than 5%. For a graphical representation of the method the bilinear approximation of the capacity curve can be imposed onto the acceleration-displacement response spectrum (ADRS) by dividing the equivalent force, F^* by the equivalent mass, m^*. The spectrum is adjusted as the ductility increases, similarly the ductility will be adjusted as the intersection of the capacity curve with the acceleration-displacement response spectrum changes. This iterative procedure is illustrated in Figure 7-2. The final displacement is obtained where the capacity curve and the ADRS converge.

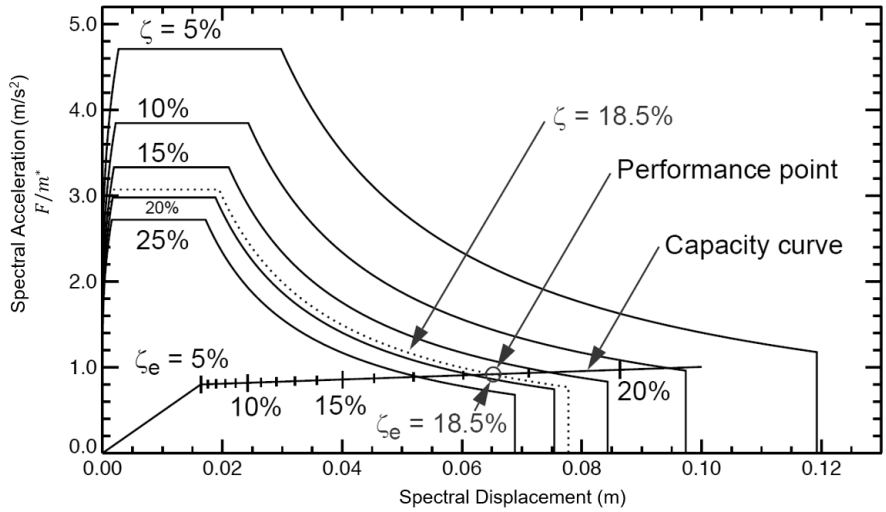

Figure 7-2: Iterative procedure for the capacity spectrum method (Monteiro, 2019,L4 p. 116)

There are several expressions that relate ductility to damping. An expression developed by Grant, et al., (2005) is used in this investigation, which is presented in Equation (7.6).

$$\xi_{hyst} = a\left(1 - \frac{1}{\mu^b}\right)\left(1 + \frac{1}{(T_e + c)^d}\right) \qquad (7.6)$$

Coefficients a, b, c and d will depend on the specific hysteretic rules used.

Table 7-1 presents the values for elastic- perfectly plastic bilinear rules as obtained from Grant, et al., (2005).

Table 7-1: Coefficients for hysteretic damping (Grant, et al., 2005)

Model	a	b	c	d
EPP	0.244	0.336	-0.002	0.25

Equation (2.22) is used to calculated total damping. For the fixed base models, the elastic damping is taken as 5%. Inserting the coefficients of Table 7-1 into Equation (7.6) and substituting Equation (7.6) in Equation (2.22) produce an expression for the equivalent damping for fixed base models as:

$$\xi_{eq} = 0.05 + 0.244\left(1 - \frac{1}{\mu^{0.336}}\right)\left(1 + \frac{1}{(T^* - 0.002)^{0.25}}\right)$$

T^* is an effective period calculated with Equation (2.50).

The response spectra are adjusted by the prescribed equation from EN 1998-1 (2004), as expressed in Equations (2.9) to (2.13).

Equivalent linearization:

FEMA 440 proposes the equivalent linearization method as an improved modification of the capacity spectrum method (FEMA 440, 2005, p. 6-1). The same iterative procedure as above is followed, but an adapted effective period, T_{eff} and damping, β_{eff} are used. Figure 7-3 illustrates the process.

Note that the two symbols for damping; β and ξ are interchangeable, where β is typically used in US codes and ξ typically used in Eurocodes. This is intentionally kept the same as the source.

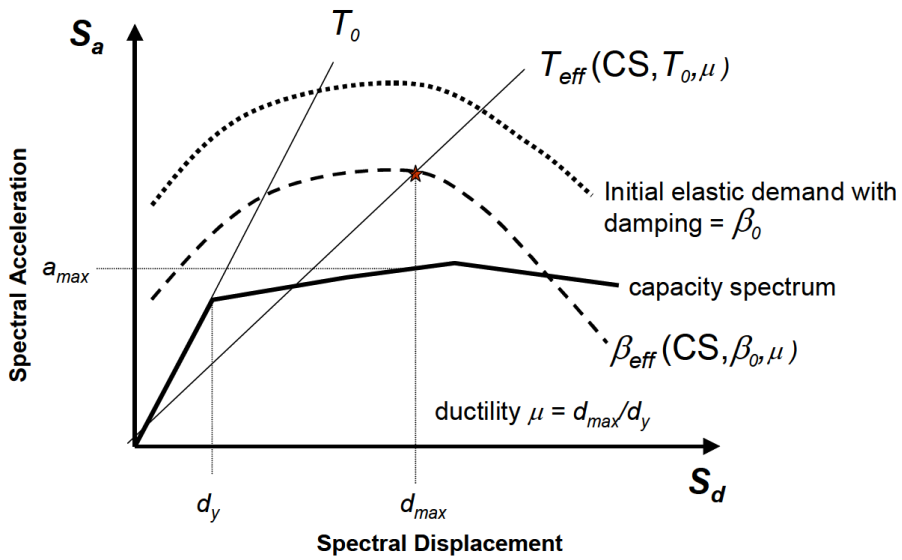

Figure 7-3: Acceleration-displacement response spectrum showing equivalent linearization approach (FEMA 440, 2005).

FEMA 440 calculates the effective damping and effective period through Equations (7.7) to (7.12).

β_{eff};

$$For\ 1 < \mu < 4: \qquad \beta_{eff} = A(\mu - 1)^2 + B(\mu - 1)^3 + \beta_0 \qquad (7.7)$$

$$For\ 4 < \mu < 6.5: \qquad \beta_{eff} = C + D(\mu - 1) + \beta_0 \qquad (7.8)$$

$$For\ \mu > 6.5: \qquad \beta_{eff} = E\left[\frac{F(\mu-1)-1}{[F(\mu-1)]^2}\right]\left(\frac{T_{eff}}{T_0}\right)^2 + \beta_0 \qquad (7.9)$$

T_{eff};

$$For\ 1 < \mu < 4: \qquad T_{eff} = [G(\mu-1)^2 + H(\mu-1)^3 + 1]T_0 \qquad (7.10)$$

$$For\ 4 < \mu < 6.5: \qquad T_{eff} = [I + J(\mu-1) + 1]T_0 \qquad (7.11)$$

$$For\ \mu > 6.5: \qquad T_{eff} = \left[K\left(\sqrt{\frac{(\mu-1)}{1+L(\mu-2)}} - 1\right) + 1\right]T_0 \qquad (7.12)$$

β_0 is the elastic damping (ξ_{el}). This is taken as 5 for the fixed base models and $T_0 = T^*$.

Table 7-2 presents the coefficients for an elastic perfectly plastic curve as obtained from FEMA 440.

Table 7-2: Coefficients for equivalent linearization (FEMA 440, 2005, Table 6-1 and Table 6-2)

A	B	C	D	E	F	G	H	I	J	K	L	Type of Linearization Curve
5.2	-0.66	11	0.12	19	0.75	0.11	-0.017	0.27	0.09	0.57	0	Bilinear Perfectly Plastic

Coefficient method:

ASCE/SEI 41-17 (2017) uses the coefficient method to determine the target displacement through Equations (7.13) to (7.16).

$$d_t = C_0 C_1 C_2 S_e(T^*)\left(\frac{T^*}{2\pi}\right)^2 \qquad (7.13)$$

C_0 is the modification factor for the transformation of a SDOF system to the MDOF system (similar to Γ). The factor is given in Table 7-3.

C_1 is the modification factor to relate expected maximum inelastic displacement to displacement calculated for linear elastic response:

$$C_1 = 1 + \frac{\mu_{strength} - 1}{\dot{a}T^{*2}} \qquad (7.14)$$

$$\mu_{strength} = \frac{m^* S_e(T^*)}{F_y^*} C_m = q_0(EN\ 1998\ method) \times C_m \qquad (7.15)$$

C_m is the effective mass factor taken from Table 7-4.

$\dot{a} = 60$ for site Class D (ASCE/SEI 7-16), similar to site Class 3 SANS 10160-4.

C_2 is the modification factor to represent the effect of pinched hysteresis shape, cyclic stiffness degradation, and strength deterioration on maximum displacement response. $C_2 \cong 1$ for T > 0.7s. However, C_2 can be calculated using Equation (7.16).

$$C_2 = 1 + \frac{1}{800}\left(\frac{\mu_{strength} - 1}{T^*}\right)^2 \qquad (7.16)$$

Table 7-3: Values for C_0 (ASCE/SEI 41-17, 2017, Table 7-5)

	Shear Buildings[a]		Other Buildings
Number of Stories	Triangular Load Pattern (1.1, 1.2, 1.3)	Uniform Load Pattern (2.1)	Any Load Pattern
1	1.0	1.0	1.0
2	1.2	1.15	1.2
3	1.2	1.2	1.3
5	1.3	1.2	1.4
10+	1.3	1.2	1.5

Note: Linear interpolation shall be used to calculate intermediate values.
[a] Buildings in which, for all stories, story drift decreases with increasing height.

Table 7-4: Values for C_m (ASCE/SEI 41-17, 2017, Table 7-4)

No. of Stories	Concrete Moment Frame	Concrete Shear Wall	Concrete Pier-Spandrel	Steel Moment Frame	Steel Concentrically Braced Frame	Steel Eccentrically Braced Frame	Other
1–2	1.0	1.0	1.0	1.0	1.0	1.0	1.0
3 or more	0.9	0.8	0.8	0.9	0.9	0.9	1.0

THA on fixed models:

Results from the different methods are compared with the average displacement response from 3 THA's of each fixed model. For design purposes the maximum

response quantities from the THA's of the 3 matched accelerograms are typically used, however, the average response quantities are used here, for comparison.

Three (3) accelerograms are chosen from the PEER Strong Motion Database, as presented by Table 7-5, and matched with the design acceleration response spectra.

To represent additional damping not captured by the hysteretic model of the fibre elements, a value of 2% tangent stiffness proportionate damping is assumed.

The assumptions about matching and damping are addressed in Chapter 9.

Table 7-5: Accelerograms chosen from PEER Strong Motion Database

Earthquake	Source	Station	Date	PGA Unmatched	PGA Matched
Chalfant Valley	PEER Strong Motion Database	Bishop - LADWP South St, 180	July 20, 1986	0.126 (g)	0.202 (g)
Umbria Marche	PEER Strong Motion Database	Castelnuovo-Assisi, 270	September 26, 1997	0.105 (g)	0.177 (g)
Loma Prieta	PEER Strong Motion Database	090 CDMG STATION 47381	October 18, 1989	0.36 (g)	0.195 (g)

Properties of the design response spectra used directly (pushover analysis) or indirectly (THA) for the nonlinear assessment of buildings are:

PGA: 0.15g

Damping, ξ: 5% elastic damping adjusted depending on the method used to determine the target displacement. Equation (2.9) together with Equations (2.10) to (2.13) are used to adjust the response spectra for other damping values.

Ground Type: Ground Type 3 of SANS 10160-4 (2017)

Results:

The target displacements of the different methods are plotted against the effective period calculated from the effective stiffness of the bilinear curve (from the EN 1998-1 (2004) *Annex B* procedure) in Figure 7-4.

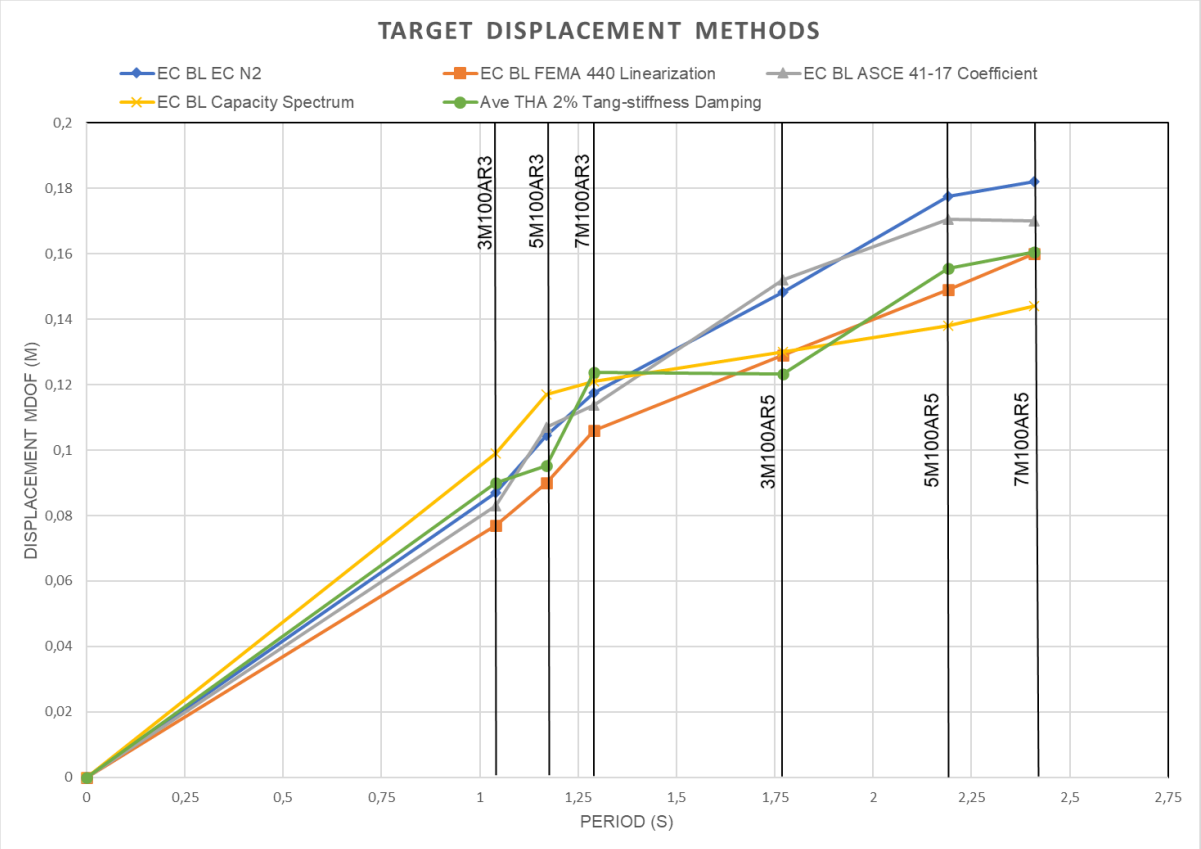

Figure 7-4: Comparison of target displacement methods

The coefficient method and the N2 method compares well with the THA for shorter periods but overestimates the displacement demand for longer periods. The capacity spectrum method overestimates the displacement demand for shorter periods and underestimates the displacement demand for longer periods. FEMA 440's equivalent linearization method slightly underestimates the displacement for shorter periods but compares well with the THA throughout.

What is significant is that the N2 method and the coefficient method used in ASCE/SEI 41-17 (2017) predict similar displacement demands and where the results diverge from the displacement demands of THA, they are conservative. For this reason, the procedure specified by ASCE/SEI 41-17 to include SSI together with the N2 based procedure of EN 1998-1 are used to predict the displacement response.

It should be noted that this conclusion is drawn from a small study of a particular structural type, however, a similar observation regarding the N2 method and the coefficient method was made by Fajfar (1999).

7.2 Including SSI in target displacement

This study follows the procedure of ASCE/SEI 41-17 to incorporate SSI in the pushover analysis. The procedure is fundamentally similar to most guidelines mentioned but incudes the method used by EN 1998-1 *Annex B* to predict the target displacement. Figure 7-5 illustrates the adapted iterative procedure used for this investigation.

The spectrum reduction factors associated with kinematic effects are conservatively taken as 1 (see Section 2.7.3). Foundation damping effects addressed in Section 2.7.4 are included in this investigation.

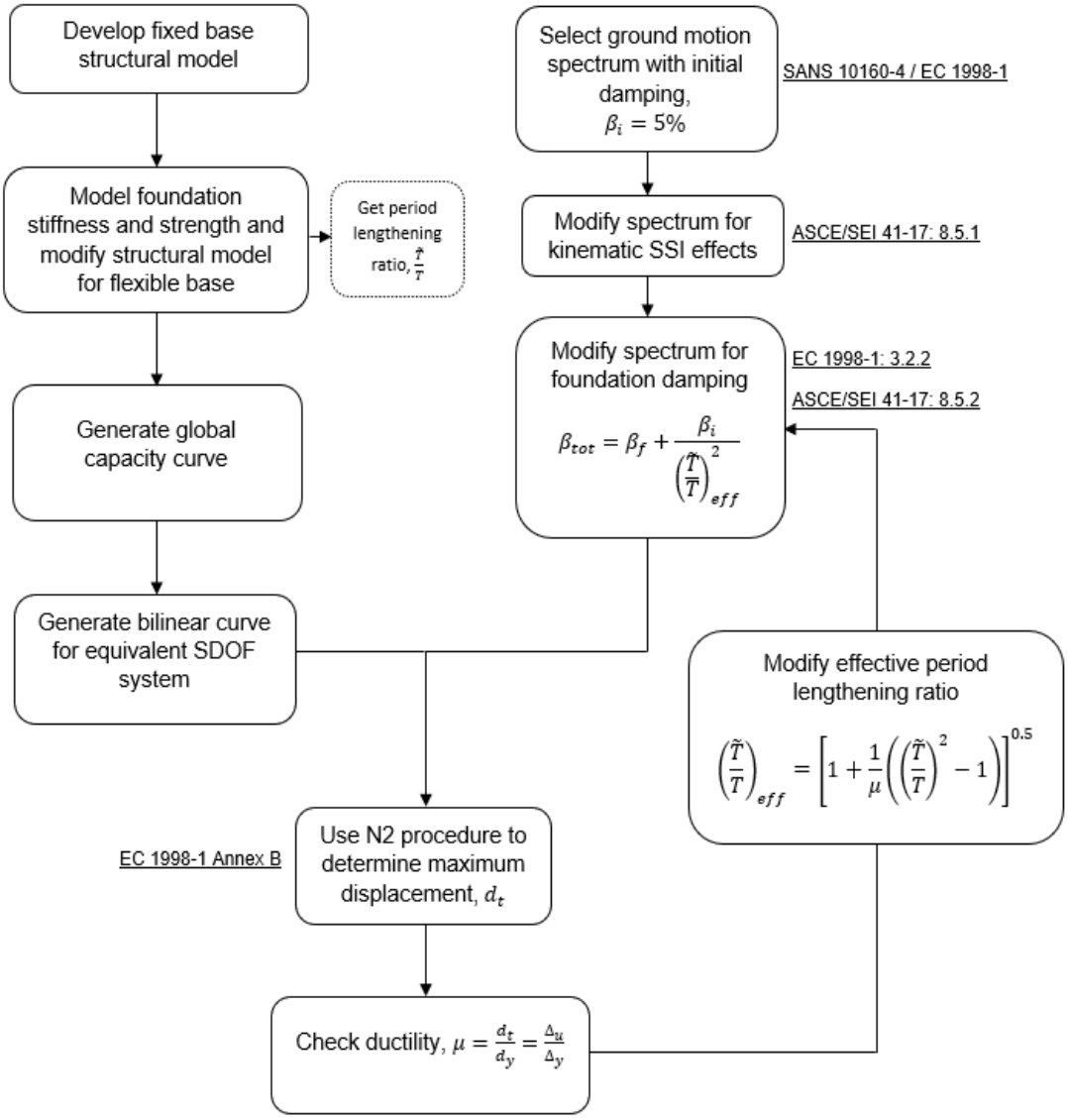

Figure 7-5: Procedure to incorporate SSI in pushover analyses

The procedure is demonstrated by considering model 7M80AR3:

$M_{fixed} = 22\,231\ kNm$	Moment produced from the linear elastic analysis on the fixed moment case.
$T_{fixed} = 1.02\ s$	Fundamental period for the fixed model using modal analysis.
$Base\ size$: $12.2 \times 2.4 \times 1\ m$	Base sized to have an ultimate moment resistance of 80% of M_{fixed}, using Equation (3.7) and soil properties of Section 4.2.
$\tilde{T} = T_{80} = 1.57\ s$	Fundamental period from 7M80AR3 modal analysis when base and springs are explicitly modelled.
$\frac{\tilde{T}}{T} = \frac{1.57}{1.02} = 1.54$	Period lengthening ratio.

Soil hysteretic damping, β_s is calculated by using Figure 2-18 and Table 2-4.

$\frac{S_{DS}}{2.5} = a_g \times S = 0.15g \times 1.15 = 0.1725g$	$S_{DS}/_{2.5}$ in ASCE 41-17 equates to the PGA adjusted by the ground type. ($a_g \times S$ in SANS 10160-4:2011).
$\beta_s = 0.032\ (3.2\%)$	Through interpolation of Table 2-4. Ground Type D is similar to Ground Type 3 in SANS 10160-4.

Radiation damping, β_{rad} is calculated using Equation (2.33) and is repeated as:

$$\beta_{rd} = \frac{1}{\left(\frac{\tilde{T}}{T_y}\right)^2}\beta_y + \frac{1}{\left(\frac{\tilde{T}}{T_{xx}}\right)^2}\beta_{xx}$$

The equation for foundation damping based on Wolf (1985) is presented NIST GCR 12-917-21 (2012) as:

$$\beta_f = \left[\frac{\left(\frac{\tilde{T}}{T}\right)^{ns} - 1}{\left(\frac{\tilde{T}}{T}\right)^{ns}}\right]\beta_s + \frac{1}{\left(\frac{\tilde{T}}{T_x}\right)^{nx}}\beta_x + \frac{1}{\left(\frac{\tilde{T}}{T_{yy}}\right)^{nyy}}\beta_{yy}$$

Where β_x is the translational component in the direction of loading and β_{yy} is the rotational component about the *strong* axis. It is unclear why the equations given in ASCE/SEI 41-17 are, conservatively, based on Pais & Kausel (1988) equations for components about the *weak* axis, which is the direction perpendicular to loading. These equations are the same in several other guidelines (FEMA 1050, ASCE/SEI 7-16, FEMA 440) and are therefore followed here. Equations (7.17) to (7.23) present the equations as given ASCE/SEI 41-17.

$$\beta_y = \left[\frac{4\left(\frac{L}{B}\right)}{\left(\frac{k_y}{GB}\right)}\right]\left[\frac{a_0}{2}\right] \qquad (7.17)$$

$$k_y = \frac{GB}{2-\upsilon}\left[6.8\left(\frac{L}{B}\right)^{0.65} + 0.8\left(\frac{L}{B}\right) + 1.6\right] \qquad (7.18)$$

$$a_0 = \frac{2\pi B}{\tilde{T} v_s}; dynamic\ stiffness\ modifier \qquad (7.19)$$

$$\beta_{xx} = \left[\frac{\left(\frac{4\psi_\upsilon}{3}\right)\left(\frac{L}{B}\right){a_0}^2}{\left(\frac{k_{xx}}{GB^3}\right)\left[\left(2.2 - \frac{0.4}{(L/B)^3}\right) + {a_0}^2\right]}\right]\left[\frac{a_0}{2\alpha_{xx}}\right] \qquad (7.20)$$

$$k_{xx} = \frac{GB^3}{1-\upsilon}\left[3.2\left(\frac{L}{B}\right) + 0.8\right] \qquad (7.21)$$

$$\psi_\upsilon = \sqrt{\frac{2(1-\upsilon)}{(1-2\upsilon)}} \leq 2.5 \qquad (7.22)$$

$$\alpha_{xx} = 1 - \left[\frac{\left(0.55 + 0.01\sqrt{(L/B)-1}\right){a_0}^2}{\left(2.2 - \frac{0.4}{(L/B)^3}\right) + {a_0}^2}\right]; surface\ stiffness\ modifier \qquad (7.23)$$

The contribution of β_y and β_{xx} to β_{rad} is based on the flexibility of the soil-structure system to fictitious periods T_y and T_{xx} that can be calculated using Equations (2.34) and (2.35), respectively.

For the 7M80AR3 model, radiation damping, $\beta_{rad} = 0.00098\ (0.098\%)$. It is observed that radiation damping contributes little to total foundation damping for base sizes and aspect ratios considered in this investigation. If the foundation system is connected with a set of ground beams, the length, *L* and width, *B* can be taken as the building

footprint, which will increase the value. It is assumed here that the foundations are unconnected. Equation (2.32) is used to calculate foundation damping as:

$$\beta_f = \left[\frac{\left(\frac{\tilde{T}}{T}\right)^2 - 1}{\left(\frac{\tilde{T}}{T}\right)^2}\right]\beta_s + \beta_{rd} = \left[\frac{(1.54)^2 - 1}{(1.54)^2}\right]0.032 + 0.0009 = \ 0.0193\ (1.93\%)$$

The bilinear approximation of the capacity curve is initially calculated using the response spectrum for 5% damping:

$d_y = 56.8\,mm$	Yield displacement.
$F_y = 1183\,kN$	Yield force.
$d_t = 186\,mm$	Target displacement (displacement demand) calculated using 5% damping spectra.
$\mu = {d_t}/{d_y} = {186}/{56.8} = 3.27$	Initial displacement ductility.

The effective period lengthening ratio is calculated from ASCE/SEI 41-17 (equation 8-22) as presented in Equation (7.24).

$$\left(\frac{\tilde{T}}{T}\right)_{eff} = \left[1 + \frac{1}{\mu}\left(\left(\frac{\tilde{T}}{T}\right)^2 - 1\right)\right]^{0.5} \qquad (7.24)$$

$$\left(\frac{\tilde{T}}{T}\right)_{eff} = \left[1 + \frac{1}{3.27}((1.54)^2 - 1)\right]^{0.5} = 1.19$$

Equation (2.31) is used to calculate the total damping, ASCE/SEI 41-17 uses 2 as the superscript in Equation (2.31):

$$\beta_{tot} = \beta_f + \frac{\beta_i}{\left(\tilde{T}/T\right)^2_{eff}} = 0.0193 + \frac{0.05}{(1.19)^2} = 0.0547\ (5.47\%)$$

Equation (2.9) is used to update the response spectrum through Equations (2.10) to (2.13).

$\eta = \sqrt{\frac{10}{(5 + 5.47)}} = 0.977$	Updated effect on response spectrum.
$d_t = 173\ mm$	Updated target displacement.
$\mu = {}^{173}/_{56.8} = 3.046$	Updated displacement ductility.
$\left(\frac{\tilde{T}}{T}\right)_{eff} = 1.20$	Updated effective period lengthening.
$\beta_{tot} = 0.054$	Updated total damping.

The target displacement converges on $d_t = 174\ mm$.

7.3 EN 1998-1 (2004) target displacement iterative procedure

If the initial assumption regarding the displacement of the first hinge mechanism, when determining the bilinear curve, is significantly different to the end result, then the area under the two curves up to the target displacement will not be equal. EN 1998-1 *Annex B* provides an optional iterative procedure where the bilinear curve is adjusted to produce equal areas under the curve. This adjustment will, in turn, affect the effective stiffness and period, therefore altering the target displacement again.

Consider the capacity curve of model 7M40AR5 in Figure 7-6. The structure does not reach any failure criteria up to the drift limit ($Limit_{drift} \cong 0.02 \times H = 0.02 \times 23.2 = 0.464\ m$).

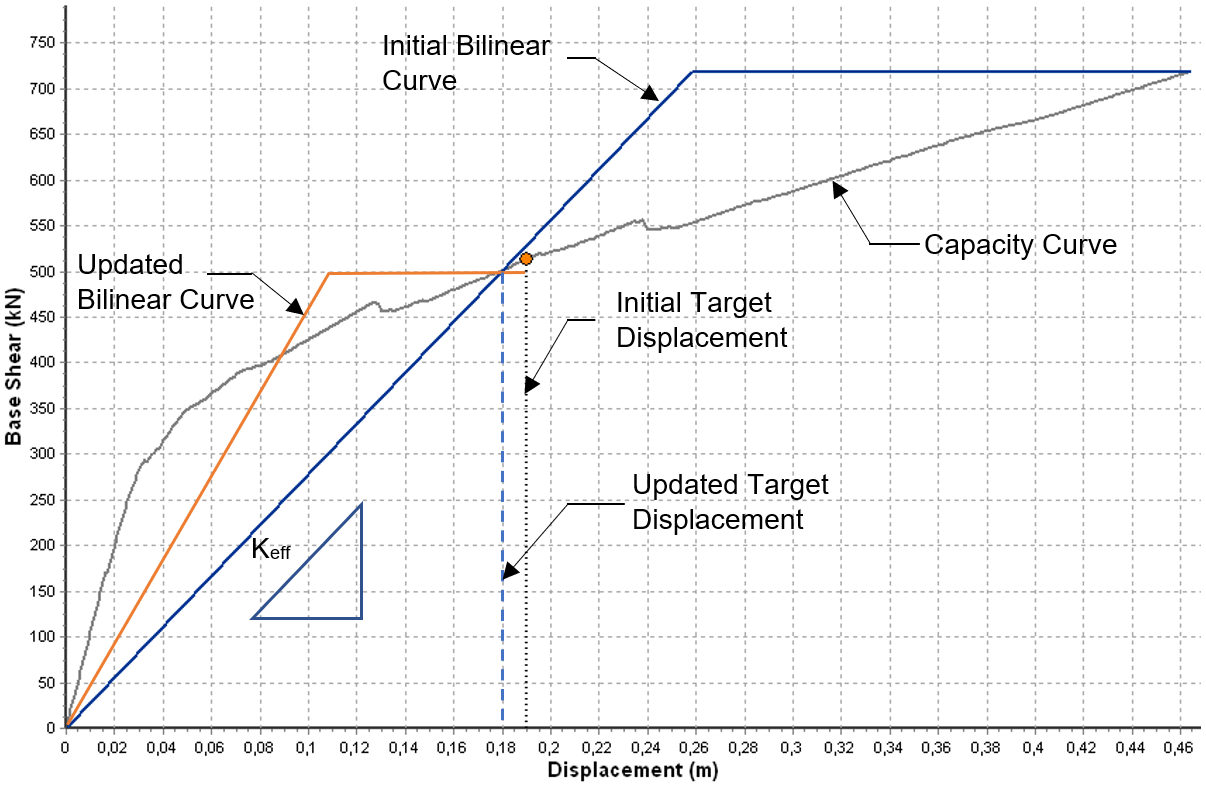

Figure 7-6: Capacity curve and corresponding bilinear curve for mode 7M40Ar5

The initial bilinear approximation is calculated to produce the same area under the curve as the capacity curve, up to the drift limits. However, the areas for the two curves up to the target displacement are very different. The target displacement lies within the elastic range of the initial capacity curve, implying no contribution of ductile behaviour to damping. An updated curve is calculated to produce the same area as the capacity up to the initial target displacement, which changes the effective stiffness and perceived ductility, therefore affecting the damping and target displacement. The process is iterated until the target displacement converges.

Even though the two bilinear curves differ significantly, the change in target displacement is relatively small in this case. This is due to the shape of the design displacement response spectrum given in Figure 2-8. Effective periods of both curves fall within the displacement plateau between the corner period, T_C and T_D, in this case between 2 and 6 seconds, where the displacement response is expected to stay relatively constant. The change is a result of additional damping due to the apparent ductility from the adapted bilinear curve.

It is expected that the iterative procedure will produce lower target displacements due to the shorter periods and the addition ductility, this is in fact the case for all models considered in this investigation. Furthermore, the maximum base shear of the bilinear curve obtained from the iterative procedure will reflect the base shear at which the target displacement is achieved on the capacity curve.

It should be noted that for most models the difference between the two bilinear curves is not as drastic as for the case considered in this section.

Models are tested against the larger target displacements produced from the non-iterative procedure, but the bilinear curves produced by the iterative procedure are considered when assessing ductility.

8 Nonlinear dynamic analysis (or THA)

Time-history analyses are used as an additional response verification in this investigation. The numerical models used for pushover analyses are kept the same for THA's. The adaptations to the models are the following sections.

8.1 Spectral matching and ground motion records

EN 1998 (2004), clause 4.3.3.4.3, specifies that if the response is obtained from at least 7 nonlinear time-history analyses, the average response quantities should be used as the design value. Otherwise, the most unfavourable value of the response quantities. EN 1998 (2004), clause 3.2.3.1.2 specifies a minimum of 3 accelerograms when spectral matching is used. Interestingly, ASCE/SEI 7-16 (2016) requires a minimum of 11 records, where in previous editions the maximum response of 3 or the mean response of 7 records was allowed.

The requirement of the larger number of motions was not based on statistical analyses, but rather judgementally selected to balance accuracy with computational effort (ASCE/SEI 7-16, 2016, p. 659). However, ASCE/SEI 7-16 recognises that fewer ground motions can be used to arrive at an acceptable estimate when matching is used (ASCE/SEI 7-16, 2016, p. 570).

The new edition to EN 1998, that is still in the draft phase, allows the use of 3 accelerograms only for low seismic regions (EN 1998-1-1 SC8 31-12-2018, 2018, p. 46).

As the THA's are used for additional verification and matched ground motion records are applied, only 3 ground motions were applied per model.

Spectral matching is the *nonuniform* scaling of a ground motion to match a target response spectrum, whereas scaling is the application of a *uniform* scale factor to the ground motion.

EN 1998 (2004), clause 3.2.3.1.2, specifies a period range for matching between $0.2T_1$ and $2T_1$. The period range for all models using eigenvalue analyses as described in Chapter 4.7 is between 1.05 and 2.85 seconds, with the pseudo-acceleration being

relatively constant after 4 seconds the period range for matching was chosen between 0.05 and 4 seconds.

The working draft of EN 1998 (EN 1998-1-1 SC8 31-12-2018, 2018, *Annex C*) requires that the scale factor must not exceed 2 or be smaller than 0.5. Table 7-5 shows that the unmatched PGA's for all the records chosen are within a reasonable range, considering that the PGA for Ground Type 3 of SANS is $S \times a_g = 1.15 \times 0.15g = 0.1725g$.

No value of the mean 5% elastic spectrum calculated from all time-histories should be less than 90% of the corresponding value of the 5% damping elastic spectrum (EN 1998-1, 2004, p. 43). Figure 8-1 shows the mean matched spectrum against the corresponding target acceleration response spectrum, with the maximum misfit (determined as 14.75%) being for extremely short periods not relevant for this investigation.

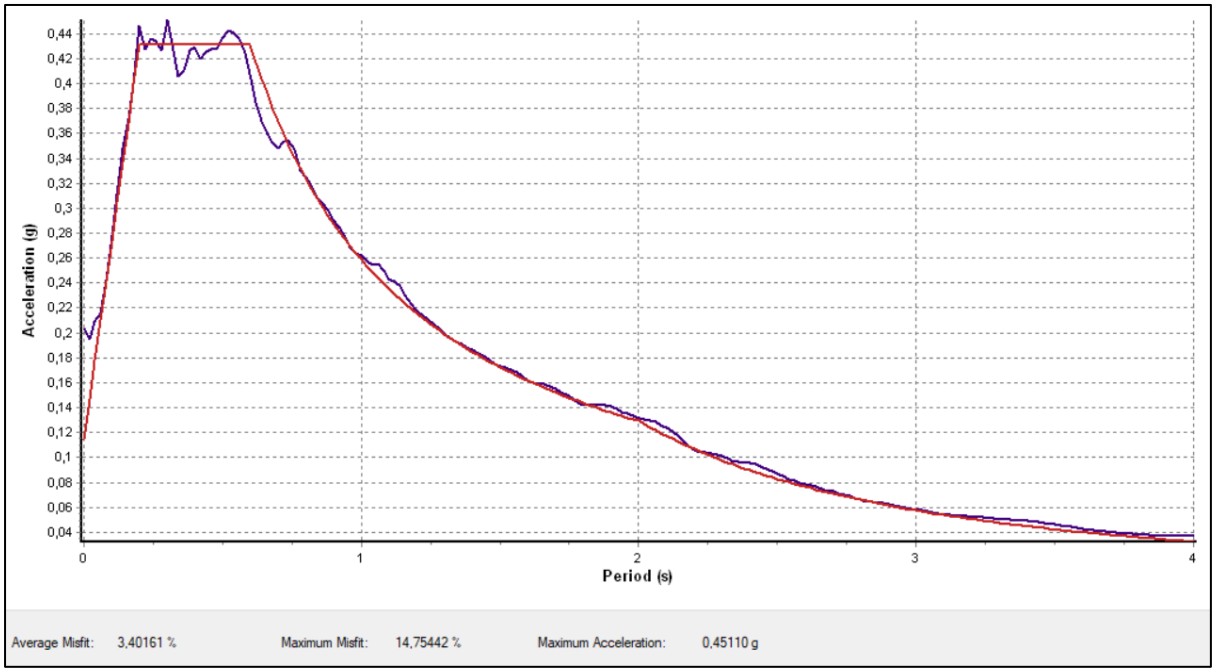

Figure 8-1: Mean matched spectrum against the target design spectrum

8.2 Additional damping

Section 2.6 addresses the different forms of damping. If the hysteretic rule models the elastic range nonlinearly, as in the case of the fibre element models, no additional

damping should be used to represent structural damping in the THA (Priestley, et al., 2007, p. 204).

The additional damping represents non-structural damping and foundation damping.

Foundation damping (around 3.2%) is conservatively ignored in the THA's of this investigation.

Non-structural damping represents hysteretic response and sliding of non-structural elements, mostly infill panels, and are introduced as tangent stiffness-proportionate damping in this investigation. Priestley, et al., (2007, p. 205) recommend an upper bound of 0.5% equivalent viscous damping for infill panels other than masonry. Owing to construction cost, masonry is used as infill panels for most buildings in South Africa. SeismoSoft User Manual (2020, p.182) recommends between 2% to 3% viscous damping as a reasonable estimate when using *tangent* stiffness-proportionate damping. Monteiro (2020) recommends 2% *tangent* stiffness-proportionate damping for buildings considered in this investigation. This investigation applies 2% *tangent* stiffness-proportionate damping for all THA's. This is expected to be conservative, as the models only consist of one frame to represent the lateral resistance of more than half the structure.

8.3 Incorporating SSI in THA

Most design guidelines are silent on the incorporation of SSI in THA. ASCE/SEI 41/17 and ASCE/SEI 7-16 permit the use of soil springs in principle but do not offer specific guidance on how it should be utilised. Kinematic effects due to SSI are indirectly incorporated by the reduction of the response spectrum when spectrum-compatible ground motion is selected, however, it is recommended that the effects of foundation damping are explicitly incorporated in the model. (NIST GCR 12-917-21, 2012, pp. 4-9 to 4-10).

Soil damping, radiation damping, and kinematic effects are conservatively ignored for the THA's of this investigation. The stiffness and capacity of the soil-springs are kept unchanged from that used for pushover analyses. Although the guidelines mentioned in this investigation allow the use of simplified bilinear spring element in THA, it has limitations that could affect the response of the THA's. Allotey & El Naggar, (2008)

proposed a generalised unload-reload curve, shown in Figure 8-2, that depends on several soil parameters not considered in this investigation. This should be further investigated.

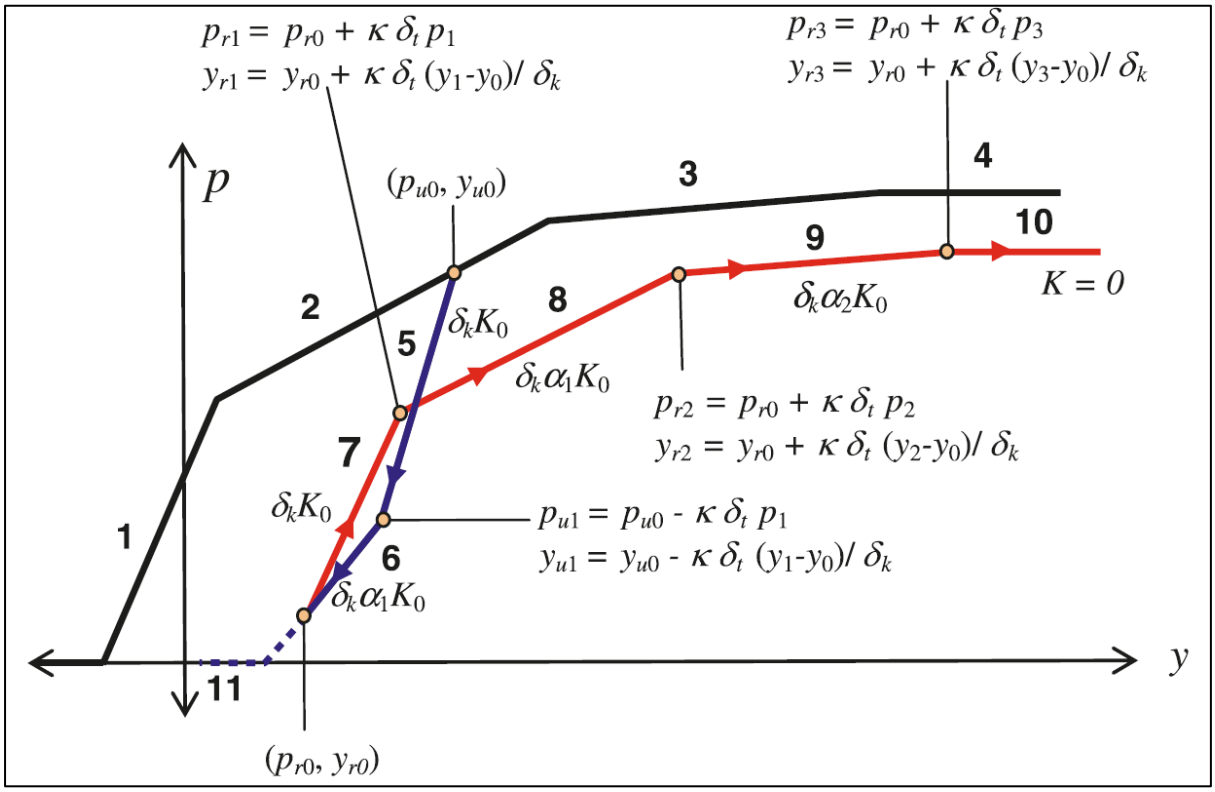

Figure 8-2: Generalised unload-reload curve for soil (Allotey & El Naggar, 2008)

Another possible limitation is the way shear-sliding resistance is typically modelled, as an uncoupled spring. This investigation does not consider shear-sliding, the horizontal spring in Figure 3-1 is therefore taken as rigid. As the foundation rotates and lifts, some areas will lose contact with the soil, which will influence the sliding shear resistance. Uncoupled horizontal elements are generally accepted for shallow foundations (NIST GCR 12-917-21, 2012, p. 2-37), but could influence the THA response, particularly the foundations reduced to resist a low percentage of the fixed moment.

9 Results and discussion

9.1 Meeting target displacement without failure

The principal objective is to assess whether structures designed according to the linear procedure (or force-based design) with the assumed behaviour factor, q = 5, meet displacement demands when tested with the nonlinear procedure (displacement-base design). This section assesses the results from the nonlinear static procedure (pushover analysis). Section 9.4 addresses the verification of these results with THA's.

Figure 9-1 to Figure 9-6 present the bilinear curves up until the target displacement (displacement demand from pushover analysis).

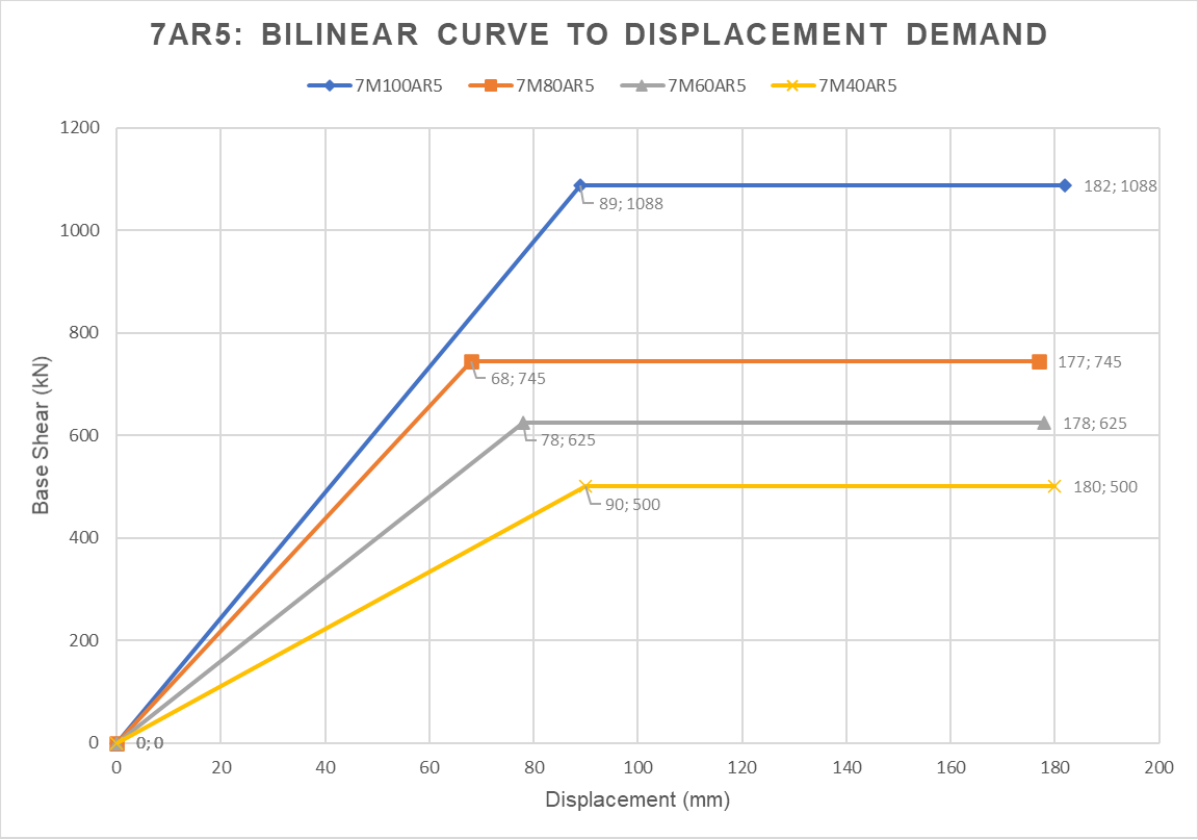

Figure 9-1: 7AR5 Idealised bilinear curve up to target displacement

For the 7-storey aspect ratio 5 models, the target displacement for each of the SSI models (models where foundations are explicitly modelled) is actually less than the target displacement for the fixed base model, as shown in Figure 9-1. This is because the effective periods are longer than the corner period, T_D. The reduction in the target displacement seen for the SSI models is the result of the adjustments in damping, due

to SSI and ductility, accounted for in the SSI adjusted method. The smallest base (7M40AR5) produces the least foundation damping and ductility, therefore requiring the largest target displacement between the SSI models.

The increase in target displacement with an increase in the effective period is better illustrated in Figure 9-2. With an aspect ratio of 3, the structural walls are longer and stiffer, therefore the effective periods are shorter, only exceeding the corner period, T_D with 7M60AR3 and 7M40AR3.

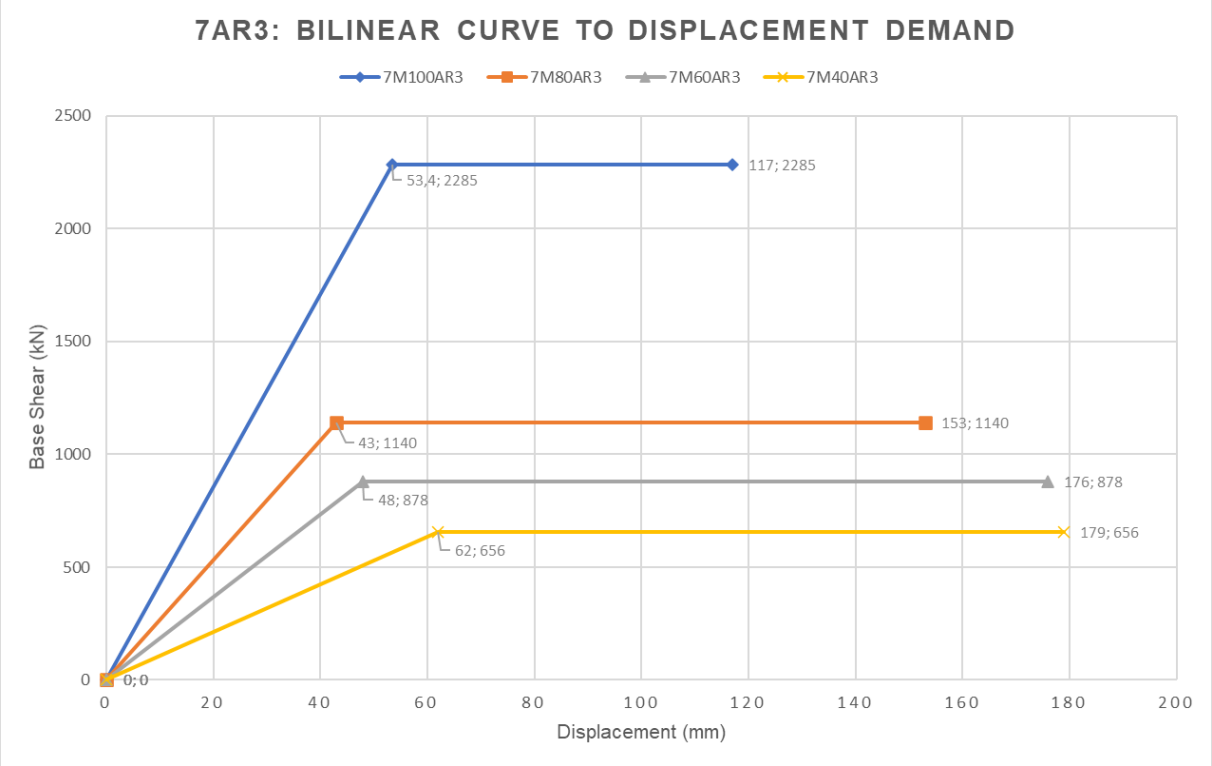

Figure 9-2: 7AR3 Idealised bilinear curve up to target displacement

The difference between the base shear of the fixed base model 7M100AR3 and the SSI models is larger than expected. This is because of the minimum reinforcing steel requirements in the boundary elements and the wall web that is assumed (see section 5.2), creating an overstrength of ,$\frac{Vpushover}{Vcode} = \frac{2285}{1392} = 1.64$, which is above the expected overstrength of approximately 1.3 to 1.5.

As in the case of the 7-storey aspect ratio 5 models, the 5-storey aspect ratio 5 models are relatively slender, therefore exceeding the corner period and reaching the "*displacement plateau*" between T_D and T_E (refer to Figure 2-8). The results from the 5-storey aspect ratio 5 presented in Figure 9-3, consistently indicate that the target

displacements are less than the fixed base model but increases as the foundation sizes are reduced, because of the reduction in foundation damping.

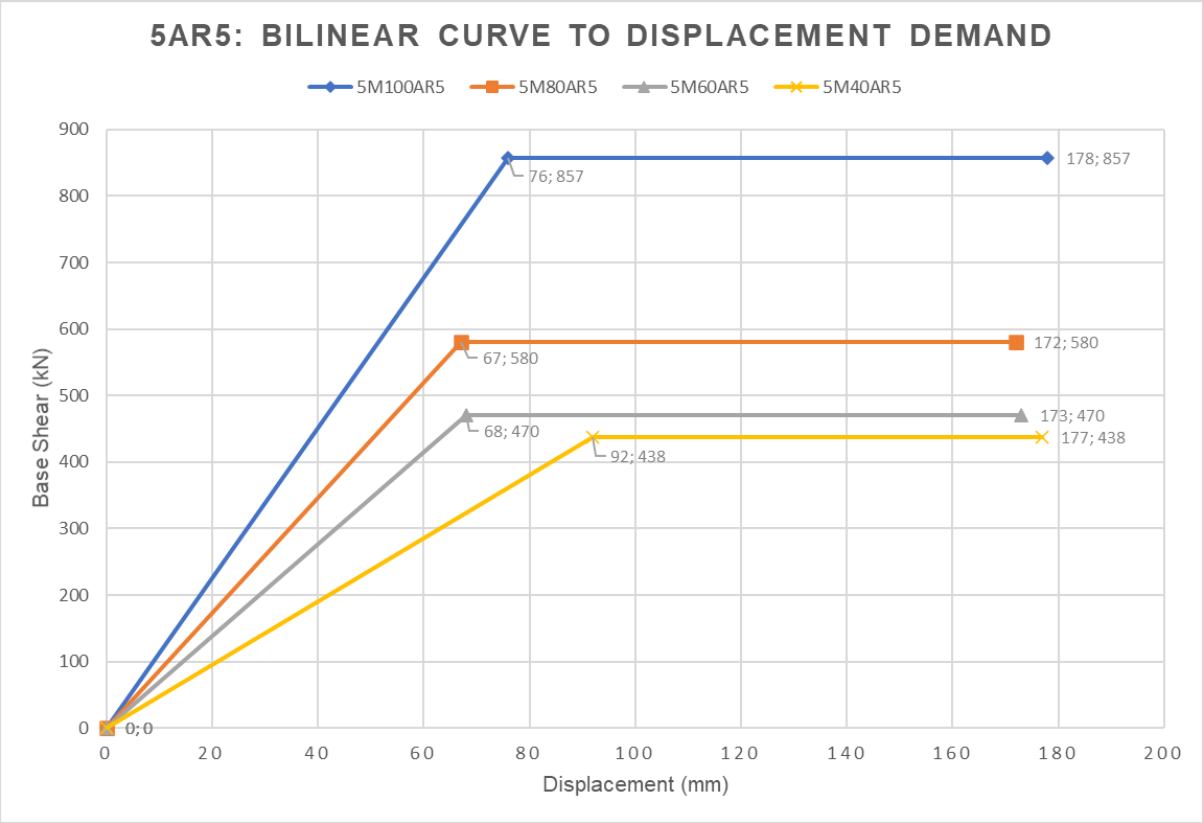

Figure 9-3: 5AR5 Idealised bilinear curve up to target displacement

A good illustration of SSI behaviour is the 5-storey aspect ratio 3 models shown in Figure 9-4. Because the effective periods are shorter than the corner periods, T_D, the target displacement increases almost linearly with base reduction. The influence of foundation damping and ductility on damping do not significantly reduce the target displacement relative to the effective period.

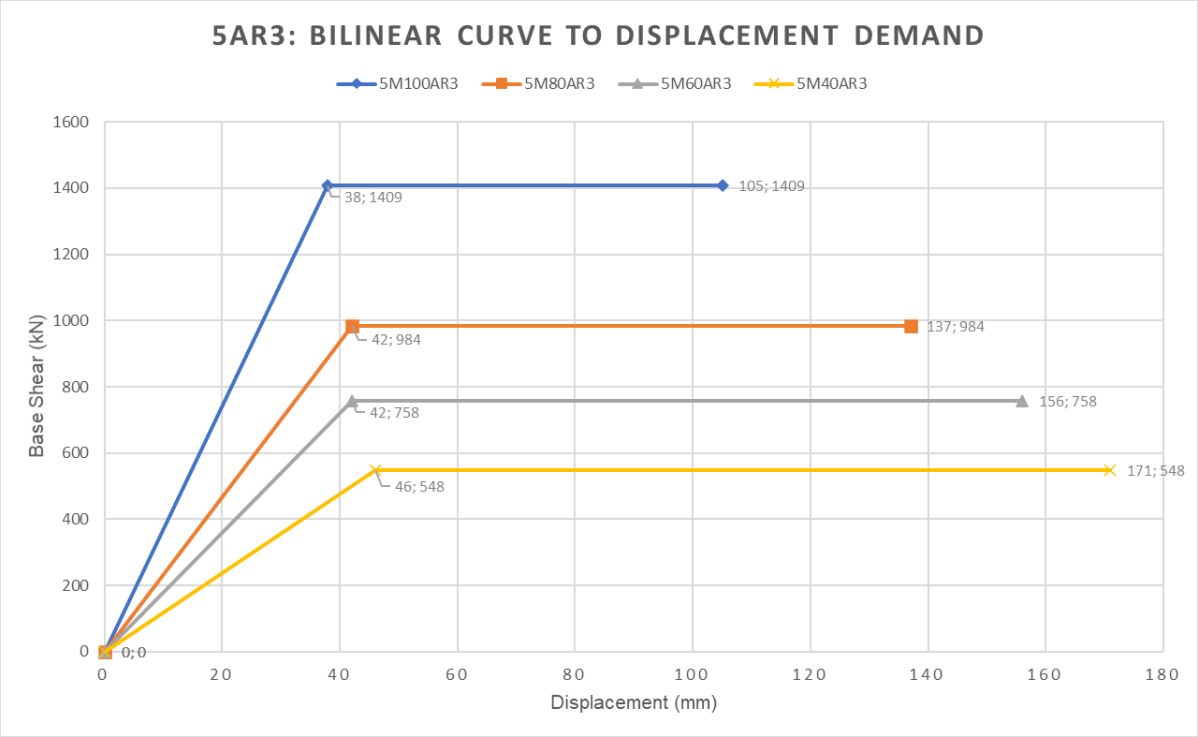

Figure 9-4: 5AR3 Idealised bilinear curve up to target displacement

Interestingly, the only model that failed before reaching the required target displacement is the fixed model 3M100AR5. It is shown in Figure 9-5 that the structure failed (crushing of confined concrete) at a displacement of 141 mm, before the target displacement of 148 mm was reached. This possibly suggests that the behaviour factor of q = 5 is not appropriate for all structural walls. Assessing the behaviour factor of fixed base structural walls do not form part of the scope of this study, however, it is useful to consider the following:

- The period used for base shear calculations is calculated from an eigenvalue analysis, which produced a period exceeding the allowable limit of 1.4 times the period calculated from empirical formulas given in SANS 10160-4 (2017). The shorter period will result in a larger design base shear, therefore requiring more steel reinforcement.
- For the 3-storey height and aspect ratio of 5 models, the structural wall is only 2.08 m in length. Considering this as a structural wall, rather than a column, might be inappropriate.

- As seen in Figure 7-4, the N2 method can produce conservative estimates for the displacement demands. The average displacement demand from the THA's is 136 mm, whereas the N2 method calculates 148 mm.
- As noted in Section 6.2.2.2, Equation (6.15) will produce conservative estimates for ultimate strain for confined concrete.

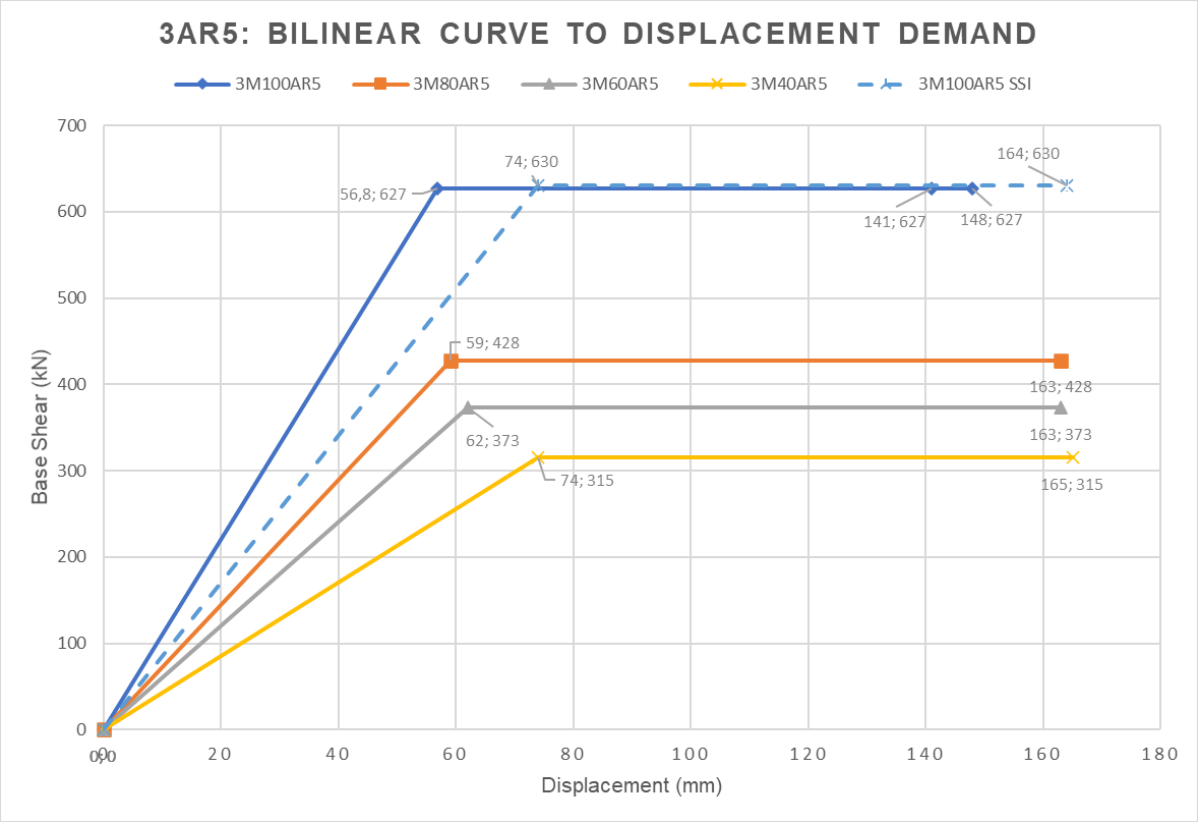

Figure 9-5: 3AR5 Idealised bilinear curve up to target displacement

When assessing the same structure, but explicitly modelling an overstrength foundation (assuming overstrength as 1.2), the SSI model reaches the updated increased target displacement of 164 mm, shown in Figure 9-5 as the dashed line. This, again, implies that code prescribed behaviour factors consider additional influences not included in the strict definition of the factor.

A similar trend of increasing target displacement with reduced foundation size is observed for the 3-storey aspect ratio 3 models in Figure 9-6.

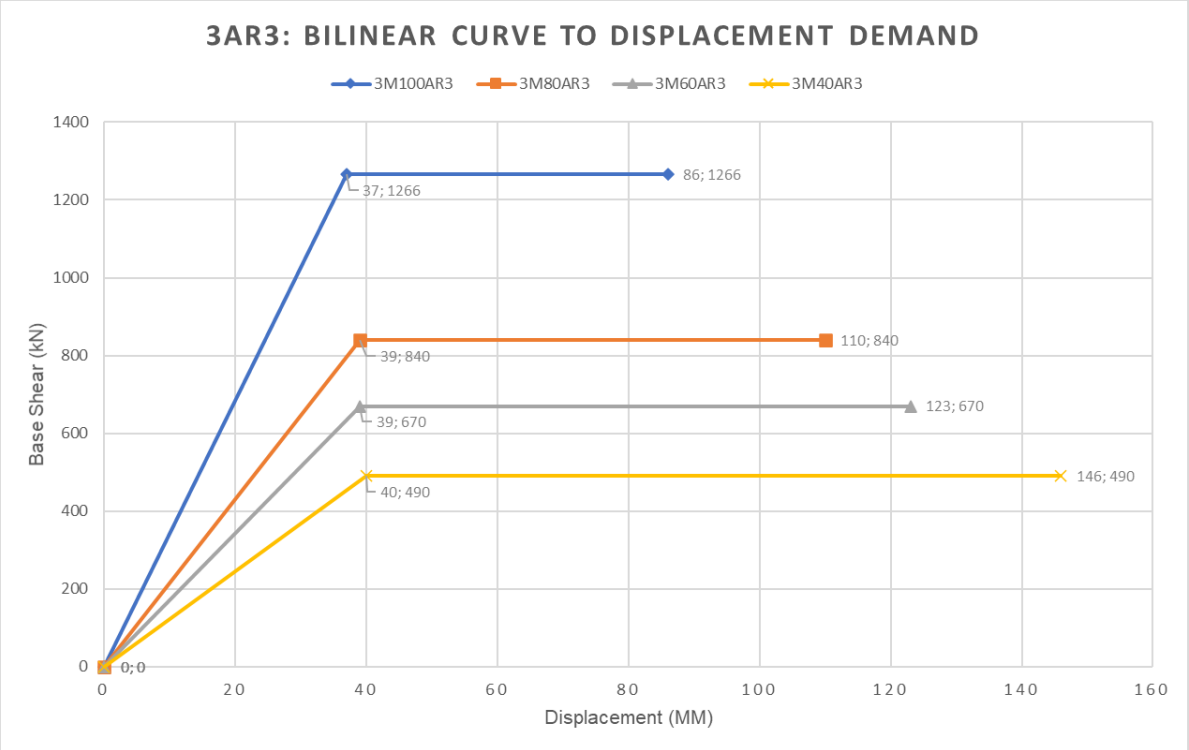

Figure 9-6: 3AR3 Idealised bilinear curve up to target displacement

All structures with explicitly modelled bases achieve their target displacement without failure, indicating that the behaviour factor of 5 is appropriate for all SSI models considered in this investigation. However, apart from the structures with periods exceeding the corner period, the ductility demand (ductility required to meet displacement demand) increases with foundation reduction for the SSI models.

Ductility capacity is a key component in defining the behaviour factor. Section 9.2 addresses relative ductility.

9.2 Relative ductility capacity and demand

As discussed in Section 2.9, one of the difficulties when assessing behaviour factors is the lack of consensus in defining ductility. For this reason, the term *relative ductility* is used in this section, as it assesses the ductility with the bilinear curve calculated using the equal energy principles of EN 1998 (2004) when determining the target displacement. This does not necessarily suggest that the same bilinear curve is used when assessing ductility for Eurocode and South African standards. A comparison can, however, be made with the idealised bilinear curves from the fixed base models calculated with the same procedure. Figure 9-7 through to Figure 9-12 illustrate the

relative ductility capacity of the fixed base models and the SSI models. Modes of failure are shown with maximum displacement capacity.

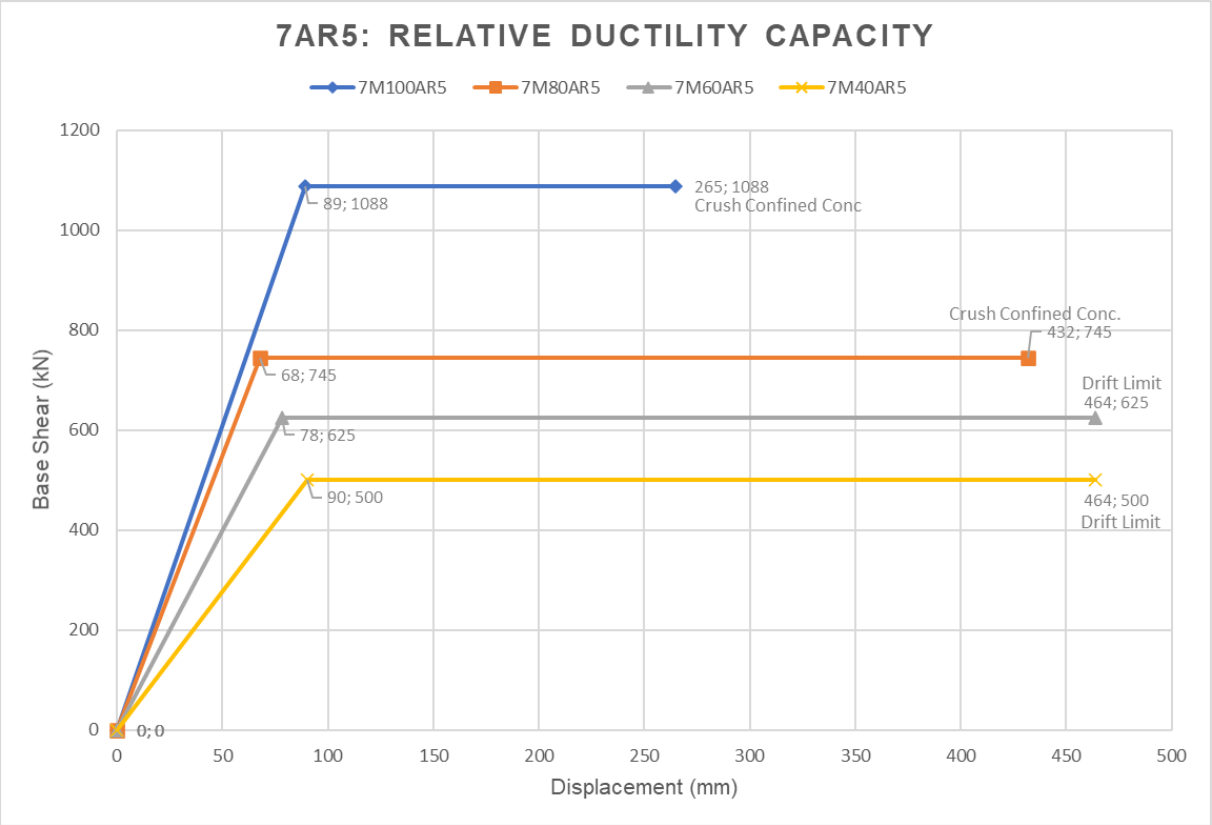

Figure 9-7: 7AR5 Relative ductility capacity

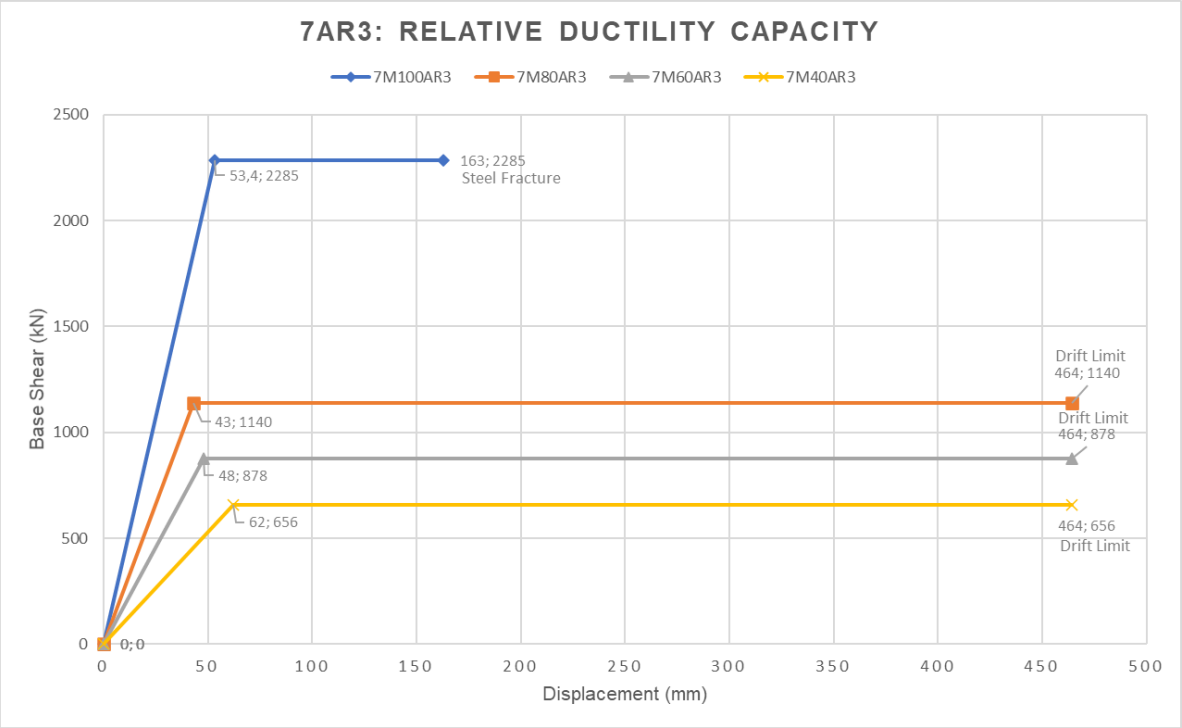

Figure 9-8: 7AR3 Relative ductility capacity

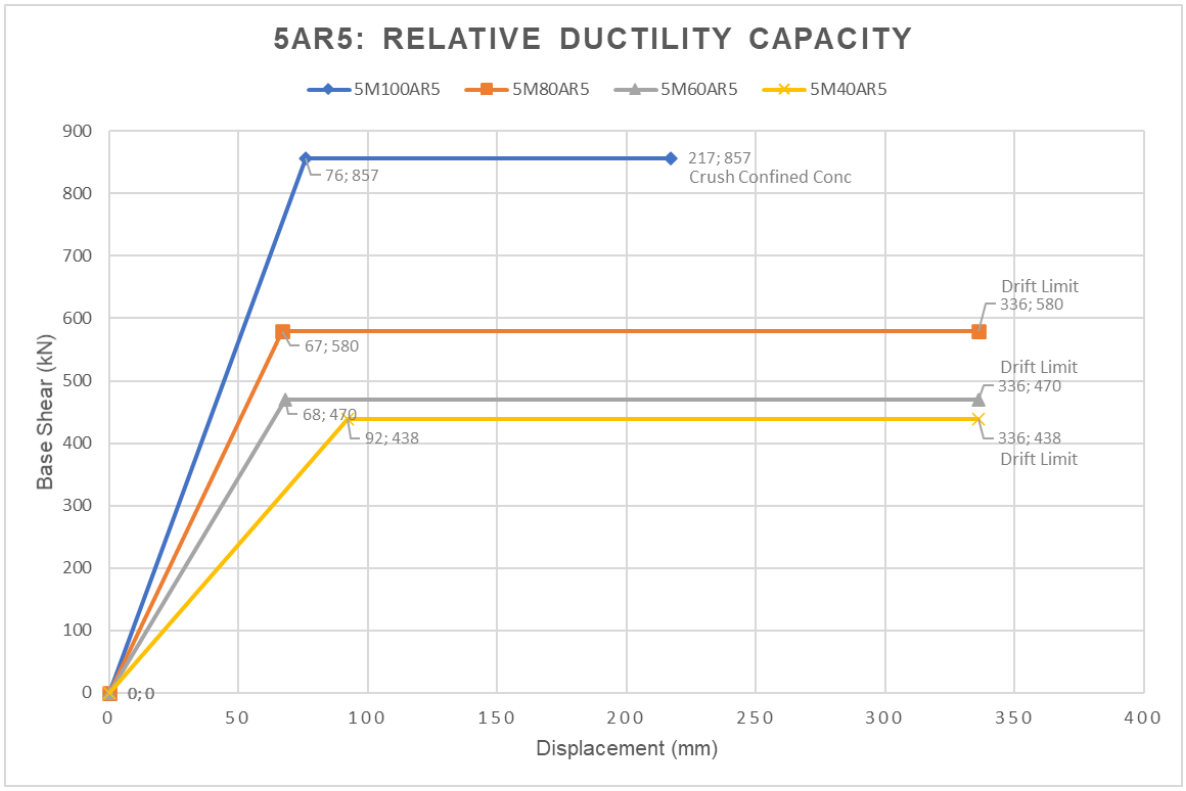

Figure 9-9: 5AR5 Relative ductility capacity

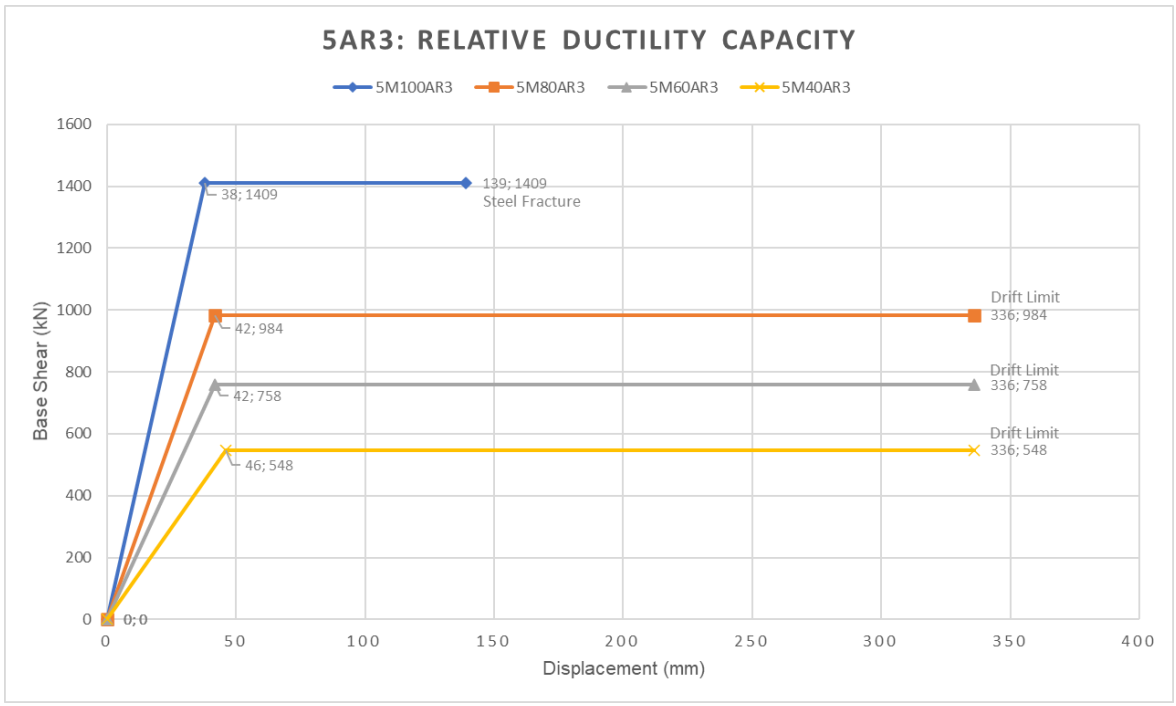

Figure 9-10: 5AR3 Relative ductility capacity

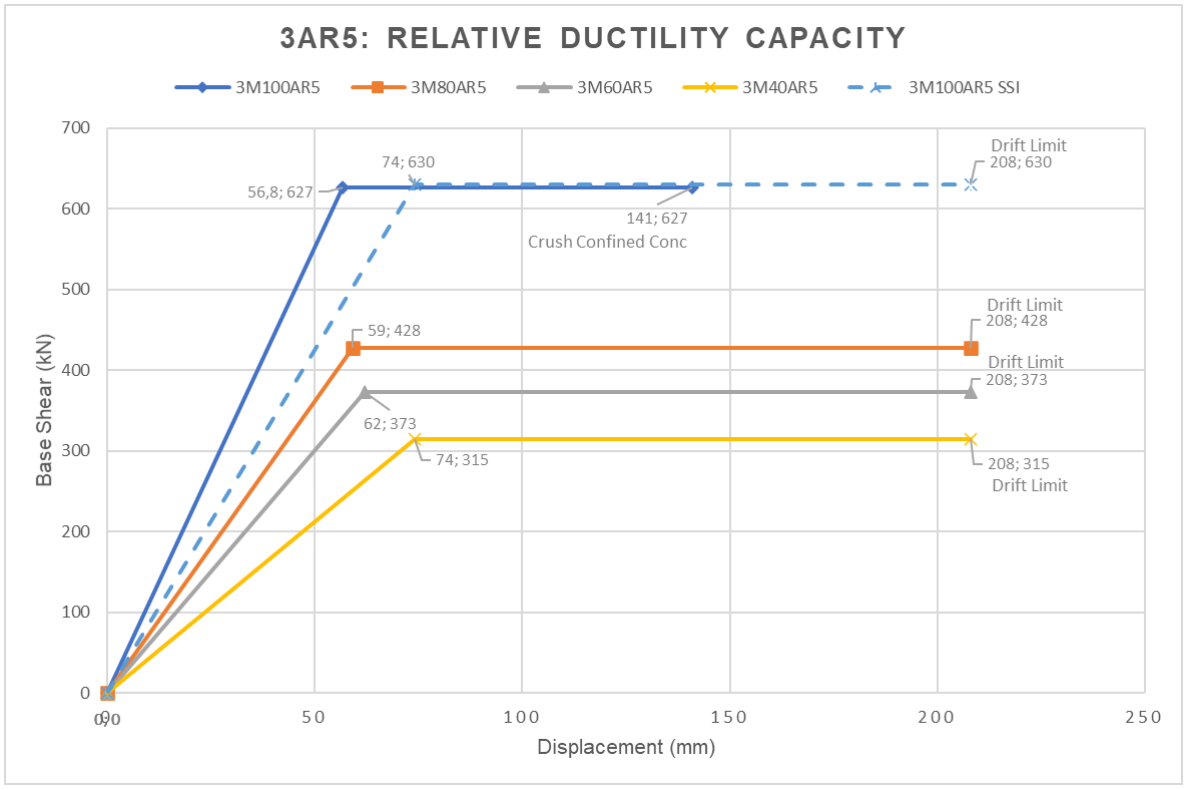

Figure 9-11: 3AR5 Relative ductility capacity

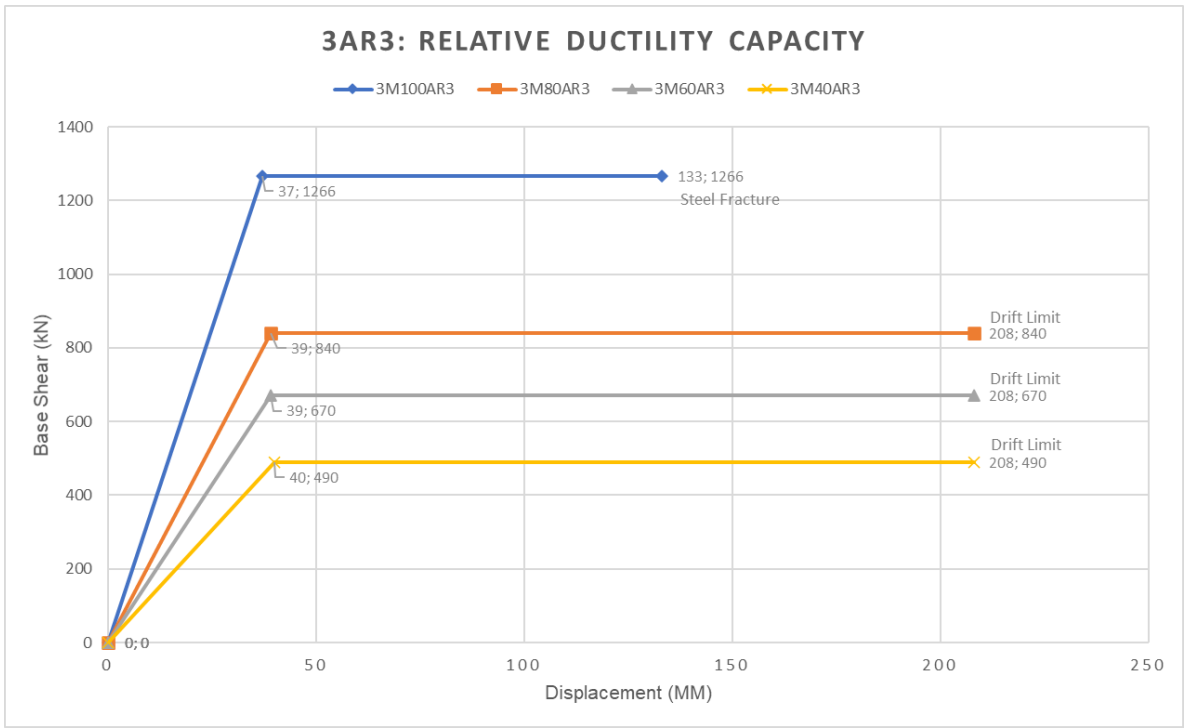

Figure 9-12: 3AR3 Relative ductility capacity

Consider the two fixed models of 3M100AR5 in Figure 9-11. It is expected that the additional flexibility owing to the rotating foundation will increase the yield displacement and the ultimate displacement by the same amount, therefore not

affecting ductility, as discussed in Section 2.9 (see Figure 2-22 and Equation (2.51)). However, this assumption does not consider the effects of the contributing frame as the foundation rotates. The frame for the 3M100AR5 SSI model is not adjusted to consider the additional rotation due to a flexible base, the only difference to the fixed base is that the foundation is explicitly modelled, yet the contributing frame provides additional resistance to achieve a proportionately larger maximum displacement, and so improving the ductility capacity from $\mu(fixed) = {}^{141}/_{56.8} = 2.48$ to $\mu(SSI) = {}^{208}/_{74} = 2.81$.

Assuming an overstrength factor of 1.5 and combining Equations (2.16) and (2.17) for this period range will arrive at behaviour factors of:

$$q(fixed) = R \times \Omega = \mu \times 1.5 = 2.48 \times 1.5 = 3.72$$

$$q(SSI) = R \times \Omega = \mu \times 1.5 = 2.81 \times 1.5 = 4.2$$

However, considering the additional influences and recalling that idealised bilinear approximations could differ significantly, the actual value is not of interest for this investigation, but rather the relative value of an improvement in relative ductility of ${}^{4.2}/_{3.72} = {}^{2.81}/_{2.48} = 1.13$.

It is observed from Figure 9-7 to Figure 9-12 that the ductility capacity of the SSI models is significantly larger than the fixed models but reduces with reducing foundation size. Furthermore, it observed in Section 9.1 that, generally, ductility demand increases with reducing foundation size. The proportions of the increase in relative ductility demand against the reduction in relative ductility capacity are, therefore, of interest and are summarised in Table 9-1 to Table 9-6.

Table 9-1: 7AR5 relative ductility

	Relative Ductility		Ductility Capacity/Ductility Demand
Model	Ductility Demand	Ductility Capacity	
7M100AR5	2.05	2.98	1.46
7M80AR5	2.60	6.35	2.44
7M60AR5	2.28	5.95	2.60
7M40AR5	2.00	5.16	2.58

Table 9-2: 7AR3 relative ductility

	Relative Ductility		Ductility Capacity/Ductility Demand
Model	Ductility Demand	Ductility Capacity	
7M100AR3	2.19	3.05	1.39
7M80AR3	3.56	10.79	3.03
7M60AR3	3.67	9.67	2.64
7M40AR3	2.89	7.49	2.59

Table 9-3: 5AR5 relative ductility

	Relative Ductility		Ductility Capacity/Ductility Demand
Model	Ductility Demand	Ductility Capacity	
5M100AR5	2.34	2.86	1.22
5M80AR5	2.57	5.02	1.95
5M60AR5	2.54	4.94	1.94
5M40AR5	1.92	3.65	1.90

Table 9-4: 5AR3 relative ductility

	Relative Ductility		Ductility Capacity/Ductility Demand
Model	Ductility Demand	Ductility Capacity	
5M100AR3	2.76	3.66	1.32
5M80AR3	3.26	8.000	2.45
5M60AR3	3.71	8.000	2.15
5M40AR3	3.72	7.30	1.97

Table 9-5: 3AR5 relative ductility

	Relative Ductility		Ductility Capacity/Ductility Demand
Model	Ductility Demand	Ductility Capacity	
3M100AR5	2.61	2.48	0.95
3M80AR5	2.76	3.53	1.28
3M60AR5	2.63	3.36	1.28
3M40AR5	2.23	2.81	1.26
3M100AR5 SSI	2.22	2.81	1.27

Table 9-6: 3AR3 relative ductility

	Relative Ductility		Ductility Capacity/Ductility Demand
Model	Ductility Demand	Ductility Capacity	
3M100AR3	2.32	3.60	1.55
3M80AR3	2.82	5.33	1.90
3M60AR3	3.15	5.33	1.69
3M40AR3	3.65	5.20	1.43

The right column shows a significant improvement in the ductility capacity – ductility demand ratio for most SSI models against the fixed models, indicating an improved safety against collapse.

It is worth noting that the actual fixed models will, themselves, rest on foundations large enough to resist the fixed moment. This is likely to improve the actual behaviour of the structure under real seismic action, but with a foundation designed to resist an overstrength moment, the mode of failure is likely to be similar to the fixed moment.

Table 9-5 shows that 3M100AR5 SSI and 3M40AR5 have similar capacity - demand ratios and model 3M40AR3 indicate a smaller ratio than 3M100AR3 in Table 9-6, indicating that the advantage of SSI is lost with such large reductions in foundation sizes, also considering the additional reinforcement required in the contributing frame.

9.3 Significance of the displacement corner period, T_D

As observed from previous sections, the natural period of the structure increases as the foundation sizes are reduced, which results in a larger displacement response until the point at which the natural period exceeds the corner period, T_D. From this point the displacement response is expected to either stay relatively constant or decrease for increasing periods, which limits the disadvantages of allowing foundation flexibility. SANS 10160-4 (2017) and EN 1998-1 (2004) specify that the corner period is taken as 2 seconds.

Faccioli, et al., (2004) performed an investigation on a large set of earthquake records to determine factors influencing displacement spectra. The main outcomes from the investigation of Faccioli, et al., (2004) that concern this study are summarised as:

- The 5% damped displacement increases essentially linearly with period up to a corner period (T_D).
- It is conservative to assume a constant spectral displacement for periods longer than T_D for moderate earthquakes.
- There is a slight tendency for corner periods to increase for soft soils, although for moderate earthquakes it is less obvious.
- The corner period appears to increase almost linearly with earthquake magnitude. Equation (9.1) establishes a relationship between moment magnitude, M_w and the corner period, T_D.

$$T_D = 1 + 2.5(M_w - 5.7), \qquad M_w > 5.7 \tag{9.1}$$

It appears that for earthquakes with moment magnitude larger than 5.5, the corner period of 2 seconds is non-conservative. A comparison was conducted on the corner period prescribed by the National Earthquake Hazards Reduction Program (NEHRP), EN 1998-1 (2004), Faccioli, et al., (2004), which is illustrated in Figure 9-13 (Priestley, et al., 2007, p. 52).

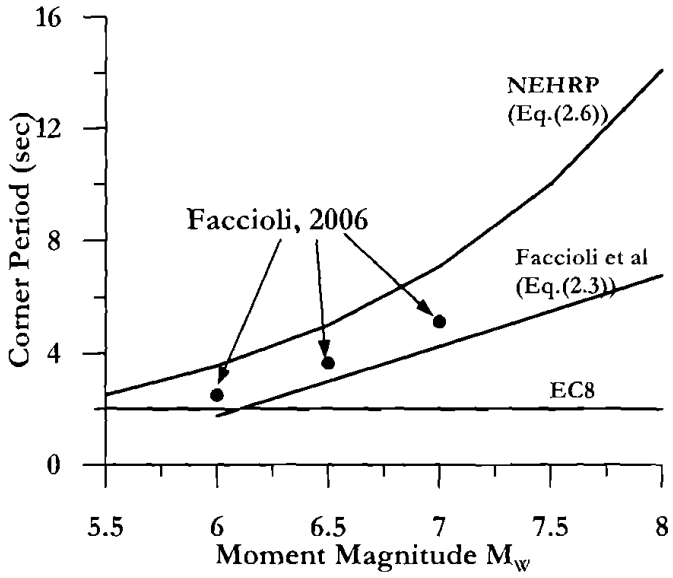

Figure 9-13: Relationship between corner period, displacement spectra and moment magnitude (Priestley, et al., 2007)

The expected moment magnitude, M_w of an earthquake in South Africa is relatively low, therefore the discrepancy between real records and the corner period prescribed by EN 1998 (2004) is expected to be small, however, the corner period for South African conditions should be further investigated.

9.4 Displacement response verification with THA

The average and maximum displacement responses from the THA's are summarised in Table 9-7 through to Table 9-12.

Table 9-7: 7AR5 THA displacement demand and target displacement

	Displacement Response, THA (mm)		Pushover Target Displacement (mm)
Model	Average	Maximum	
7M80AR5	41	43	177
7M60AR5	125	144	178
7M40AR5	155	183	180

Table 9-8: 7AR3 THA displacement demand and target displacement

	Displacement Response, THA (mm)		Pushover Target Displacement (mm)
Model	Average	Maximum	
7M80AR3	110	112	153
7M60AR3	131	174	176
7M40AR3	133	155	179

Table 9-9: 5AR5 THA displacement demand and target displacement

	Displacement Response, THA (mm)		Pushover Target Displacement (mm)
Model	Average	Maximum	
5M80AR5	121	123	172
5M60AR5	115	127	173
5M40AR5	127	151	177

Table 9-10: 5AR3 THA displacement demand and target displacement

	Displacement Response, THA (mm)		Pushover Target Displacement (mm)
Model	Average	Maximum	
5M80AR3	96	107	137
5M60AR3	133	143	156
5M40AR3	110	118	171

Table 9-11: 3AR5 THA displacement demand and target displacement

	Displacement Response, THA (mm)		Pushover Target Displacement (mm)
Model	Average	Maximum	
3M80AR5	120	133	163
3M60AR5	119	125	163
3M40AR5	110	123	165

Table 9-12: 3AR3 THA displacement demand and target displacement

	Displacement Response, THA (mm)		Pushover Target Displacement (mm)
Model	Average	Maximum	
3M80AR3	95	100	110
3M60AR3	95	106	123
3M40AR3	88	93	146

The only displacement response that exceeds the predicted target displacement is 7M40AR5, where the maximum demand exceeds the target displacement by 3 mm. The structures perform surprisingly well when subjected to the ground motions. The

results are, however, irregular. An apparent abnormality of a maximum response of 43 mm for 7M80AR3 is observed, however, it is observed that the average response does not deviate significantly from the maximum. The model was subjected to various adjustments for variables such as:

- Ground motion records, matched and unmatched.
- Reduced time step.
- More stringent convergence criteria.
- Upper bound of 2 x soil stiffness and bearing capacity.
- Various soil damping ratios.

The resulting displacement responses do not deviate significantly from above.

Further investigations are recommended with more ground motion records and advanced stress-strain curves to represent the soil hysteretic behaviour.

10 Conclusions

10.1 Displacement response

The main objective of this study is to assess the behaviour factor when SSI is incorporated in structural wall buildings. All SSI models reach their target displacements with significant additional capacity, therefore confirming that the behaviour factor adequately (and possibly conservatively) represents the expected ductility when linear (force-based) methods are used. The conclusions from the outcome of the pushover analyses are:

- The target displacement increases with the reduction in foundation size.
- The increase in target displacement for structures with fundamental periods larger than the corner period, T_D is mainly the result of a reduction in damping with a reduction in foundation size. The more slender buildings with wall aspect ratios of 5 illustrate this principle.
- For structures with fundamental periods smaller than the corner period, T_D the increase in target displacement is more significant due to the linear relationship between displacement response and fundamental period for periods between T_C and T_D. The more rigid buildings with wall aspect ratios of 3 illustrate this principle.
- The required base shear associated with the target displacement reduces with a reduction in foundation size.
- The influence of foundation damping is relatively small for foundation sizes considered in this investigation.

The displacement responses from the THA's verifies that the structures achieve their displacement demands without failure, however the displacement responses are more inconsistent than that of the pushover analysis. The recommendations for further investigation regarding THA's are:

- Include a more advanced soil hysteretic model.
- Increase the ground motion records to 7, or even 11.
- Include coupled horizontal springs to represent the sliding shear resistance.

10.2 Ductility capacity to ductility demand

With a standalone structural wall, the ductility capacity is likely to either remain constant or reduce, depending on the mode of failure. This will reduce the ductility capacity to demand ratio, as the lengthened period will result in larger displacement demands. However, if the frame is designed to contribute to lateral resistance, due to the additional foundation rotation, then a significant improvement in capacity and safety is observed, without the reduction in ductility and therefore no reduction in the behaviour factor. The observations regarding ductility capacity to ductility demand ratio are:

- Significant improvements from the fixed base models to the M80 models are observed.
- For buildings with a wall aspect ratio of 5, the improvements for the reduced foundation sizes remain relatively constant per building height.
- For building with wall aspect ratios of 3, the improvements decrease with reduction in foundation size per building height.
- The improvements decrease with a reduction in the number of storeys and therefore the number of contributing frames.
- A reduced ductility capacity to demand ratio is observed for the 3M40AR3 model relative to the 3M100AR3 model, indicating a deterioration in safety relative to the fixed model. The ductility capacity to demand ratio is 1.5 for 3M100AR3 and 1.4 for 3M100AR3, which could still be considered acceptable considering that the mode of failure for 3M100AR3 is strain related, therefore associated with structural damage and safety, where the mode of failure for 3M40AR3 is the drift limit, therefore associated with damage of non-structural elements, not collapse.
- An improvement for the 3M100AR5 SSI model relative to the fixed base model is observed. This improvement is consistent with the improvements for models; 3M80AR5, 3M60AR5 and 3M40AR5, suggesting that the fixed base models will inherently possess better safety against collapse than what is predicted, given that the structure is attached to a frame.

10.3 Compatibility

It is observed that the actual displacement response and rotation when SSI is incorporated in the analysis differs from the displacement response of the fixed base model. For the sake of compatibility between the actual rotation of the concrete wall and the frame attached to it, incorporating SSI in the analysis is recommended.

10.4 Further research

Further research recommendations are:

- Include a more detailed hysteretic curve to represent the soil response in THA's.
- Include shaking table tests to confirm results.
- Consider several frame elements with various spans.
- Consider the effects of shear failure in the frame.
- Investigate the cyclic behaviour of unconfined frame elements like slabs.
- Include kinematic effects.
- Perform an economical study on the additional reinforcement required in the frame elements against the reduction in foundation size and optimise the economic compromise between the beneficial effects of SSI and the disadvantages in repairing foundation settlement and residual tilt.
- Certain soil types can undergo liquefaction under cyclic loading, which is detrimental to the safety of the building. Investigate the areas in South Africa where these soil types may be present.
- Investigate the influence of different soil types on rocking behaviour.
- Investigate the effects of shear strength and deformation on ductility.

11 Bibliography

Allotey, N. & El Naggar, M. H., 2008. Generalized dynamic Winkler model for nonlinear soil-structure interaction analysis. *Canada Geothecnical Journal,* Issue 45, pp. 560-573.

Allotey, N. & El Naggar, M. H., 2003. Analytical moment-rotation curces for rigid foundations based on a Winkler model. *Soil Dynamics and Earthquake Engineering,* Volume 23, pp. 367-381.

ASCE/SEI 41-17, 2017. *Seismic evaluation and retrofit of existing buildings,* Reston,Virginia: American Society of Civil Engineers.

ASCE/SEI 7-16, 2016. *Minimum design loads and associated criteria for buildings and other structures,* Reston, Virginia: American Society of Civil Engineers.

Bachmann, H. et al., 2002. *Erdbebengerechter Entwurf und Kapazitatsbemessung eines Gabaubes mit Stahlbetontragwanden,* Zurich: SIA - Schweizerischer Ingenieur- und Architektenverein.

Bommer, J. J. & Elnashai, A. S., 1999. Displacement spectra for seismic design. *Journal of Earthquake Engineering,* 3(1).

Bowles, J. E., 1996. *Foundation Analysis and Design.* 5th ed. SIngapore: McGraw-Hill.

Chopra, A. L., 2012. *Dynamics of Structures.* 4th ed. Upper Saddle River: Pearson Prentice Hall.

Crouse, C., 2001. *Commentary on soil-structure interaction in U.S. seismic provisions.* Tsukuba, Japan.

Dwairi, H. M. & Kowalsky, M. J., 2007. Equivalent Viscous Damping in Support of Direct Displacement-Based Design. *Journal of Earthquake Engineering,* 11(4), pp. 512-530.

EN 1992-1-1, 2004. *Eurocode 2: Design of concrete structures - Part -1-1: General rules and rules of buildings ,* CEN: European Committee For Standardization.

EN 1998-1-1 SC8 31-12-2018, 2018. *Working Draft Part 1-1 of EN 1998 with general rules as resulting from splitting the previous Part 1 dated of 18/12/2018. It contains the previous chapters 4, 5, 6 and the relevant annexes.*

EN 1998-1, 2004. *Eurocode 8: Design of structures for earthquake resistance - Part 1: General rules, seismic actions and rules for buildings,* CEN: European Committee of Standardization (CEN).

EN 1998-5, 2004. *Design of structures for earthquake resistance Part 5: Foundations, retaining structures and geotechnical aspects,* CEN: Eurpean Committe for Standardization.

Faccioli, E., Paolucci, R. & Rey, J., 2004. Displacement Spectra for Long Periods. *Earthquake Spectra,* 20(2), pp. 347-376.

Fajfar, P., 1999. Capacity spectrum method based on inelastic demand spectra. *Earthquake Engineering and Structural Dynamics,* Issue 28, pp. 979-993.

Fajfar, P., 2000. A nonlinear analysis method for performance-based seismic design. *Earthquake Spectra,* Issue 16, pp. 573-593.

Fardis, et al., 2005. *Designers' guide to Eurocode 8: Design of buildings for earthquake resistance.* London: ICE Publishing.

FEMA 1050, 2015. *Recommend Provisions for Seismic Regulations for New Buldings and other structures, Part1: Provisions, prepared by the Building Seismic Safety Council for the Federal Emergency Management Agency,* Washington, D.C.

FEMA 274, 1997b. *NEHRP commentary on the guidelines for seismic rehabilitation of buildings,* Washington, DC: Prepared by the Building Seismic Safety Council for the Federal Emergency Management Agency.

FEMA 356, 2000. *Prestandard and commentary for the seismic rehavilitation of buildings,* Washington, DC: Prepared by ASCE for the Federal Emergency Management Agency.

FEMA 440, 2005. *Improvement of Nonlinear Static Seismic Analysis Procedure, prepared by the Applied Technology Council for Federal Emergency Management Agency,* Washington, D.C.

FEMA P-2006, 2018. *Example Application Guide for ASCE/SEI 41-13 Seismic Evaluation and Retrofitting Exsiting Buildings with Additional Commentary for ASCE/SEI 41-17, Prepared by Applied Technology Council for Federal Emergency Management Agency,* Wahington, D.C.

Feng, Y., Kowalsky, M. J. & Nau, J. M., 2014. Fiber -Based Modeling of Circular Reinforced Concrete Bidge Columns. *Journal of Earthquake Engineering,* Issue 18, pp. 714-734.

Gazetas, G., 1991. *Foundation Engineering Handbook.* New York: Van Nostrand Reinhold.

Grant, D. N., Blandon, C. A. & Priestley, M. J. N., 2005. *Modelling Inelastic Response in Direct Displacement-Based Design,* Pavia: IUSS Press.

Le Roux, R. C., 2010. *Assessment of seismic drift of structural walls designed according to SANS 10160 - 4,* Stellenbosch: Stellenbosch University.

Mander, J. B., Priestley, M. J. N. & Park, R., 1988. Theorectical stress-strain model for confined concrete. *Journal of Structural Engineering,* 114(8), pp. 1804-1826.

Mirza, S. A. & MacGregor, J. G., 1979. Variability of Mechanical Properties of Reinforcing Bars. *Journal of the Structural Division,* 105(5), pp. 921-937.

Monteiro, R., 2019. *Seismic Design of Building Structures,* Stellenbosch: Stellenbosch University.

Monteiro, R., 8 August 2020. *Tangent stiffness-proportionate damping for infill masonry panels,* ricardo.monteiro@iusspavia.it.

NIST GCR 12-917-21, 2012. *Soil-Structure Interaction For Building Structures,* Gaithersburg: National Institure of Standards and Technology (NIST).

NIST GCR 17-917-46 v1, 2017. *Guidelines for Nonlinear Structural Analysis for Design of Buildings, Part1: General,* Gaithersburg: National Institure of Standards and Technology.

Pais, A. & Kausel, E., 1988. Approximate formulas for dynamic stiffnesses of rigid foundations. *Soil Dynamics and Earthquake Engineering,* 7(4), pp. 213-227.

Pauley & Priestley, 1992. *SEISMIC DESIGN OF REINFORCED CONCRETE AND MASONRY BUILDINGS.* New York: John Wiley & Sons, Inc.

PEER NGA Database, 2020. *Pacific Earthquake Engineering Research Center: NGA Databse.* [Online]
Available at: https://peer.berkeley.edu/peer-strong-ground-motion-databases
[Accessed 3 June 2020].

PEER Report 2017/06, 2017. *Guidelines for Performance-Based Seismic Design of Tall Buildings. Developed by the Pacific Earthquake Engineering Research Center (PEER) as part of the Tall Buildings Initiative.,* Berkeley: Pacific Earthquake Engieering Research Center. University of California, Berkeley.

Pinho, R. & Antoniou, S., 2005. *"A displacement-based adaptive pushover algorithm for assessment of vertically irregular frames," European Workshop on the Seismic Behaviour of Irregular and Complex Structures.* Thessaloniki, Greece.

Priestley, M. J. N., Calvi, G. M. & Kowalsky, M. J., 2007. *Displacement-Based Seismic Design of Structures.* Pavia: IUSS PRESS.

PROKON version 3.1, 2018. *Prokon Software Consultants.* [Online]
Available at: https://prokon.co.za/

Response-2000, 2001. *Response-2000. Response Concrete Sectional Analysis using the Modified Compression Field Theory*.

Retief, J. V. & Dunaiski, P. E., 2009. *Background to SANS 10160: Basics of Structural Design and Actions for Buildings and Industrial Structures.* Stellenbosch: SUN MeDIA.

SABS 0144, 1995. *Detailing of steel reinforcement for concrete,* Pretoria: South African Bureau of Standards.

SANS 0100-1, 2000. *Structural Use of Concrete,* Pretoria: South African Bureau of Standards.

SANS 10160-1, 2011. *Basis of structural desing and action for buildings and industrial structures; Part 1: Basis for structural design,* Pretoria: SABS Standards Division.

SANS 10160-1, 2019. *Basis of structural design and actions for buildings and industrial structures: Part 1: Basis of structural design,* Pretoria: South African Bureau of Standards.

SANS 10160-2, 2011. *Basis of structural design and actions for buildings and industrial structures; Part 2: Self-weight and imposed loads,* Pretoria: SABS Standard Division.

SANS 10160-4, 2011. *Basis of Structural Design and Actions for Buildings and Industrial Structures, Part4: Seismic action and general requirments for buildings,* Pretoria: South African National Standards.

SANS 10160-4, 2017. *Basis of structural design and actions for buildings and industrial structures. Part 4: Seismic actions and general requirements for buildings,* Pretoria: SABS Standards Division.

SANS 920, 2005. *Steel bars for concrete reinforcement,* Pretoria: Standards South Africa.

Seismosoft, 2020. *SeismoStruct 2020 - A computer program for static and dynamic nonlinear analysis of framed structures.* [Online]
Available at: https://seismosoft.com

SIA 262:2003, 2003. *Concrete Structures,* Zurich: Swiss Society of Engineers and Architects, Swiss Standard 505 262.

Stewart, J., Seed, R. & Fenves, G., 1999. Seismic soil-structure interaction in buildings. Part 1: analytical methods. *Journal of the Geotechnical and Geoenvironmental Engineering Division of the ASCE,* I(125), pp. 26-37.

Van der Merwe, J. E., 2009. *Rocking shear wall foundations in regions of moderate seismicity. MScEng Thesis,,* Stellenbosch: University of Stellenbosch.

Veletsos, A. S. & Meek, J. W., 1974. Dynamic behavior of building-foundation systems. *Earthquake Engineering and Structural Dynamics,* Volume 3, pp. 121-138.

Wolf, J. P., 1985. *Soil-Structure Interaction.* William J. Hall ed. Englewood Cliffs: Prentice-Hall.